2016

Optical Redox Imaging of Metabolic Activity

Syed Anwar Hyder Zaidi
Wright State University

OPTICAL REDOX IMAGING OF METABOLIC ACTIVITY

A thesis submitted in partial fulfillment
of the requirements for the Degree Of
Master of Science in Biomedical Engineering

by

SYED ANWAR HYDER ZAIDI
B.E. E.C.E, Osmania University, 2014

2016
Wright State University

Wright State University

GRADUATE SCHOOL

October 10th, 2016

I HEREBY RECOMMEND THAT THE THESIS PREPARED UNDER MY SUPERVISION BY Syed Anwar Hyder Zaidi ENTITLED Optical Redox Imaging of Metabolic Activity BE ACCEPTED IN PARTIAL FULFILLMENTOF THE REQUIREMENTS FOR THE DEGREE OF Master of Science in Biomedical Engineering.

_____

Ulas Sunar, Ph.D.

Thesis Director

_____

Jaime E. Ramirez-Vick, Ph.D.

Chair, Department of Biomedical, Industrial and Human Factors Engineering

Committee on
Final Examination

_____

Jaime Ramirez-Vick, PhD

_____

Debra Mayes, Ph.D.

_____

Ulas Sunar, Ph.D.

_____

Robert E.W. Fyffe , Ph.D.

Vice President for Research
Dean of the Graduate School

ABSTRACT

Zaidi, Syed Anwar Hyder. M.S.B.M.E, Department of Biomedical, Industrial and Human Factors Engineering, Wright State University, 2016. Optical Redox Imaging of Metabolic Activity

Fluorescence imaging can be used to determine tissue metabolism, which is an indication of the cellular functionality. Metabolic contrast is useful for the early detection of several medical conditions such as cancer, diabetes, lung diseases etc.

This study aims to use fluorescence imaging to quantify NADH and FAD, which are cellular metabolic indicators. A parameter known as Redox ratio, can be used to study metabolic state of several tissue types and disease states.

To quantify the Redox ratio, three fluorescence imaging systems were optimized to measure the fluorescence signal from NADH and FAD. The first system was a camera based model suitable for laboratory and clinical settings. The second and third were compact versions of the same instrument. The systems were characterized and brain cancer cells were measured using the camera based system and the compact model, which resulted in a similar Redox ratio.

List of Abbreviations

ADP - Adenosine Diphosphate

APD – Avalanche Photo Diode

ATP - Adenosine Triphosphate

CCD - Charged Coupled Device

DNA- Deoxyribose Nucleic Acid

DPN - Di-phosphopyridine Nucleotide

FAD - Flavin Adenine Dinucleotide

FWHM – Full Width Half Maxima

HB02 – Oxy-Hemoglobin

HHB – Deoxy-Hemoglobin

I.C – Integrated Circuit

IRS - Infrared Absorption Spectroscopy

LASER - Light Amplification by Stimulated Emission of Radiation

LCD – Liquid Crystal Display

LED - Light Emitting Diode

MM – Multi Mode

NADH - Nicotinamide Adenine Dinucleotide

NMR - Nuclear Magnetic Resonance

NIR- Near Infrared

PI – Inorganic Phosphate

PMT – Photo Multiplier Tube

RNA - Ribonucleic Acid

R.R – Redox Ratio

SM – Single Mode

S.S – Stokes Shift

TPN - Triphsphopyridine Nucleotide

UV-VIS – Ultraviolet- Visible

XPS - X-ray Photoelectron Spectroscopy

Contents

List of Figures

List of Tables

Acknowledgements

I would like to take this opportunity to thank all the people who have helped me in completing my work. First, I would like to thank Dr. Ulas Sunar for giving me this opportunity and believing in me with the project. He has guided and helped me throughout my entire journey and I have learned a lot from him. I would also like to thank Dr. Jamie Ramirez-Vick and Dr. Debra Mayes for being a part of my committee.

I would also like to thank Dr. Daniel Rohrbach and Jeremy Kress for supervising my work. I am also grateful to my Lab mates Chien, Aaron and Zahra Meghjani for continuously encouraging me throughout my work.

Last, I would also like to thank my parents Dr. Murtuza Zaidi and Dr. Najafi Begum for being pillars of my moral support. I would also like to thank My Sister Nishat Zaidi and brother Aman Zaidi for encouraging me all the time.

Dedicated to

My Mom and Dad who have always loved and supported me in every step of my life.

Introduction and Background

1.1 Introduction

Mitochondria play a very essential role in a cellular metabolism. Dysfunction in mitochondria may lead to several diseases as shown in the Figure 1.1 [1-2]. Pioneer works of Warburg showed the involvement of mitochondria in a tumor cell [3]. Since then, a number of studies were performed to investigate the presence of mitochondrial dysfunction[1] in many conditions such as aging[4,5], neurodegenerative diseases like Parkinson's and Alzheimer's [6-8], tissue damage post stroke[9] , spinal cord injury[10], cardiovascular diseases[11], liver and kidney[12,13], diabetes and obesity[14-16], cancer[17-25] and many other medical conditions.

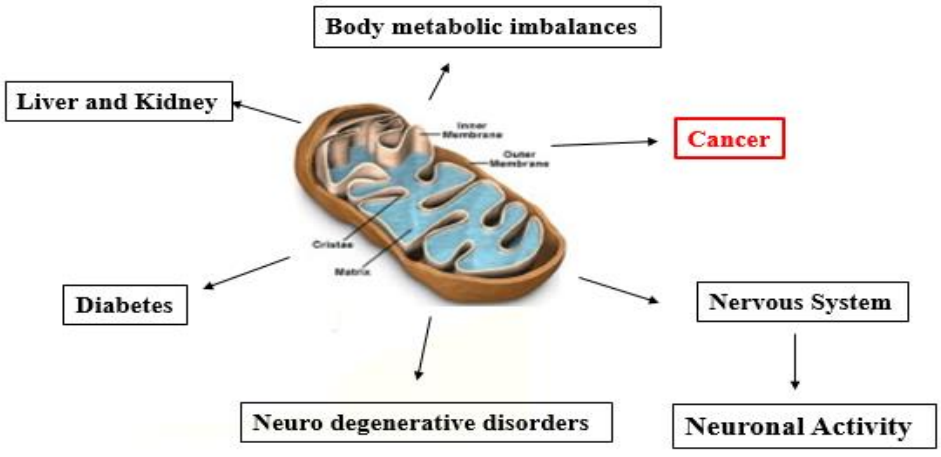

Figure 1.1: Mitochondrial dysfunction
Adapted for Mayevsky et al, 2009 [2]

Pioneer works of Chance et al showed a relation between function of mitochondria in health and disease by quantifying NADH redox state in mitochondria [26-28]. Since then several studies were performed in various pathophysiological conditions to study metabolic changes in experiments, animals and patients [29-30].

1.1.1 Cancer

Cancer can be one the of the consequences of mitochondrial dysfunction. Cancer is defined as an abnormal growth or uncontrolled division of cells [31]. There are several types of cancer which including breast, oral, brain, prostate and many more. Figure 1.2 shows the cancer cases and mortality rate in both developed and underdeveloped countries.

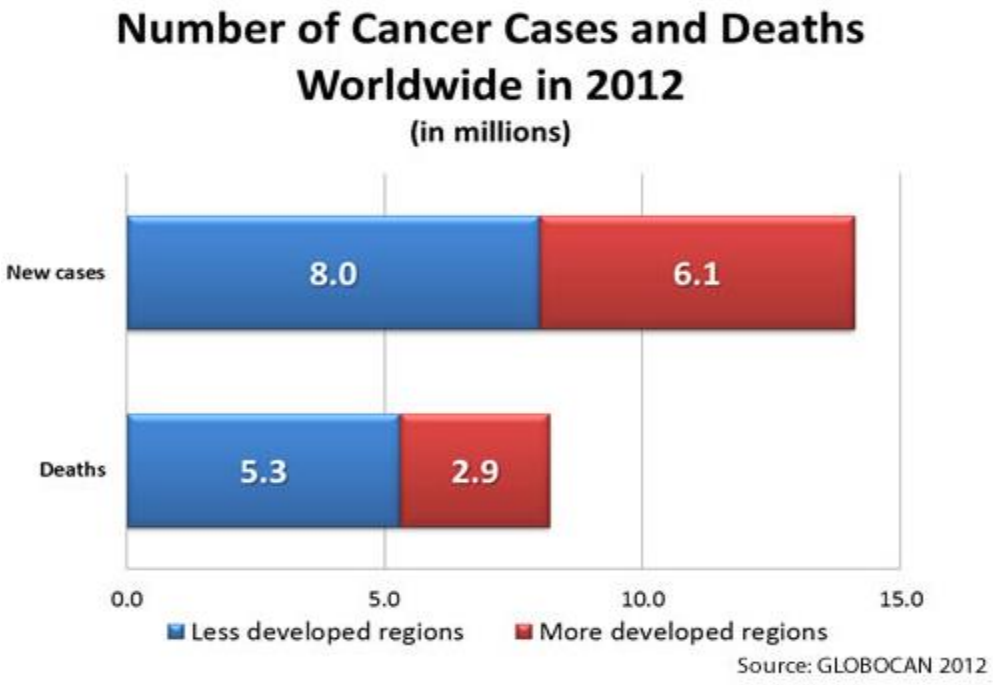

Figure 1.2: Cancer statistics [32]

1.1.1.1 Brain Cancer

Brain tumors can be benign or malignant and only the latter is termed as brain cancer. Cancerous cells compete with the healthy cells and take up their space, blood and nutrients to grow and spread [33]. The exact cause of brain cancer is not clearly [33]. Not all brain tumors show symptoms and some are detected only when a CT or MRI scan is done [33].

Common symptoms include headache, weakness, nausea, changes in intellectual capacity or emotional response gradually, difficulty in walking and in speech, but some of these are not limited to brain tumors alone and can be missed easily [33]. CT and MRI are generally performed for the diagnosis.

If a tumor is suspected, then a biopsy will be performed followed by pathophysiological examination to detect the presence of cancer. Biopsy of the brain is usually one piece which is enough for diagnosis, however removing aby brain tissue for a biopsy can cause further brain damage and might also cause infection.

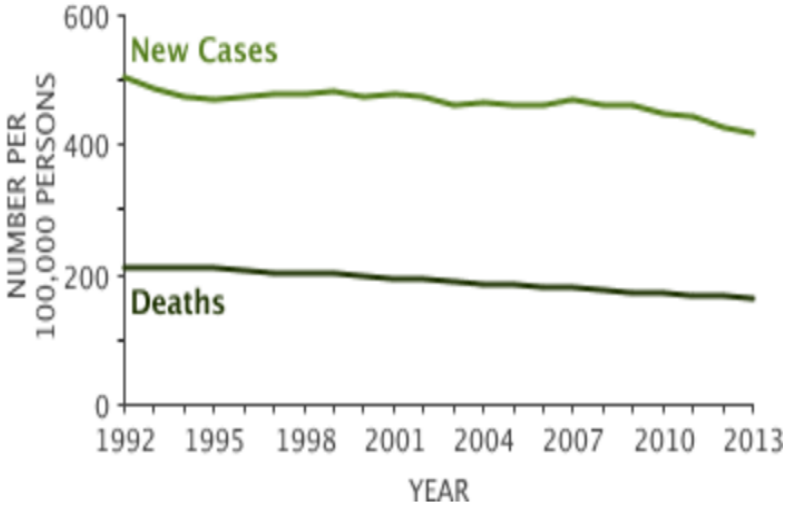

Figure 1.3: Brain cancer statistics [34]

Generally, treatment of neuronal tumors involves surgery for the removal of the tumor followed by radiation or chemotherapy to remove any remaining cancerous cells [33].

1.1.2 Motivation

As per the 2012 census there were about 14.1 million cancer cases around the world [35]. Around 256,213 cases of brain tumors [36] have been reported worldwide in 2012. As per 2016 census, 1,685,210 new cancer cases and 595,690 cancer deaths have occurred in The United States, making it the major cause of death in 21 states [37]. Approximately 78,000 brain cancer diagnoses have been reported in the U.S. Hence there is an urgent need to develop a device which can accurately identify the presence of cancer noninvasively in its early stages to avoid mortality.

Presence of cancer alters metabolism of the cell which is associated with cell growth and proliferation [38-39]. Usually cancer cells have increased metabolism which is used as a tool for investigating or detecting cancer in the body [40]. A wide range of clinical instruments have already been developed which can accurately identify the presence of cancer but are expensive and require the patient to visit the hospital for diagnoses. Thus, an instrument should be developed which is portable (Wearable), low cost and user friendly which could potentially make cancer diagnoses easy and detectable in its early stages. The aim of this study is to develop a portable, inexpensive and wireless device capable of measuring the fluorescence emitted by fluorophores such as Nicotinamide Adenine Dinucleotide (NADH) [41] and Flavin Adenine Dinucleotide (FAD) [42] which are involved in cellular metabolic pathways.

1.2 Background of Redox Ratio

1.2.1 Mitochondria

Mitochondria are found in all Eukaryotic cells where they play a large role in cellular metabolism and energy generation. Structure of mitochondria is shown in Figure 1.4. Overall, mitochondria have several important functions, the most important functions being oxidation of food materials and cellular respiration [43]. Cellular respiration is the process where the breakdown of complex food molecules through oxidation within the cell leads to the release of considerable amounts of energy [44]. Complex molecule compounds known as respiratory substrates are oxidized during this process. Carbohydrates are the preferred substrates, but proteins and fats can be used as well [45].

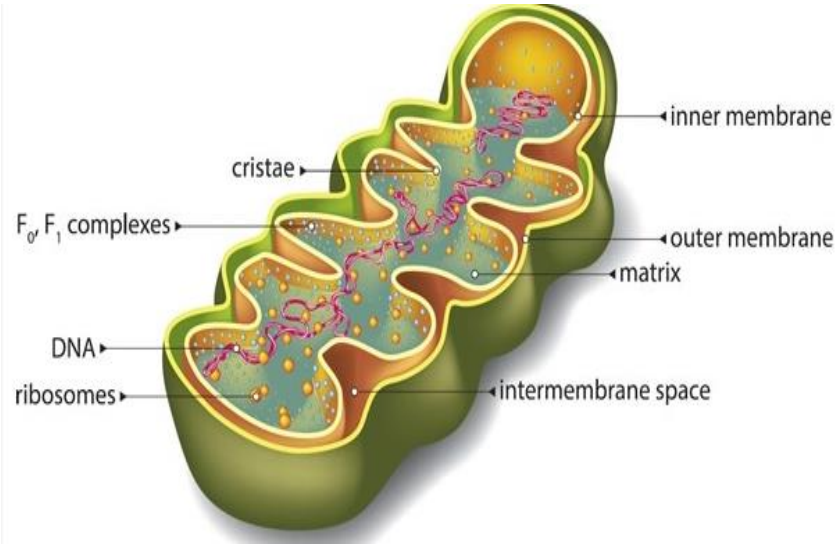

Figure 1.4: Mitochondria structure [46]

When respiratory substrates are broken down in the presence of oxygen it is called aerobic respiration. All the energy is not released free into the cell in a single step. It is released in

a series of reactions which are controlled by enzymes [47]. The chemical energy thus obtained is held in the form of Adenosine triphosphate (ATP) [48], which can then be utilized as a source of energy for the cell [49-50]. Energy released by oxidation in respiration is used to synthesize ATP and not used directly. The amount of energy that is produced depends on the quantity of oxygen present inside the cell [51]. This energy is produced through a process called the electron transport chain. Redox reactions such as respiration extracting energy through this process.

Energy trapped in ATP is utilized in various processes for the organism and the carbon components produced during respiration is used for bio synthesis of various other molecules in the cells [52]. ATP synthase is an important enzyme providing energy for the cell through the synthesis of ATP. ATP is formed from a reversible reaction of Adenosine diphosphate (ADP) and Inorganic Phosphate (PI) popularly known as ATP-ADP cycle.

$$ADP + PI + free \rightarrow ATP$$

Thus, Mitochondria are also often referred to as miniature biochemical factories wherein respiratory substrates and other food stuff are completely broken down and oxidized to carbon dioxide and water. Energy generated during this process is stored as reduced coenzymes and prosthetic groups which later undergo oxidation and form ATP which is rich in energy. ATP generated out of mitochondria is used in many energy requiring processes [53].

1.2.2 Electron Transport Chain

As mentioned in the previous section, energy is produced in the cell through a process called the electron transport chain, which is responsible for the generation of energy within the cells.

The electron transport chain is a chemical series of electron donation and electron acceptance. A continuous transportation of electrons form an electron donor to a more electronegative acceptor takes place. This process continues to the most electronegative acceptor at the end of the chain [54]. Finally, the energy is released by the conversion of ATP from ADP as mentioned in the previous section 1.2.1. The entire process is called oxidative phosphorylation.

There are two proteins in the mitochondrial inner membrane, NADH and FAD, which get oxidized by complex chemical reactions resulting in the release of a proton across the membrane. A Figure of electron transport chain is shown in Figure 1.5.

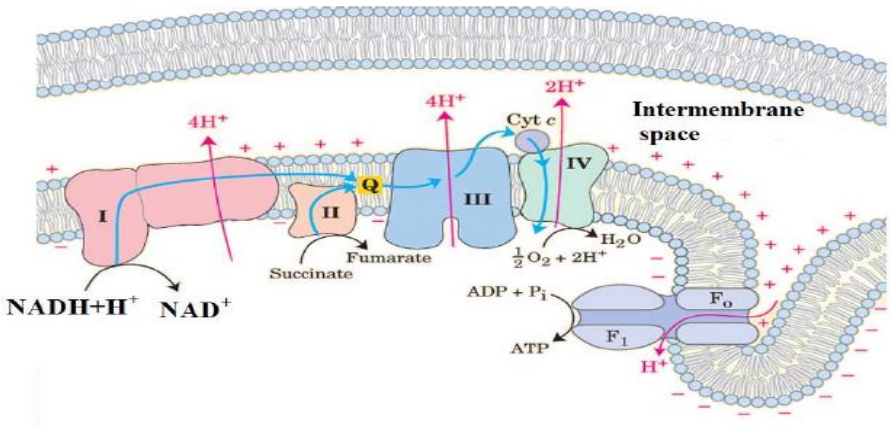

Figure 1.5: Electron transport chain [54-55]

1.2.3 Mitochondrial Oxidative Stress

In the process of electron transport chain, a small number of electrons do not participate in this process and directly leak to oxygen [54]. This leads to the formation of free radical which cause a phenomenon known as oxidative stress.

Oxidative stress is defined as the excess or deficiency of oxygen in the cell, caused by the imbalance of reactive oxygen produced in the cell and the system's inability to repair the resulting damage caused by it [54,56]. Disturbance in the normal redox reaction in the cell produces peroxides and free radicals which can have toxic effects [57], which can have a damaging effect on the cell [54]. Therefore, for the proper functionality of the cell, quantity of oxygen present in the cell and its surroundings play a very vital role [58-60].

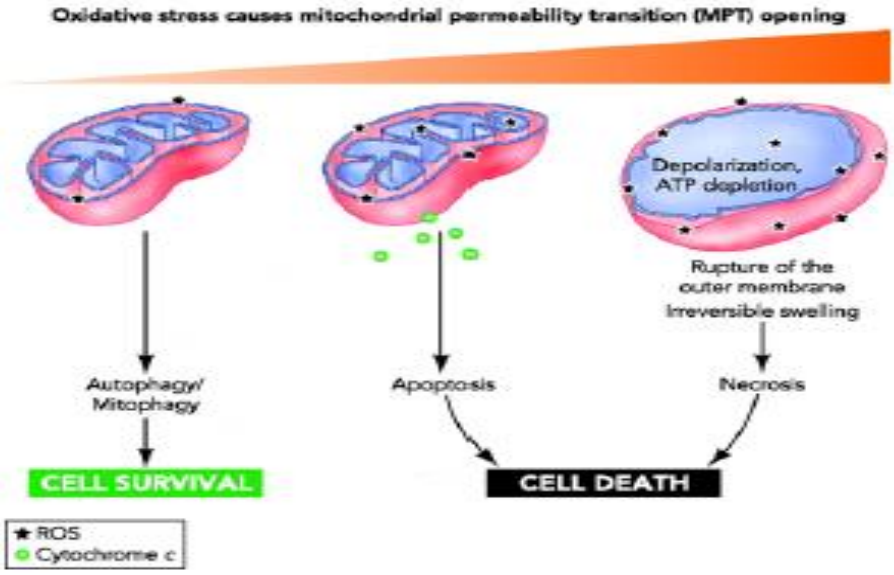

Figure 1.6: Mitochondrial dysfunction and death of the cell [63]

Oxidative stress is responsible for causing several diseases and aging in a cell [61-63]. The amount of energy produced in the cell is a function of the quantity of oxygen present in the cell. Oxidative stress, the imbalance of oxygen present in the cell, can cause various malfunctioning in the cell and can also lead to cell death [54]. The Figure 1.6 shows the mitochondrial dysfunction and ultimately the death of the cell [63].

Oxidative stress is seen in a number of neurological diseases such as Amyotrophic Lateral Sclerosis [64], Parkinson's disease [65], Alzheimer's disease [66], Huntington's disease [67], and Multiple sclerosis[68-69].

Several diseases are caused by poor functioning of the cell due to the improper balance of oxygen in the mitochondria which accelerates cell death [70]. Thus, determining the amount of oxygen present inside the cell can prove a very useful tool for feedback of the health of the cell. This is very important in situations relating to mitochondrial dysfunction and oxidative stress [54]. In such situations, oxidation state (redox state) can be used to determine the health of the tissue.

1.3 Optical Imaging

In this section, optical imaging, especially fluorescence imaging is explained.

1.3.1 Optical Imaging

Imaging performed using light as tool is termed as optical imaging. This imaging technique has emerged in the past decades as a strong tool for determining the anatomy [71], physiology [72], metabolic [73], and molecular function [74] of the tissue under

investigation [54]. In this research, measurement of redox ratio can be done without using harmful radiation on the subject [54]. Moreover, optical imaging techniques have the advantage of being non-invasive, inexpensive and being very sensitive for detection purposes [75]. The one disadvantage of optical imaging is that penetration depth limiting access to tissue anatomy is less when compared to other imaging modalities like MRI, CT etc. [76].

Optical imaging can use a wide spectral range covering ultraviolet light to infrared light. For this research, we use ultra violet (UV) light as the excitation wavelength for both NADH and FAD. When the photons from the optical sources interact with the tissue, they either are absorbed or scattered.

1.3.2 Light Transport in Tissue

A common model for tissue imaging is the semi-infinite geometry, as shown in Figure 1.7. In semi-infinite geometry, there is a single interface, typically with air above and tissue below. When the light is incident on the surface, multiple processes can occur. Some percentage will undergo specular reflection and never enter the tissue. For photons that enters the tissue, they will either be scattered in random directions and or absorbed depending upon the wavelength used and the property of the tissue. Thus, there are two main optical parameters that define the light transport in tissue: absorption and scattering parameters. I will be introducing briefly these parameters in the next sections.

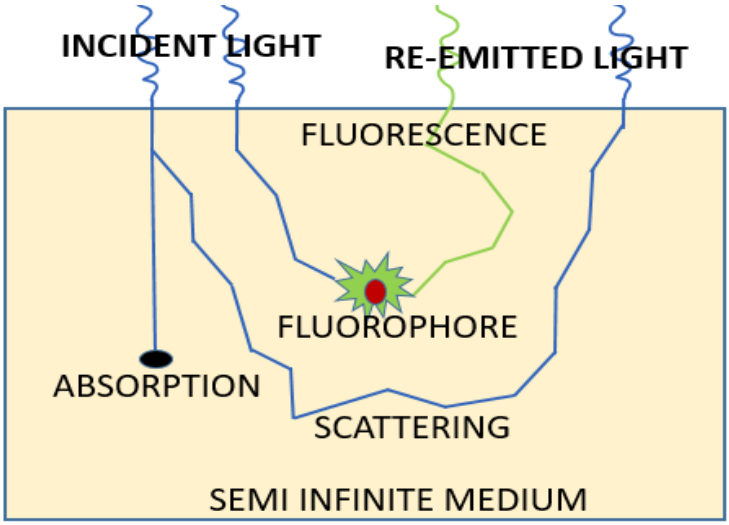

Figure 1.7: Interaction of light with the tissue

1.3.2.1 Light Absorption

The relation between absorption of light in a non-scattering, absorbing medium was first given by Bourger in 1729 and then by Lambert in 1760 [77]. Per this study when light with an intensity $\mathbf{I_0}$ passes through a cuvette having a thickness d then the light obtained at the other end will have a lower intensity comparatively [77].

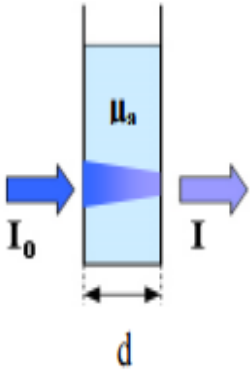

Figure 1.8: Absorption of light in a non-scattering medium [77]

The absorption of light in tissue is due to various chromophores present in the body such as water, oxy-hemoglobin (HBO2), deoxy-hemoglobin (HHB), lipids, porphyrins, melanin, NADH and Flavin's, collagen, elastin, and lipo-pigments depending on the wavelength range we are investigating [54]. In the Near Infrared (NIR) wavelength region, the main absorption occurs due to oxy-hemoglobin (HbO2), and deoxy-hemoglobin (Hb) chromophores. Thus, for tissue oxygenation studies, this wavelength range is commonly used.

The Figure 1.9 shows the absorption spectrum of HHB and HBO2

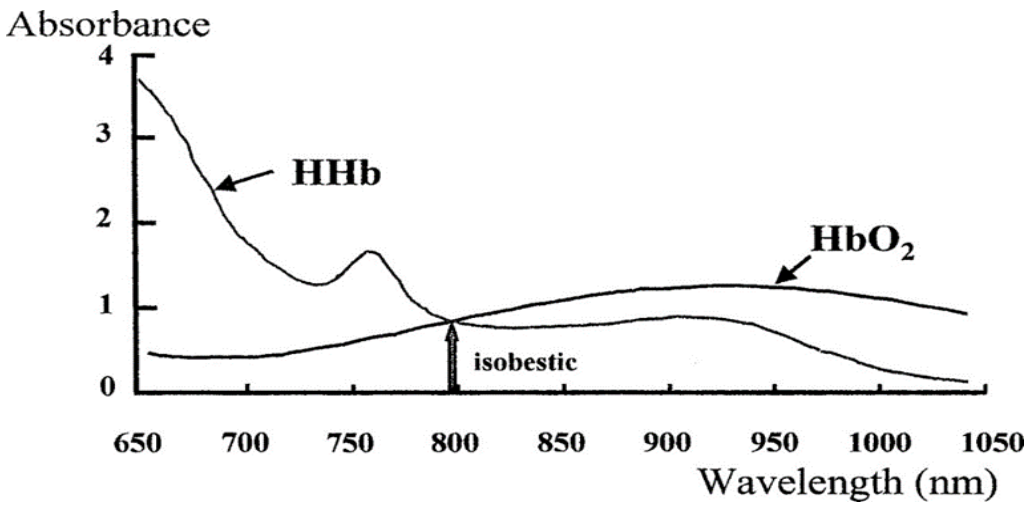

Figure 1.9: Absorption Spectra of a oxy and deoxy hemoglobin[78]

1.3.2.2 Light Scattering

Light Scatter in a tissue because the cells and cellular organelles that make up a tissue have a mismatched refractive index. [79]. When the refractive index changes between various

organelles within the cells, which account for a large portion of solid content of the tissue, scattering occurs [77]. In the visible and near-infrared wavelengths, scattering is the major mechanism in the propagation of light through the tissue. Even in thin tissue, photons are likely to scatter multiple times before reaching the boundary [77]. Scattering causes the photons to travel a greater distance within a tissue thereby increasing the probability of the photon getting absorbed which is shown in the Figure 1.10 [77]

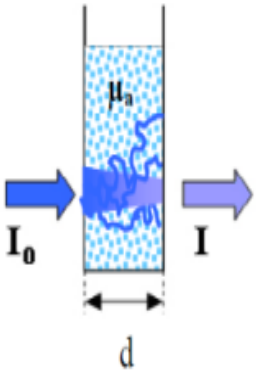

Figure 1.10: Scattering of light [77]

Scattering is affected by several factors namely age, tissue oxygenation, and wavelength of light [80]. For instance, in brain scattering increases with age, from birth to adulthood. This occurs because as people age there is a two-fold increase in lipid and protein content. In addition, the lipid in white matter, is increased by seven folds [81].

In biological tissue, light scatters multiple times and is characterized by a term known as the reduced scattering coefficient (μ_s'). Reduced scattering coefficient is the reciprocal of the total distance travelled by the photon before it gets completely randomized.

Due to variation in the size of cancer cells, there is a difference in the reduced scattering coefficient between normal and cancerous cells [82].

1.3.2.3 Penetration Depth

In fluorescence spectroscopy, the light source and detector are generally placed on the surface of the tissue, therefore primarily superficial information is collected. The penetration depth is low because of two factors. First, fluorescence is a weak signal. This means the source and detector are typically placed very close to each other to detect the signal. Light that reaches the detector travels a "banana curve", and as Figure 1.11 shows, the separation between the source and detector influences the penetration depth. The depth can be increased by increasing the source-detector separation but that would limit the signal detected. Thus, there is a tradeoff between intensity of collected light and penetration depth.

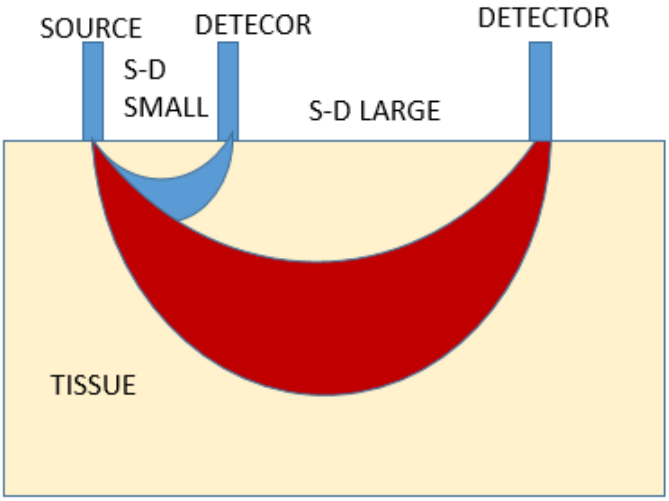

Figure 1.11: Penetration depth in smaller source detector separation (S-D small) and large source detector separation (S-D large)

The second factor affecting the penetration depth of light in tissue is the choice of wavelength. As discussed in previous sections, shorter wavelength light tends to undergo more absorption and scattering events, limiting the penetration depth. For fluorescence spectroscopy, a shorter wavelength is used in most studies which further reduces the penetration depth [83-85]. The relationship between penetration depth and wavelength is shown in the Figure 1.12 [86]

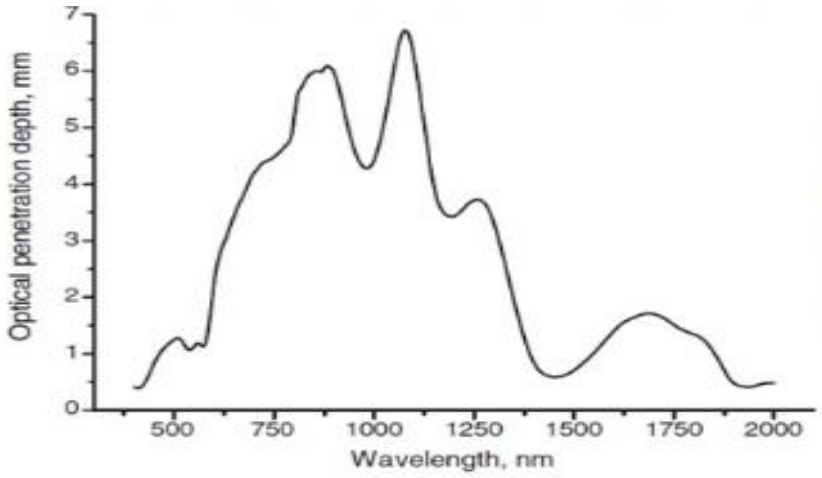

Figure 1.12: Penetration depth as a function of wavelength [86]

1.3.3 Fluorescence Imaging

In this section the principles of fluorescence imaging will be discussed.

1.3.3.1 Mechanism of Fluorescence Imaging

Fluorescence is defined as the process wherein a fluorophore absorbs an excitation photon and then emits a lower energy photon. [87]. The process of fluorescence is divided into two stages namely the Excitation state and the Fluorescence emission state.

Excitation: In this process a photon of energy called excitation energy is supplied to the fluorophore by means of a light source (lamp, laser, light emitting diode, etc.), promoting the molecule to jump to higher energy state as shown in Figure 1.13. Each fluorophore has specific excitation and emission wavelengths where more absorption and emission occurs.

The process of fluorescence can be depicted by the Figure below

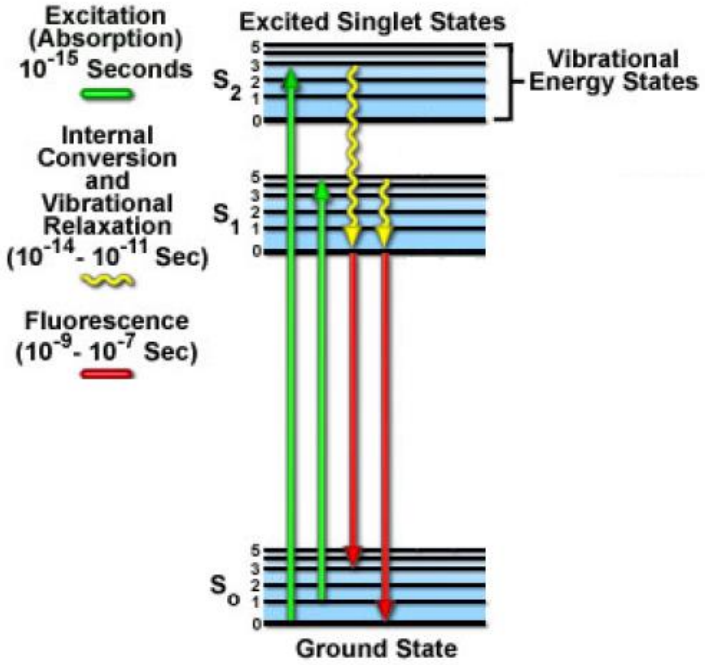

Figure 1.13: Stages of fluorescence [54,88]

An important parameter of every fluorophore is the fluorescence quantum yield. This parameter is defined as the ratio of excitation photons to emission photons.

Fluorescence emission: The fluorophore returns to the ground stage by emitting a photon of energy called emission energy. Photon energy is inversely related to the wavelength, or directly related to the frequency of the light. Due to the dissipation of energy that occurred

in the excited state, the emitted energy will be lower than the absorbed energy and the wavelength of the fluorescence photon will be longer. The separation between excitation and emission wavelength is known as Stokes shift, which is shown in Figure 1.14.

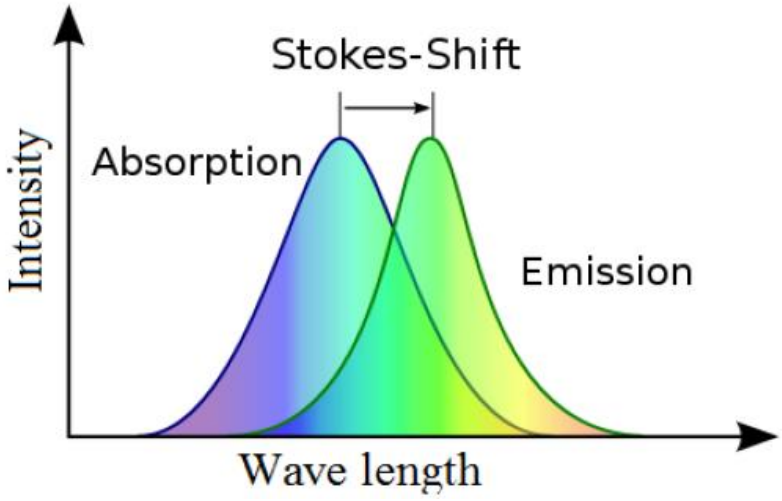

Figure 1.14: Stokes shift [54,89]

In vivo fluorescence gets affected by factors such as (i) movement artifacts (ii) Blood oxygenation changes (iii) Variation in tissue absorption properties (iv) Tissue blood volume variation [90]. Work has been done to nullify their effect for more accurate measurement. For instance, movement artifacts can be corrected by making proper contact, effects of absorption can be nullified by the subtraction technique [91-92], correction in blood volume can be done by taking measurements on thin slices of the imaging tissue [93] or by using the reflected light [94].

Early works of Chace et al and others showed that it was possible to link intrinsic mitochondrial fluorophores to metabolism [95-105]. Fluorescence imaging, can be used to

determine the metabolism of cells which can be used as tool to determine tissue functionality.

1.3.3.2 Intrinsic Mitochondrial Fluorophores

Only a few fluorophores involved in cellular metabolic process are auto-fluorescent and these can be used to study the metabolism of the tissue [54]. These fluorophores include tryptophan, collagen, NADH, Flavin's, and porphyrins [54]. As discussed earlier, NADH and FAD are essential in mitochondrial metabolic activity and play a very important part of the electron transport chain. Therefore, NADH and FAD fluorescence can be used to study the oxidation state (redox state) of the mitochondria [106].

NADH is fluorescent in its reduced state and gives no fluorescence in oxidized form whereas FAD is fluorescent in its oxidized form. We use a parameter known as redox ratio to measure the metabolic state of the tissue and mitochondrial redox. The fluorescent signals emitted from these fluorophores can be used as indicators of tissue vitality and metabolism [107-109].

NADH has its peak excitation at 340nm (ultraviolet) and peak emission at 460nm (blue). FAD on the other hand has two excitation wavelengths. One is at 340nm (ultraviolet) and the other is at 448nm (blue) while the peak emission of FAD is at 520nm (green) as shown in Figure 1.15.

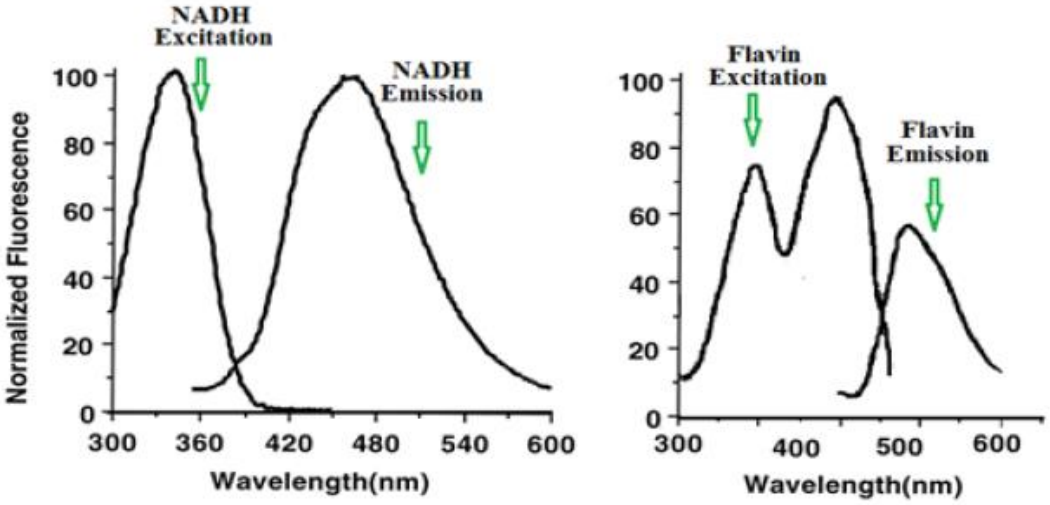

Figure 1.15: Excitation and emission wavelengths of NADH and FAD [110-111]

The NADH redox ratio is defined as the ratio of concentration of NADH to the summation of concentration of FAD and NADH.

$$\text{NADH REDOX RATIO (R.R)} = \frac{\text{CONCENTARTION OF NADH}}{\text{CONCENTRATION OF FAD+CONCENTRATION OF NADH}} \quad (1.1)$$

Whereas, FAD redox ratio is defined as the ratio of concentration of FAD to the summation of concentration of FAD and NADH.

$$\text{FAD REDOX RATIO (R.R)} = \frac{\text{CONCENTARTION OF FAD}}{\text{CONCENTRATION OF FAD+CONCENTRATION OF NADH}} \quad (1.2)$$

Because of important role played by these intrinsic mitochondrial fluorophores, fluorescence imaging techniques has widely been used in biomedical research to study the path-physical state of tissues [112-113], diagnose and/or monitor various diseases in heart [114-115], kidney [116-117], liver [118], lung [107], skeletal muscles [119], cervix [120] and brain [121].

1.3.3.3 Applications of Fluorescence Imaging

As mentioned in the previous section, fluorescence imaging can be used for several applications. A few of them are discussed in this section.

1.3.3.3.1 Brain Application

Mayevsky and Chance et al detected the fluorescence emission from the brain in various conditions such as Anoxia, Ischemia etc. [29,122-124]. Their study concluded that Redox ratio is the best way to evaluate mitochondrial function and tissue oxygen balance.

Fluorescence is used to study the changes occurring during brain stimulation. The study was done by observing the NADH changes occurring due to cortical and ischemic change during myocardial infarction [125]. Changes occurring in NADH signal can be used to determine the metabolic changes [126]. Redox ratio can also be used to differentiate between normal and cancer tissues in the brain and the study concluded that normal brain tissue had higher FAD redox (FAD/FAD+NADH) compared to a cancer tissue [127]. The reason for this being FAD gives fluorescence in oxidized form and NADH in reduced form.

1.3.3.3.2 Other Applications

Fluorescence from NADH and FAD can be used to differentiate between normal oral keratinocytes and squamous carcinoma cells form various origin [128]. Detection of FAD fluorescence can be used diagnose the presence of malignant oral mucosa since the cancer region would have no FAD fluorescence emission [129].

FAD redox is another parameter which can be used to detect oral malignancy [130]. It was seen that normal cells and post treated cancer had more redox ratio in comparison to the cancer cells. NADH and FAD can be used to detect cancer in neck and head area. Pauli et also conclude that out of all endogenous fluorophores only NADH and FAD could effectively differentiate between normal and cancer cells [131].

FAD Redox ratio can be used to differentiate normal tissue from cancer tissue in breast biopsy's [132]. FAD redox can also be used to differentiate between (aggressive) and less metastatic (indolent) tissues in the breast [133]. Tryptophan to NADH ratio was also used to discriminate normal, aggressive and non-aggressive cancer tissues in the breast. The study concluded that the ratio was maximum for aggressive followed by less aggressive cancer tissue and was least for normal tissue [134].

NADH redox (NADH/FAD) can be used to study changes in a rat's perfused lung [135]. The ratio can be used to evaluate the pulmonary ischemia-reperfusion on lung tissue [136]. NADH redox can also be used to evaluate the condition of respiratory chain in a rat's lungs due to ischemia, hypoxia and Ischemia-reperfusion [107].

Fluorescence emitted by NADH and FAD can be used to differentiate normal, benign and cancer tissue in prostate [137]. NADH fluorescence can used to determine the presence of cancer in prostate tissue. It was seen that cancer tissue had more NADH fluorescence in comparison to normal tissue [138]. By recording the emission at various excitation wavelengths of NADH, an excitation- emission matrix can be constructed which can be used to detect the presence of cancer in prostate tissue.

Fluorescence emitted by NADH and FAD to investigate the presence of retinal pigmentosa in mice [139]. Fluorescence of the two fluorophores can be used to determine the effects of oxidative on mitochondrial redox in salt sensitive hypertension [140]. NADH fluorescence can be used to differentiate between normal and cancerous bronchial tissue [141]. NADH and FAD fluorescence can be used to study the photo aging process [142]. Metabolic state of the tissue based on auto fluorescence can be used to discriminate between normal and cancer cells of the bladder [143].

1.4 Discussion

In the next chapter (Chapter 2) instrumentation and results of standard bench top camera based systems will be explained in detail which is more suitable for Laboratory and Clinical environment. There is also a need for combat and wireless device

In chapter 3 and chapter 4, instrumentation and results of compact systems will be explained in detail.

Instrumentation and Results of Camera Based Model

2.1 Introduction

The first design was made looking at relevant literature, suitable for clinical and Lab environment. This model provides high resolution images.

2.2 Instrumentation `

This section deals with sources and the detectors which are generally used for the design of a fluorescence measurement device. All the source and detectors, along with their pros and cons would be discussed in this section

2.2.1 Light Sources

The two common light sources which are used in optical instrumentation is a Laser diode or a Light Emitting Diode (LED).

2.2.1.1 Light Emitting Diode

Light emitting diode knows as LED's are inexpensive, efficient and rugged [144]. They are also available in number of wavelength ranges. Their only disadvantage is that they have a wide spectral bandwidth (~20nm to ~60nm FWHM) and this can cause problems in sensitive optical measurements where precise wavelength is required. In the case of fluorescence measurements, a light source need not have high precision in wavelength fluorophore has an excitation spectrum which is a wide and thus precision is not important. Thus, LED's are the ideal light sources for Fluorescence measurements.

2.2.1.2 Laser Diodes

Laser diodes are of two types namely single mode(SM) and multimode(MM) laser diode. A SM has a smaller core radius than a MM laser. SM laser supports larger bandwidth than a SM laser. A SM laser has lower signal losses compared to a MM laser. A SM laser are more coherent than a MM laser. Both SM and MM laser are expensive and are chosen depending upon type of application.

2.2.2 Detector Sources

The common light sources used in optical instrumentation are the PIN diodes, Avalanche Photo Diode(APD), Photo Multiplier Tube(PMT), Spectrometer and Multispectral camera.

2.2.2.1 Pin Diodes

PIN diodes are very inexpensive and have a good quantum efficiency and dynamic range [144]. Most of the PIN diodes have peak sensitivity in the 600nm -800nm range. They do not have very high sensitive as they do not have an internal amplifier but this can be

designed. They are usually used in application where sensitivity is not very important and for shorter source and detector separation [144].

2.2.2.2 APD

Avalanche photo diodes are comparatively more sensitive than PIN diodes but they tend to have a smaller dynamic range [144]. They have an in-build amplifier which tend to increase their sensitivity. These are expensive than PIN diodes and they require a high voltage supply for their operation. They are used in applications where the source-detector separation distance is large.

2.2.2.3 PMT

Photo multiplier tube and APD have about the same sensitivity and dynamic range. PMT's can provide a farther more gain compared to a APD. The operating voltage is even higher for a PMT when compared to a APD. The disadvantage of PMT is that it that they are highly sensitive to supply voltage fluctuations, their gain depends on spectra and their linearity is poor [144].

2.2.2.4 Spectrometer

A spectrometer is a device which collects the light, separates the light based on their wavelength and displays the intensity values at specific wavelengths. A spectrometer can have a desired spectral response as this depends on the groove density which can be altered. The optical resolution (wavelength) can also be varied by varying the opening slit of a spectrometer. A spectrometer is very sensitive device but is expensive compared to PMT

and APD. As a spectrometer gives a complete spectrum of a wide range of wavelengths, thus it is a commonly used in fluorescence applications.

2.2.2.5 Multispectral Camera

A multispectral camera is like a spectrometer as it captures the imaging surface and provides the intensity at a specific wavelength within an image. It is equal or has a greater sensitivity than a spectrometer. A multispectral camera is the most expensive detecting module. Most of multispectral cameras are equipped with a filter mechanism which can be used and only a desired range of wavelength can be measured which eliminated the use of additional optical filters. The main advantage of using a camera is that it can take the image from a greater separation distance and provide accurate results. Another advantage of the camera is that it provides a complete image of imaging surface unlike point measurements in other detecting modules.

2.3 Camera Based Module

In this section the Light source unit and the light detector unit of the camera based model will be explained in detail.

2.3.1 Light Source Unit (LSU)

2.3.1.1 LED

The light source chosen for the camera based model was a high-power LED from Mightex. The wavelength chosen was 365nm as this was capable of exciting both NADH and FAD.

The product number of this LED is LCS-0365-02-22. The specification of the LED is given in the Table 2.1.

PARAMETER	VALUE
WAVELENGTH	365nm
OPERATING CURRENT	500mA
OPERATING VOLTAGE	3.8V
OUTPUT POWER	80mW

Table 2.1: Specifications of LED (Camera model)

2.3.1.2 LED Driver

The LED driver used to run the LED was SLC series LED driver from Mightex. The part number of this driver is SLC-SA04-US. The LED driver is connected to P.C by means of USB or a RS 232 interface. The LED's cathode and anode are connected to the driver as marked and the desired supply current is varied by means of a software. By varying the supply current, optical power of the LED could be varied. The specifications of the LED driver are given in the Table 2.2.

Table 2.2: Specifications of LED Driver (Camera model)

PARAMETER	VALUE
SUPPLY VOLTAGE	9-12V
SUPPLY CURRENT	<4000mA
DRIVING VOLTAGE (max)	Supply voltage-0.5V
CURRENT RESOLUTION	12 bit

2.3.2 LED Testing

The most important testing for a source used for optical applications is its power or stability testing. It is very important for the source to be stable as variation in its power can lead to false diagnoses. For instance, at a certain optical power a certain amount of fluorescence intensity is expected. Due to instable power, if the optical power of the LED falls below its normal value then the emitted fluorescence will also be low leading to false readings. Thus, it is very important that the source be highly stable. In this experiment the current was set to give a power of around 55mW.

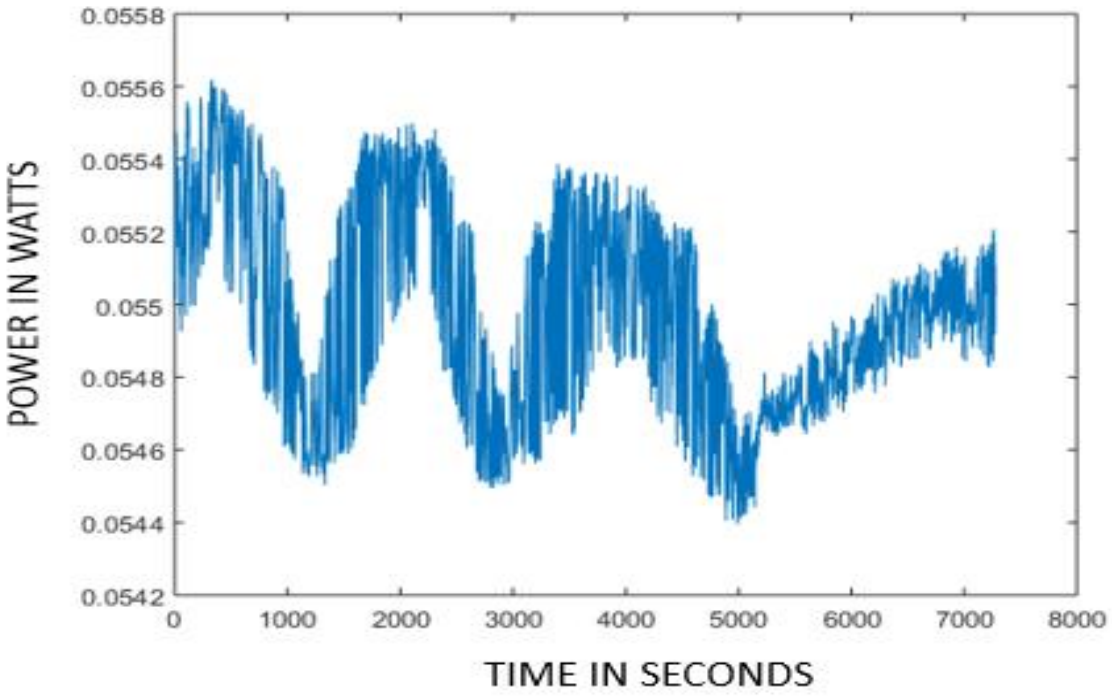

Figure 2.1: Power stability of the LED (Camera based)

The mean and standard deviation from the LED stability test is shown in the Table 2.3.

Table 2.3: Specifications of LED Driver (Camera model)

PARAMETER	VALUE
MEAN	55mW
STANDARD DIVIATION	220nW

2.3.2 Light Detector Unit (LDU)

The detector used to detect fluorescence in the camera based module was a Nuance Multispectral Camera from Perkin Elmer. The camera has a USB interface with the P.C and the images are taken using a Multispectral Imaging software. The camera can capture images in both RGB mode and fluorescence mode depending upon the type of application. The resolution of the camera is 14 bit and various binning and acquisition times can be used to capture the image. The filter cube in the camera acts like a filter and can be set to pass a desired range of wavelengths. The specifications of camera are given in Table 2.4.

Table 2.4: Specifications of the Multispectral Camera

PARAMETER	VALUE
SUPPLY VOLTAGE	5V DC
WAVELENGTH RANGE	400nm- 700nm
CAMERA RESOLUTION	14 bit (4096 intensity levels)
OPTICAL RESOLUTION	10nm
ACQUISTION TIME	10ms – 7s
BINNING	1x1, 2x2, 4x4
FILTER CUBE RANGE	10nm-full range

2.3.2.1 Detector Testing

Testing the detector is essential to see if the device is calibrated and is working accurately. As a device becomes old calibration is required so that the detection is precise. The Multispectral Camera used in the design was tested by means of a detector card from Thorlabs Inc (Part no: VRC2). The purpose of using this detector card was because of its absorption and emission property. This was like fluorescence excitation and emission and was the best way to test the device. The absorption and emission of the detector card from Thorlabs is shown in the Figure 2.2.

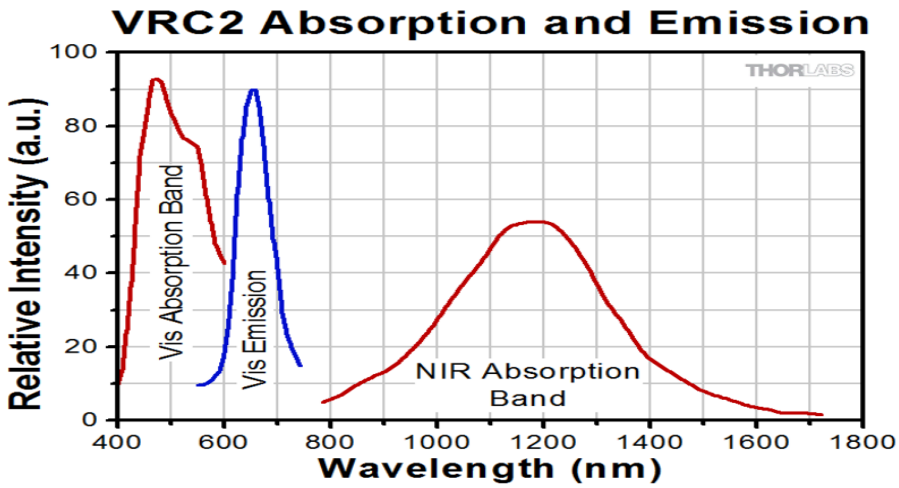

Figure 2.2: The absorption and emission of the detector card (Thorlabs.com)

https://www.thorlabs.com/newgrouppage9.cfm?objectgroup_id=296&pn=VRC2#3218

The absorption wavelength used for detector testing was a 532nm Laser pointer from E-Bay. The distance between the detector card and camera was around 22 cm. A camera Lens was used to focus the camera on the detector card.

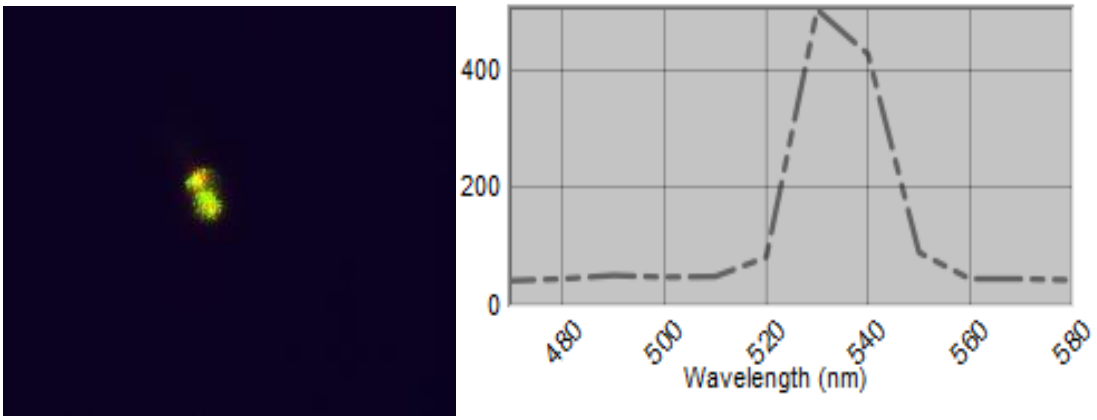

Figure 2.3: Excitation light from the laser pointer and its spectrum (Filter: 480-580nm)

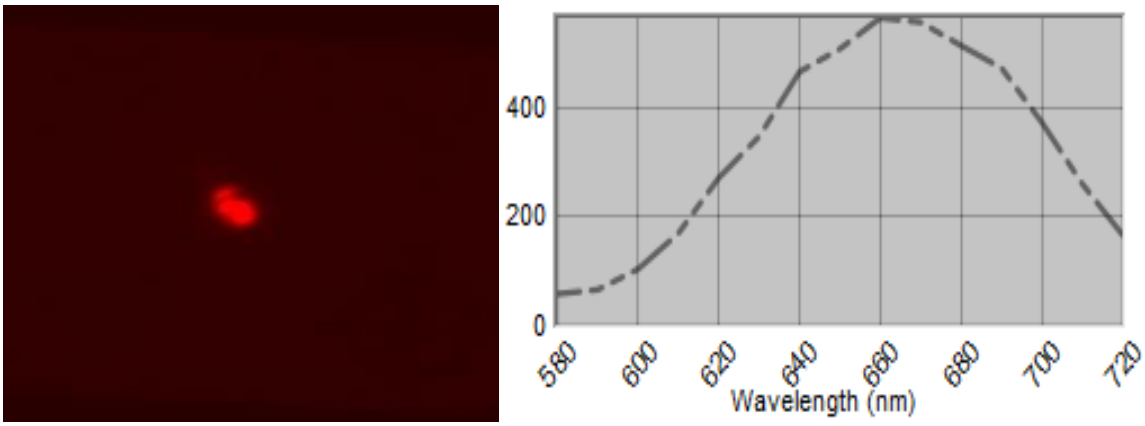

Figure 2.4: Emission light from the Detector card and its spectrum (Filter: 580-720nm)

The result (Figures 2.3 and Figure 2.4) obtained using the camera was very like the specification sheet from Thorlabs Inc which show that the camera was calibrated and accurate.

2.3.3 Experimental Setup

The setup used for fluorescence detection was simple and straight forward. The light from the LED was collimated onto the imaging surface at a small angle so that it does not

obstruct the camera's imaging path. The distance between the LED and the imaging surface was about 10cm. The emitted fluorescence was detected by the camera placed at 27cm from the imaging surface. The camera was equipped with a tunable filter cube which could pass desired range of wavelengths and stop unwanted wavelengths. A camera Lens was also attached in front of the camera to focus the camera onto the imaging surface. The complete setup of the camera based model used for all the experiments is shown in the Figure 2.5.

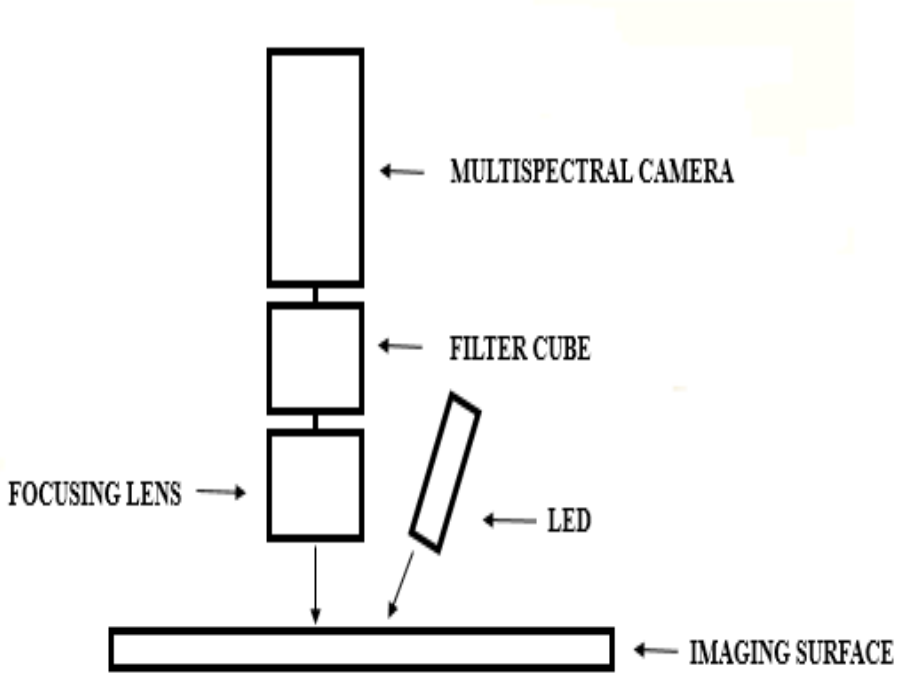

Figure 2.5: Block Diagram of Camera Based Model Setup

A screen shot of Multispectral Imaging software used to capture images in all these experiments is shown in the Figure 2.6

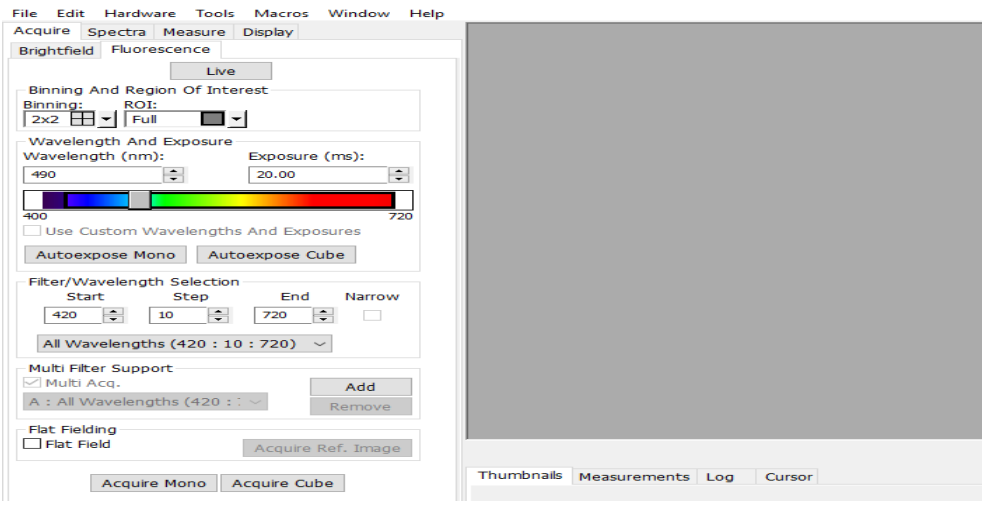

Figure 2.6: Multispectral Imaging software

2.4 Phantom Experiment

In this section the phantom experiment conducted using the camera based model will be explained in detail.

2.4.1 Experimental Procedure

The phantom experiment was done to test the linearity of NADH and FAD using the camera based model with increasing concentration. Four concentrations of NADH and FAD were made and placed in a 96 well palette, the LED at 365nm was illuminated on the four wells having different concentrations to excite NADH and FAD. Initially the reflectance at 365nm was taken to eliminate the effects of improper illumination and then the emission spectra was captured. The fluorescence was corrected for reflectance, image processing was performed and finally a linearity curve was plotted. The setup used to perform all the experiments in shown in the Figure 2.7

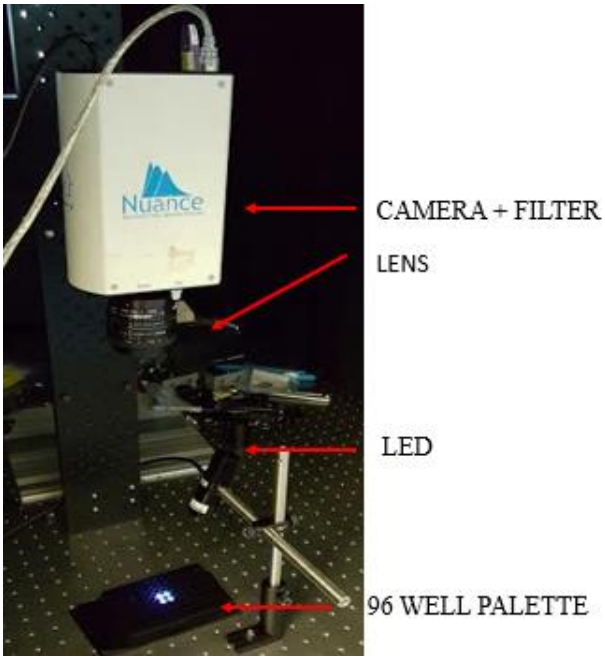

Figure 2.7: Setup

2.4.2 Phantom Preparation

Phantoms were prepared using the powdered form of NADH and FAD from Sigma Aldrich Inc. The part number for NADH is N8129 and the part number of FAD is F6625. Four concentrations of NADH solution at 0uM, 70uM, 140uM, 280Um and FAD at 0uM, 40uM, 80uM, 160Um were prepared and placed in placed in a 96 well palette and imaging was done. Solution and molecular weights of components used is shown in Table 2.5

The solution of desired Molarity was prepared per the formula shown below

$$\text{MOLARITY} = \frac{\text{MOLES OF SOLUTE}}{\text{LITERS OF SOLUTION}} \tag{2.1}$$

$$\text{MOLES OF SOLUTE} = \frac{\text{WEIGHT}}{\text{MOLECULAR WEIGHTT}} \tag{2.2}$$

Table 2.5: Solution used and Molecular weights

PARAMETER	VALUE
SOLUTION	0.1M HCL
MOLECULAR WEIGHT OF NADH	829.51
MOLECULAR WEIGHT OF FAD	709.40

A stock solution of NADH and FAD in 2.5ml Tris 0.1M HCL solution was prepared and then further diluted to give the required concentrations. The part no of Tris 0.1M HCL is T2319 Sigma Aldrich Inc. NADH of 4.2mM in 2.5 ml of Tris H.C.L was prepared and then further diluted to get lower concentrations. Diluting 5 µL in 295 µL intra-lipid solution (Intra-lipid + Ink) gave a concentration of 70 µM. Similarly, diluting 10 µL, 20 µL in 290 µL and 280 µL intra-lipid solution gave a concentration of 140 µM and 280 µM respectively. Similarly, FAD of 2.4mM in 2.5 ml of Tris H.C.L was prepared and then further diluted to get lower concentrations. Diluting 5 µL in 295 µL intra-lipid solution gave a concentration of 40 µM. Similarly diluting 10 µL and 20 µL in 290 µL and 280 µL intra-lipid solution gave a concentration of 80uM and 160 µM respectively.

The optical properties of Intra-lipid are shown in the Table 2.6.

Table 2.6: Optical properties of Intra-lipid

COEFFICIENT	VALUE (cm-1)
REDUCED SCATTERING	10
ABSORPTION	0.1

2.4.3 Experiment

The camera based model is setup as described in the section 2.3.3 . Initially four concentrations of NADH were placed in 96 well palette to form a square structure so that the light from LED can evenly illuminate all the four concentrations. For NADH reflectance the images were taken in 2x2 binning (Combining adjacent pixels in an image), fluorescence mode with an acquisition time of five seconds. Similarly, FAD fluorescence images were taken in 2x2 binning with an acquisition time of two and a half seconds. The results are shown in Figures 2.8-2.11

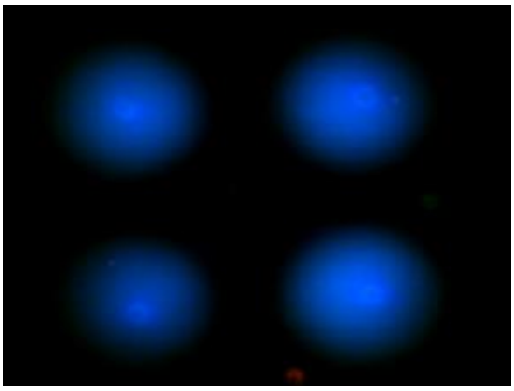

Figure 2.8 : Reflectance of FAD

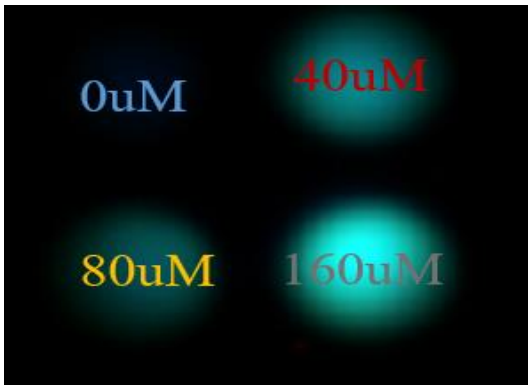

Figure 2.9 : Different concentrations of FAD

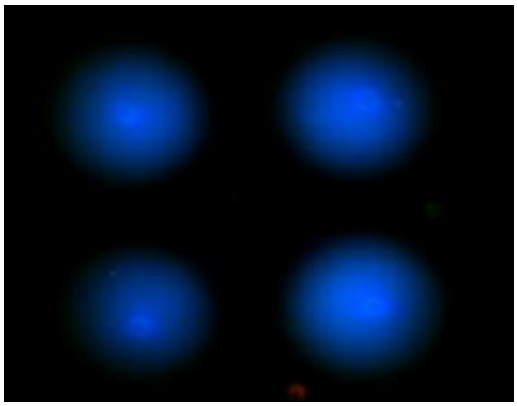

Figure 2.10 : NADH Reflectance

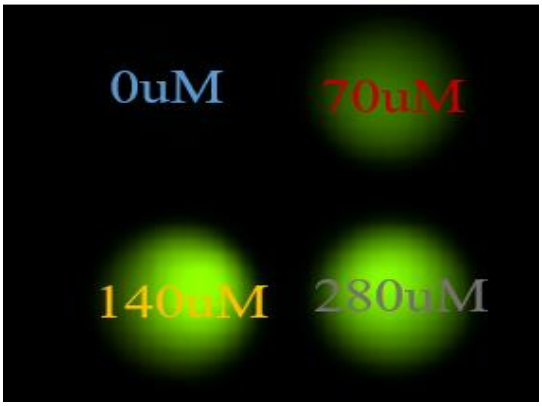

Figure 2.11 : Different concentrations of NADH

The spectrum of these images is shown in the Figures 2.12,2.13

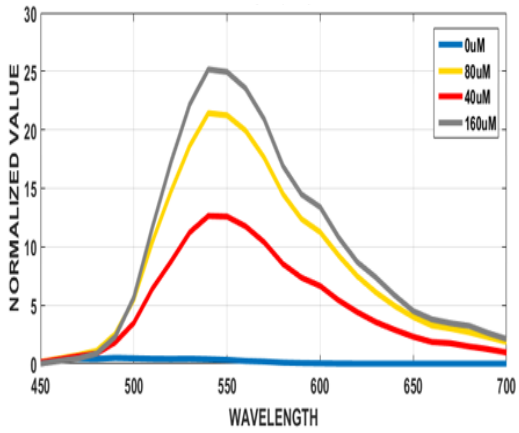

Figure 2.12 : FAD spectrum

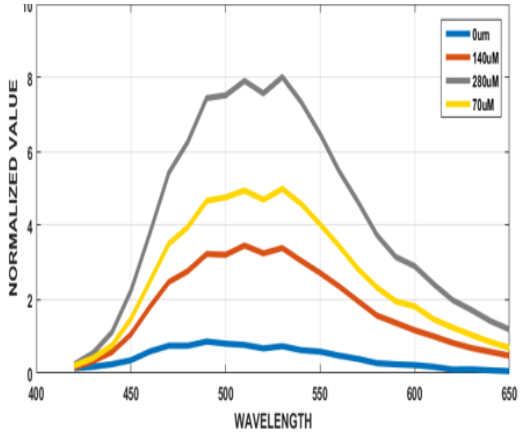

Figure 2.13 : NADH spectrum

After acquisition, images are saved in .im3 file format. The images in .in3 format can be opened by using the Multispectral imaging software only. The software also gives the provision to select and portion of an image and visualize the spectrum of the selected portion. This can be exported to Xcel and then MATLAB was used to perform data analysis. It is also possible to extract a channel from the .im3 cube and save as .TIFF or .JPEG image and perform image processing on it. For this experiment the channels at which NADH and FAD gave peak were extracted and image processing was performed.

2.4.4 Image Processing

As mentioned in the previous section the peak channels were and processing was performed on them. The following steps were done to perform image analysis. Initially the reflectance image was selected and the four different concentrations were separated. The same procedure was done to NADH and FAD fluorescence images. Next the reflectance

image was divided with its corresponding fluorescence image for correction purposes. Next the random pixel created by division (misalignment of the image) were removed. Results are shown in the Figures 2.14,2.15

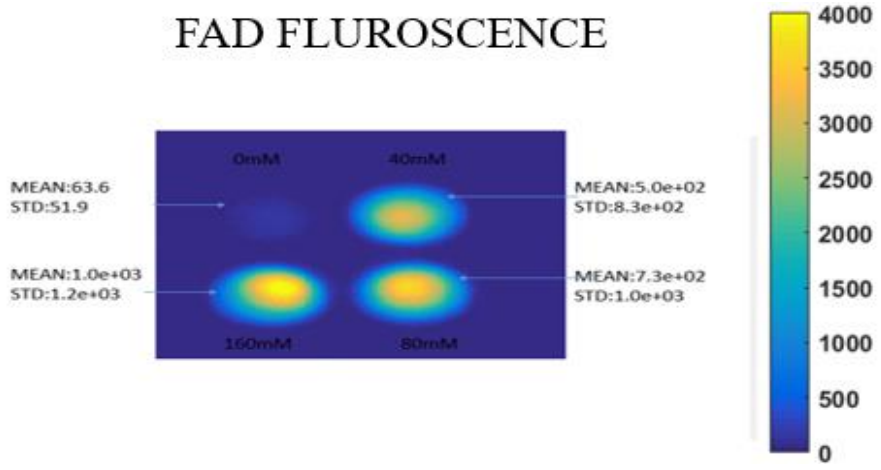

Figure 2.14: FAD image after image processing

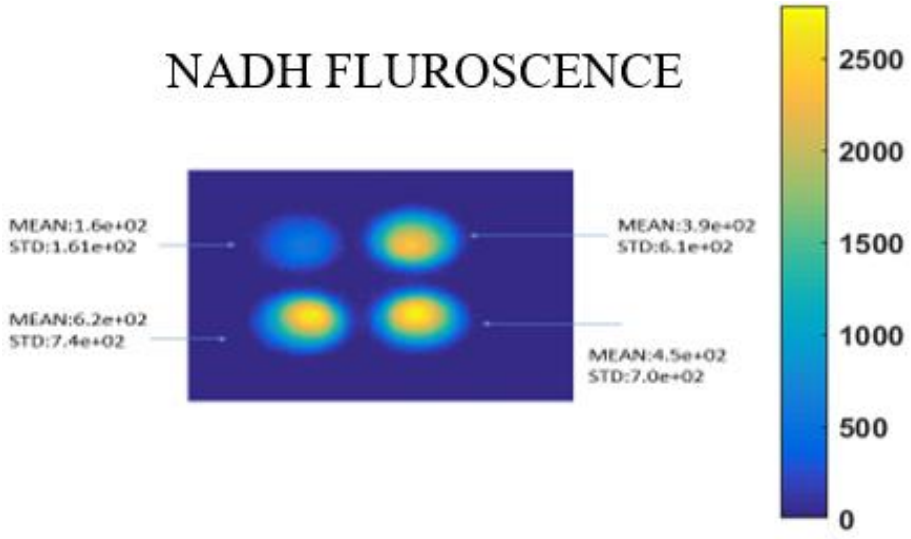

Figure 2.15: NADH image after image processing

Finally, the mean of each concentration was taken and linearity curve was plotted. The linearity curves for NADH and FAD fluorescence is shown in the Figures 2.16,2.17

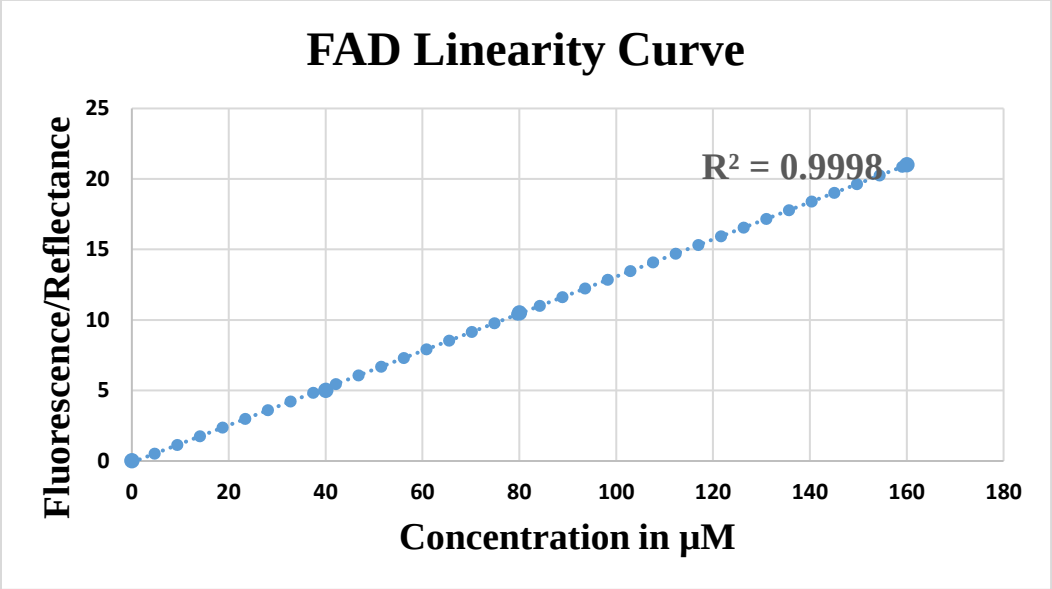

Figure 2.16: FAD linearity curve

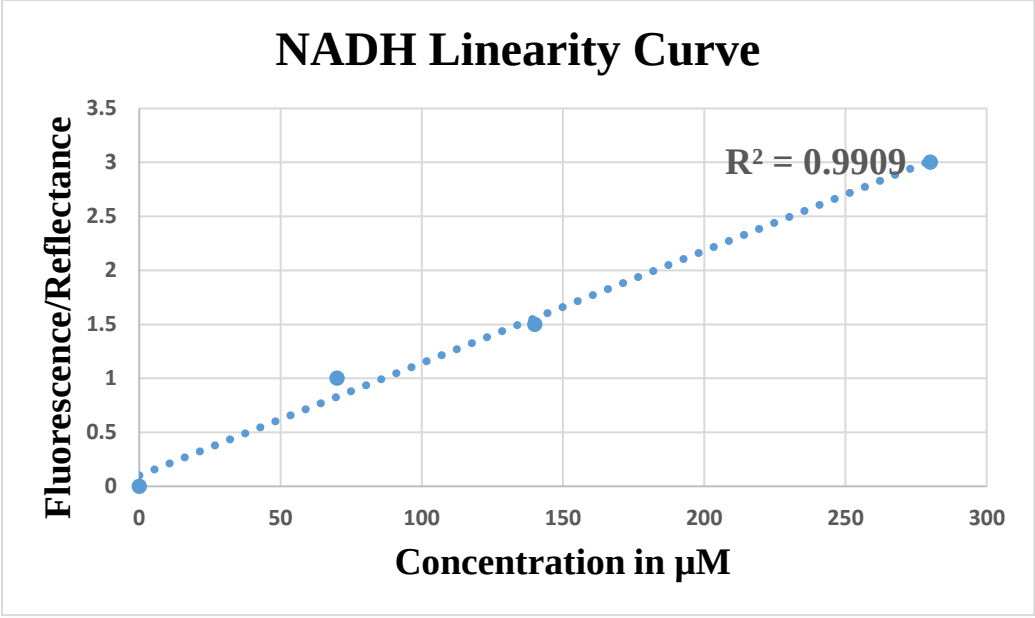

Figure 2.17: NADH linearity curve

2.5 Ex-Vivo Experiments

In this section the experiments performed ex-vivo on mice placenta and cancer cells will be discussed.

2.5.1 Measurement 0f FAD in Placenta

In this experiment, mice placentas were used to detect FAD fluorescence. The setup used in the experiment is like setup shown in Figure with an excitation light of 450nm.

Experiment was performed on three placentas numbered 7-9 which is showed in the Figure 2.18.

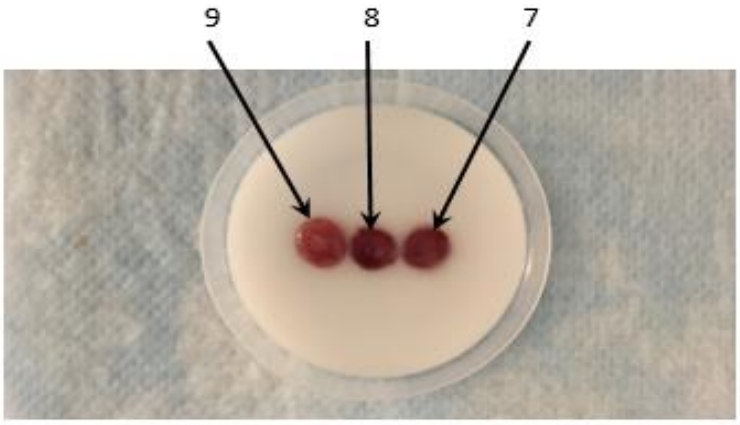

Figure 2.18: Placenta

2.5.1.1 Results

The images were taken at integration time 2 seconds. As the aim of this study was to determine the FAD signal from the sample, peak channel for FAD emission (520nm) and excitation (450nm) were extracted from the image cube and image processing was

performed on it and average of normalized fluorescence in each sample was calculated. The results from the placenta is shown in the Figure 2.19,2.24.

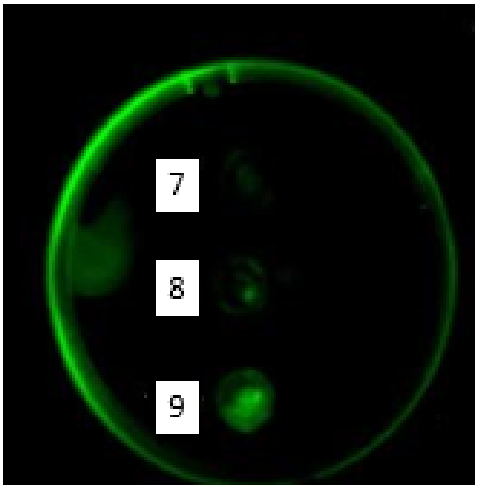

Figure2.19: Image cube

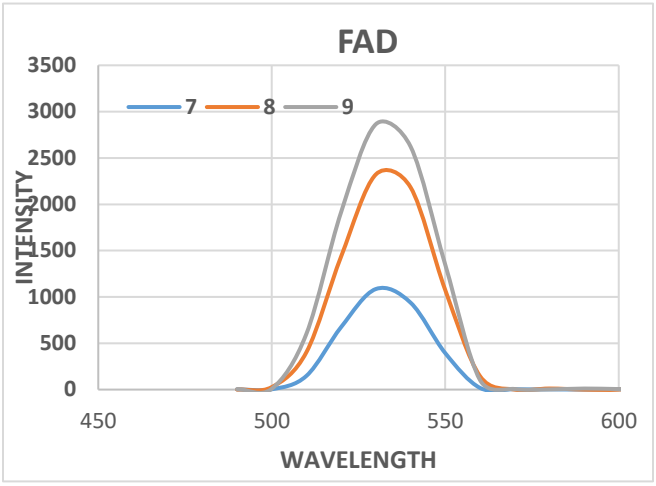

Figure 2.20: Spectrum

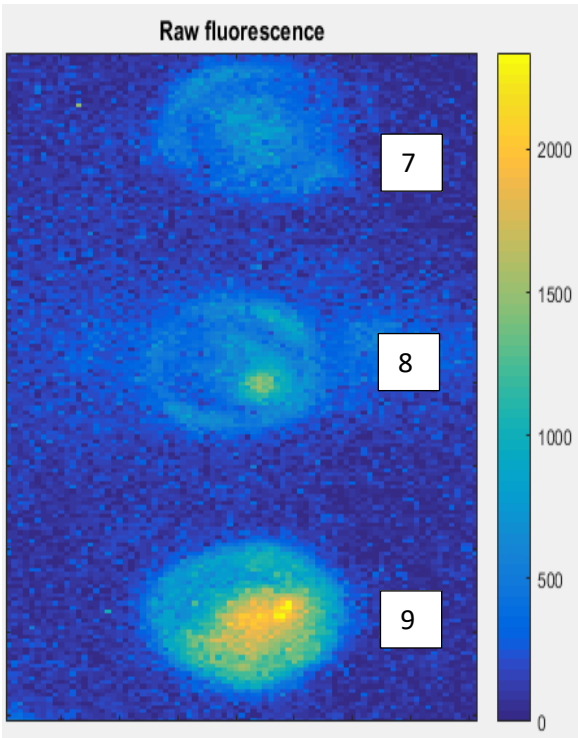

Figure 2.21: Raw fluorescence

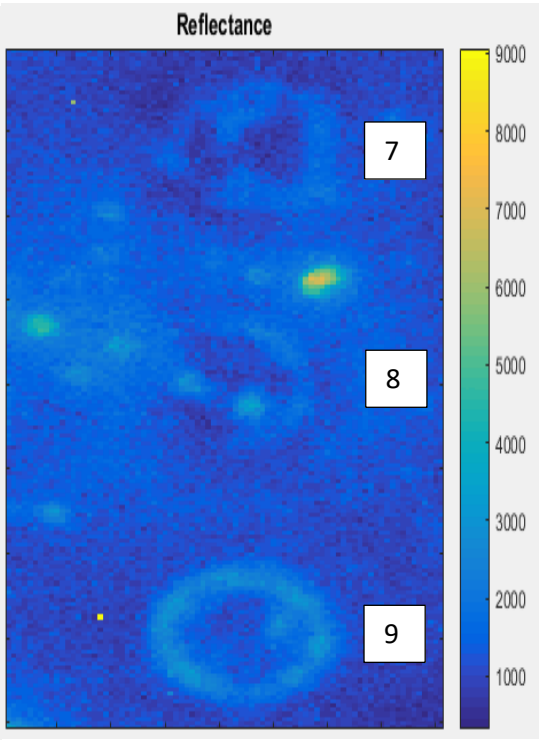

Figure 2.22: Reflectance

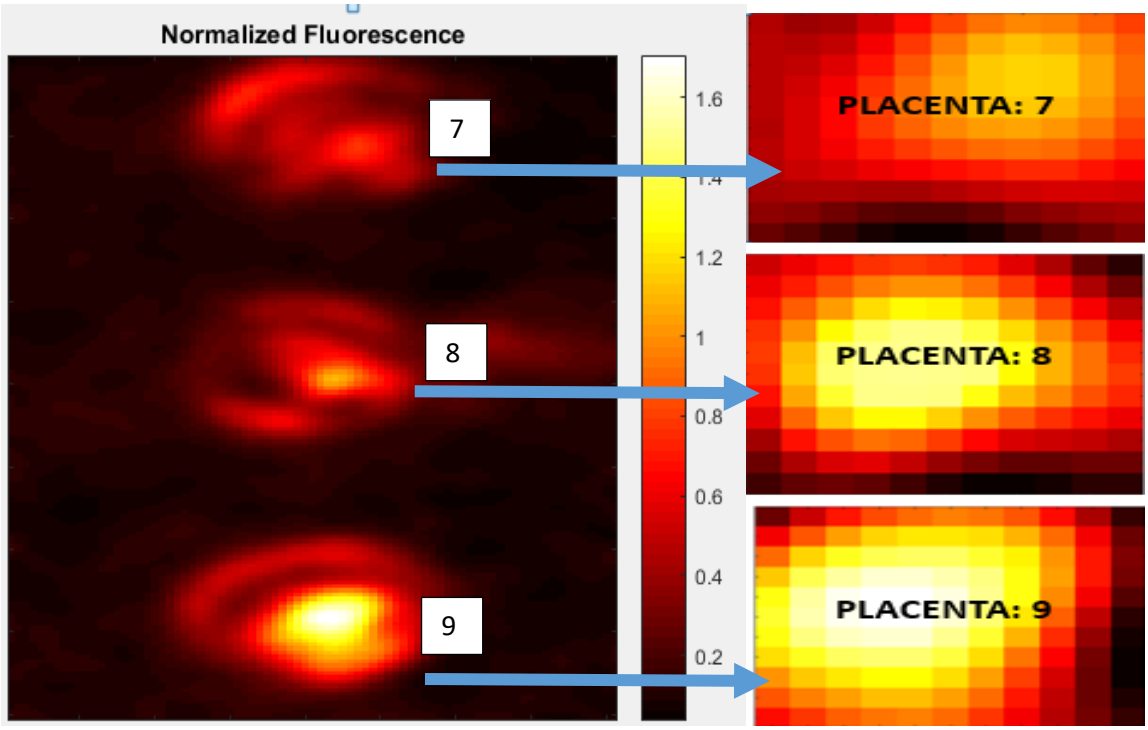

Figure 2.23: Normalized fluorescence

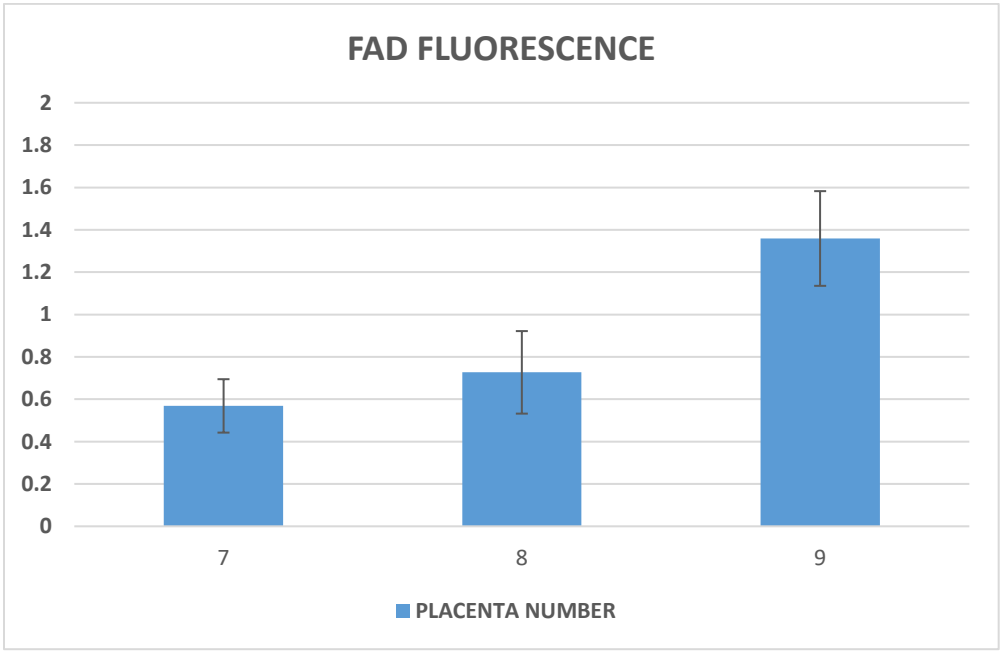

Figure 2.24: Normalized fluorescence for each placenta

From the resultant data, placenta number 9 had maximum fluorescence and that is since it has less blood comparatively to placenta 7 and 8. Presence of blood increases reduces fluorescence intensity. Whereas the fluorescence intensity from placenta 7 and 8 are close to each other. This also shows that using a single fluorescence intensity as results may be misleading and redox ratio is a better and accurate parameter.

2.5.2 Brain Cancer Cells

In this experiment cancer cells from brain were used to obtain the FAD redox ratio which is defined as the ratio of FAD concentration to the summation of NADH and FAD concentration. The setup used in the experiment is like setup shown in Figure with an excitation light of 365nm. Brain cancer cells is shown in the Figure 2.25

Figure 2.25: Cancer cells

2.5.2.1 Results

The images were taken at integration time 2 seconds. As the aim of this study was to determine the FAD redox ratio, peak channel for FAD (520nm), NADH (460nm) emission

and excitation (410nm) were extracted from the image cube and image processing was performed on it and average of redox ratio from the cancer cells was calculated. The results from brain cells is shown in the Figure 2.26-2.30.

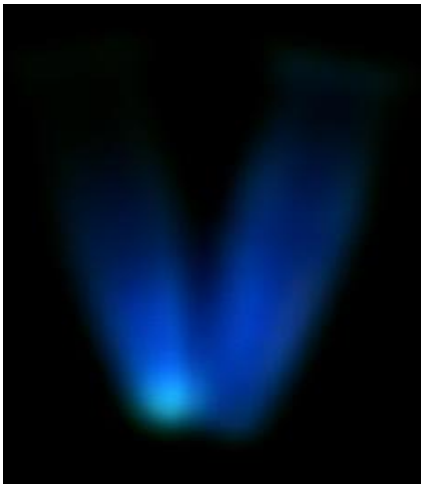

Figure 2.26: Image cube

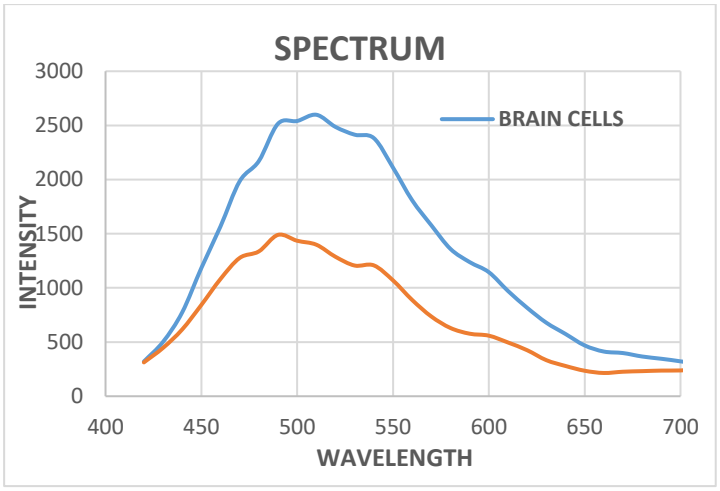

Figure 2.27: Spectrum-Cancer Cells

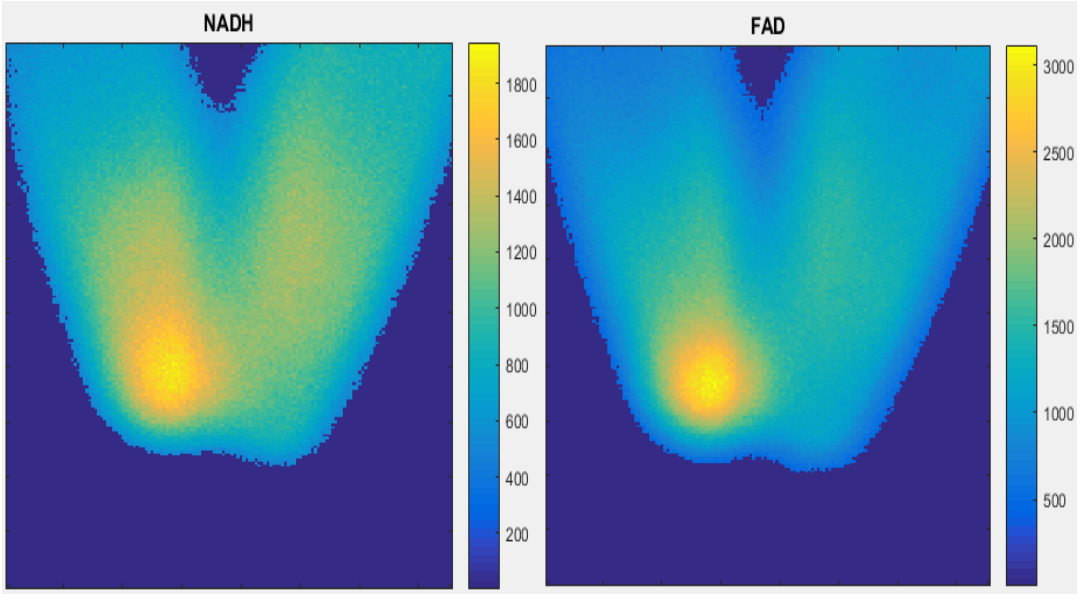

Figure 2.28: NADH-460nm

Figure 2.29: FAD-520nm

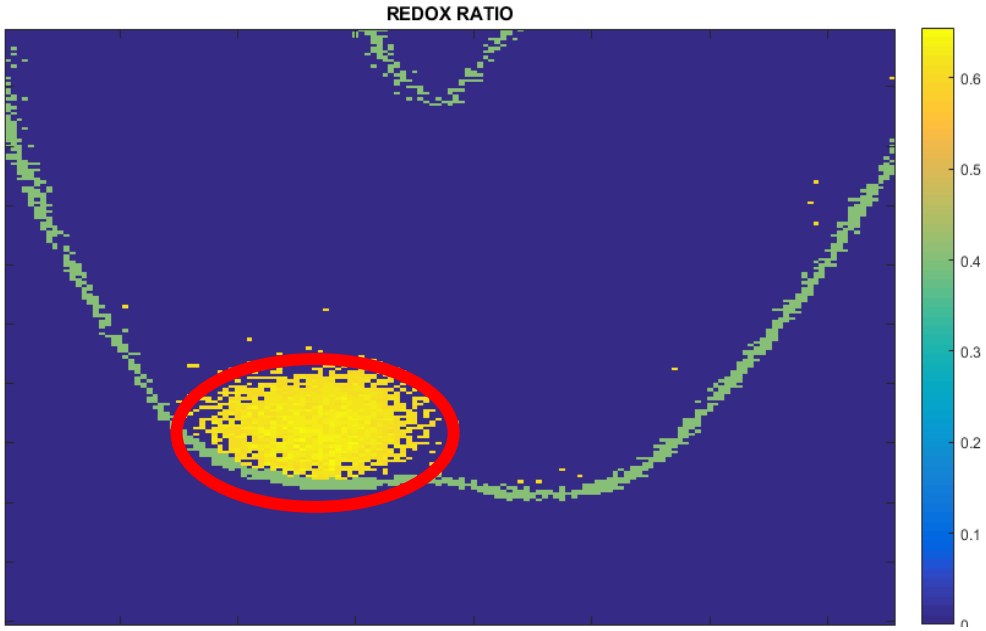

Figure 2.30: Redox Ratio-Cancer Cells

Table 2.7: Mean and standard deviation of redox ratio – Cancer cells

REDOX RATIO	VALUE
MEAN	0.6297
STD	0.0016

The obtained redox ratio is close to the literature value [132].

2.5.3 Brain Normal Cells

Similar steps were performed for normal cells as described in section 2.52. Initially Image cube was captures, peak emission of NADH and FAD was extracted from the image cube,

image processing was performed on the extracted images and finally FAD redox ratio was calculated. The results obtained are shown in the Figure

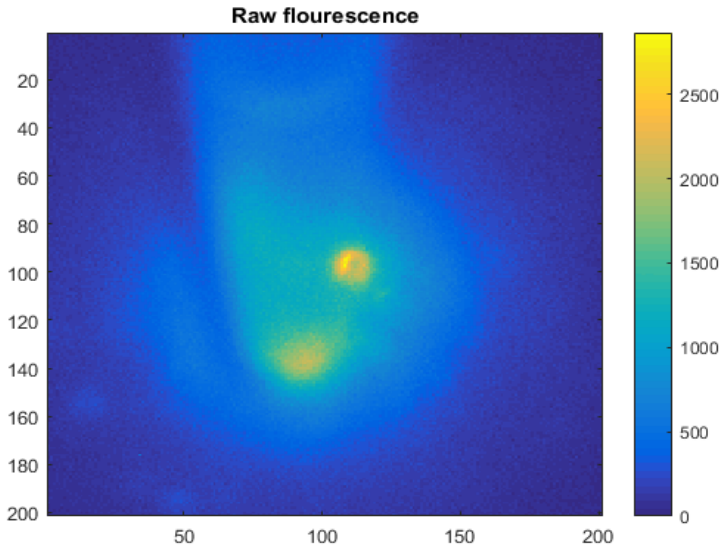

Figure 2.31: Normal cells

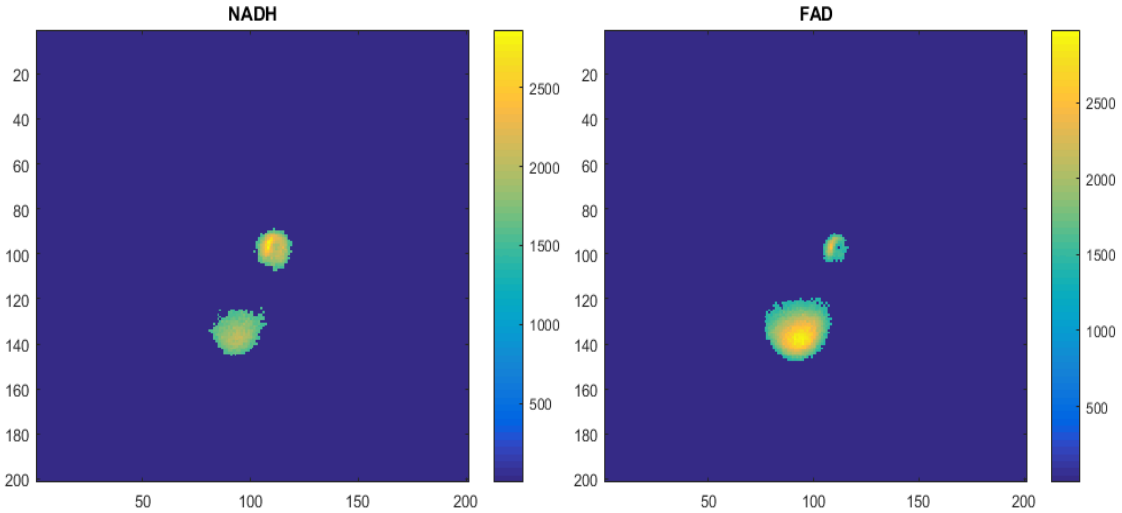

Figure 2.32: NADH-460nm

Figure 2.33: FAD-520nm

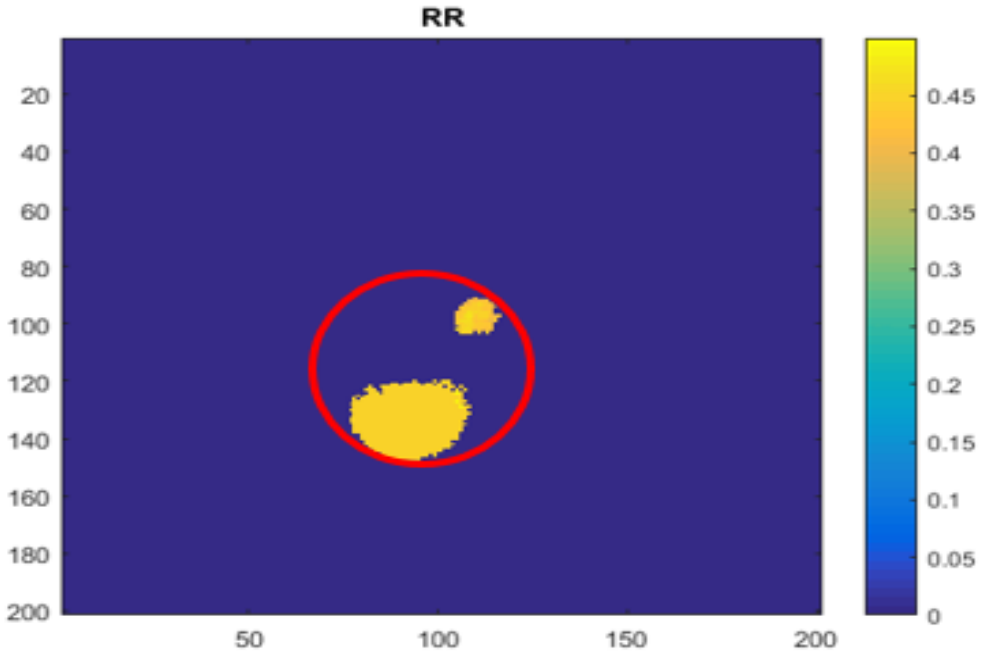

Figure 2.34: Redox Ratio-Normal cells

Table 2.8: Mean and standard deviation of redox ratio – Normal cells

REDOX RATIO	VALUE
MEAN	0.4414
STD	0.0019

The obtained redox ratio is close to the literature value [132].

2.5.4 Comparison of Normal and Cancer Redox Ratio

This section gives a comparison of redox ratio in cancer cells when compared to normal cells. Table 2.8 gives a comparison of redox ratio in both normal and cancer cells.

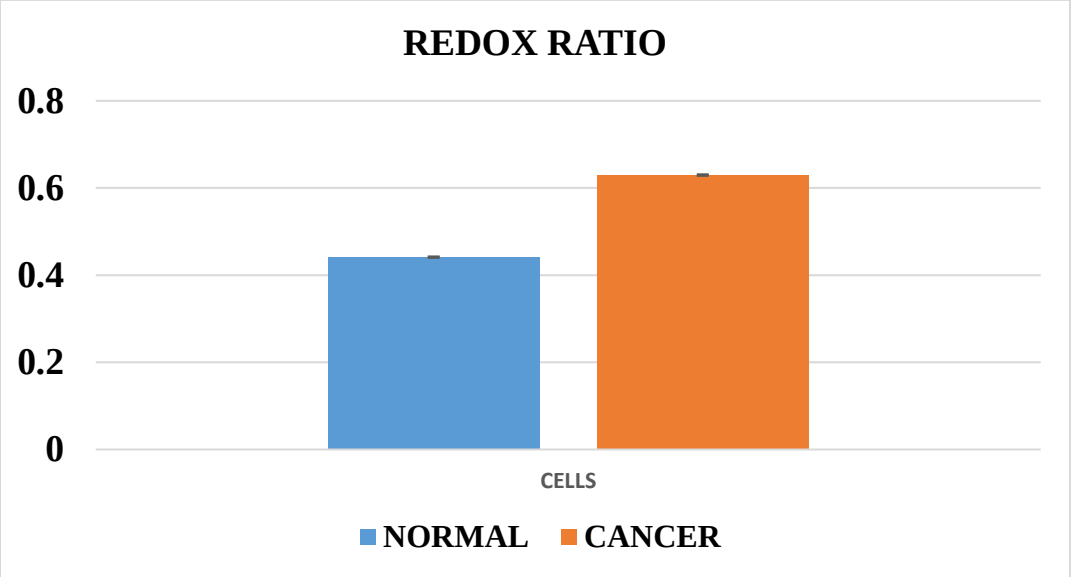

Figure 2.35: Mean and standard deviation of redox ratio – Both cells

Table 2.8: Mean and standard deviation of redox ratio – Both cells

REDOX RATIO	NORMAL VALUE	CANCER VALUE
MEAN	0.4414	0.6297
STD	0.0019	0.0016

The obtained redox ratio is close to the literature value [132].

2.6 CONCLUSION

The camera based model is accurate, linear and can also detect low concentration value of fluorophore. It provides an image of measurements which could be useful differentiate the

diseased area in a normal tissue. The limitations of this model are that the setup is expensive, occupied space and wired. To overcome these limitations a compact and wireless model was designed which would be explained in the next chapter.

Instrumentation and Results of Compact Model

3.1 Introduction

As a metabolometer has the capability of detecting a number medical disorders, making a compact, wireless and inexpensive device could serve several advantages. This chapter the instrumentation of the compact and wireless fluorescence model will be discussed. The aim was to make the device compact and low cost. The various parts used and the reason for their selection will also be mentioned in this chapter.

Some previous works have been done to make the device compact. Chance et al made a miniature Fluorescent Metabolometer to detect the fluorescence intensities and display them on a LCD screen [145]. This model was compact but did not use any wireless operation. Kornilin et al used a compact model to detect the auto fluorescence model from the skin [146]. Another fluorescence detection model was built of a size of a pill which could detect bleeding in the stomach [147].

3.1.1 Significance of Compact and Wireless Model

Mentioned in this section is the significance of the designed device over other instruments.

3.1.1.1Compact and Light Weight

There are several advantages of having a compact device. The first one being, it could be moved anywhere without the need of the patient to come to a specific location, like in most of medical diagnoses. This could be very advantageous in cases of old, weak and patients with mental disorders. Having compact and low weight makes a device wearable and could be used to provide continuous monitoring of a person's medical condition and this could be particularly useful in military applications.

3.1.1.2Wireless

Having a wireless device also has several advantages. Having a wired device could limit patient's movement and could attract his/her attention during continuous monitoring [148]. Having wires in hospital environment could also lead tripping hazards [149]. Having wires in a device would increase size and weight of a device [150]. Additionally, making a device wireless and compatible with a mobile device could make the device use friendly and easy to use.

3.1.1.3 Inexpensive Device

Building an inexpensive device could make the cancer detection possible even in underdeveloped countries which do not have sufficient medical technology and equipment's to detect cancer. By building such device there is a possibility that the mortality rate due to cancer in underdeveloped countries could be reduced.

3.2 Instrumentation

In this section, all the electronics used for instrumentation of the small model will be mentioned.

3.2.1 Light Source Unit

As the aim for the compact model was to make the device low cost, Light Emitting Diodes (LED's) were used as the source units for the device. These are usually cheap, compact and are available in number of optical power specifications. The wavelength chosen for the compact model was a 365nm LED from Marktech Optoelectronics Inc. The part number of the LED is 1125-1254-ND. This wavelength was chosen as both NADH and FAD are excited using this and to eliminate the use a second source unit

The specifications of the LED are shown in the Table 3.1

Table 3.1: Specifications of the LED

PARAMETER	**VALUE**
WAVELENGTH	365nm
SUPPLY VOLTAGE	3.5 V
SUPPLY CURRENT	100mA
OPTICAL POWER	54mW

The LED had a high optical power of 54mW at a forward current of 100mA. This optical power is high for in vivo applications and was reduced by reducing the forward current.

The spectrum and V-I characteristics of the LED are shown in Figure 3.1 and Figure 3.2.

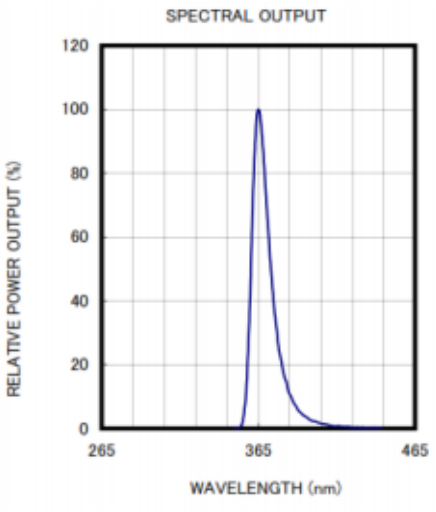

Figure 3.1 : LED spectrum[151]

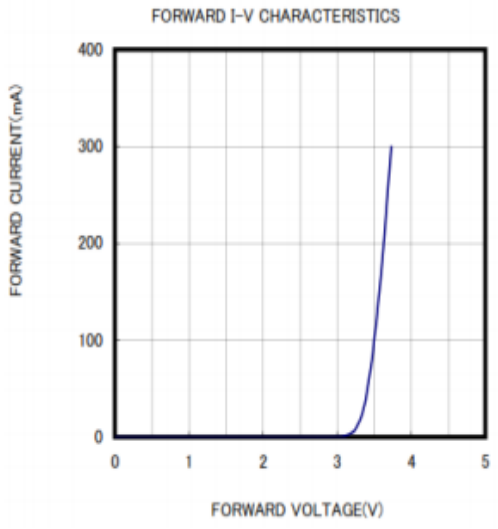

Figure 3.2 : V-I characteristics [151]

3.2.1.1 LED Driver

The LED driver used in this model is a constant current source. This is used to prevent the fluctuations in current or voltage effect on the optical power illuminated form the LED. This is important as fluctuations in the LED's optical power can vary the fluorescence emitted by the fluorophore which may lead to false diagnosis. To avoid these problems a constant current source is used as a LED driver. This is constructed using a LM 317 I.C chip from Texas Instruments. This is a voltage regulator and upon circuit design, this can be converted to a constant current source where the output current depending upon the load resistor. By using this I.C chip, LED would give a constant output irrespective of changes in input voltage or current. While designing this constant current driver, it is important to keep in mind that the power supply used in the circuit should be at least 2.5V greater than

the forward voltage of the LED for its proper operation. The circuit used for the constant current source is shown in the Figure 2.3.

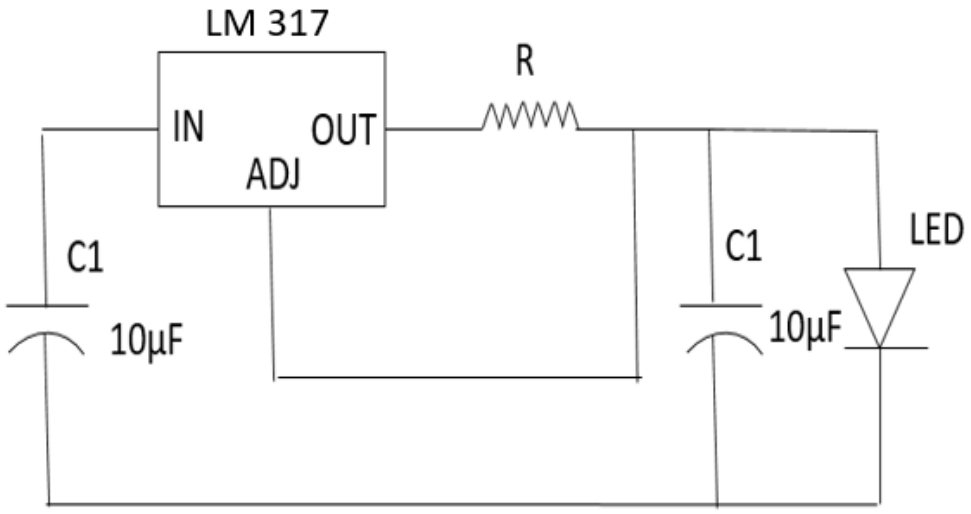

Figure 3.3: Circuit of constant current source

Here the value of resistance R is chosen depending on the following equation

$$\text{I (Current)} = \frac{1.25}{R} \tag{3.1}$$

3.2.1.2 Light Source Unit Testing

The most important testing of the source used for optical applications is its power or stability testing. It is very important for the source to be very stable because variation its power can lead to false positives during diagnosis. The LED stability testing is shown in the Figure 3.4. Results of stability test is given in Table 3.2.

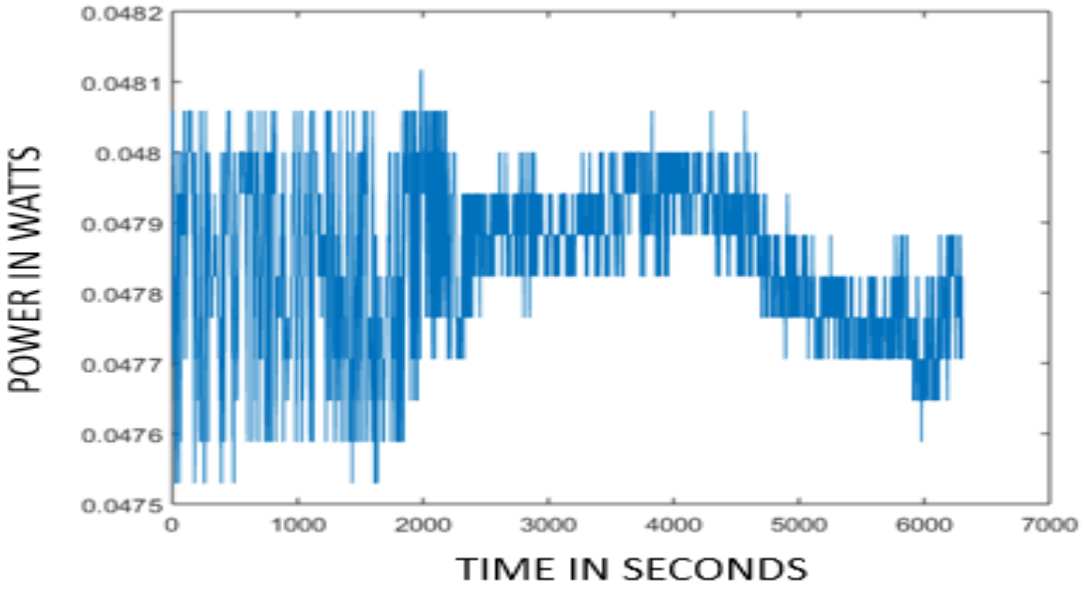

Figure 3.4: Stability test for LED (Compact model)

Table 3.2: Stability test of LED (Compact model)

PARAMETER	VALUE
MEAN	47.85
STANDARD DIVIATION	182nW

3.2.1.3 Switching

The switch was used to turn on and off the LED on receiving the digital inputs from the control unit. Initially Multiplexer was used to turn on and off the LED. The part number of the multiplexer is CD54HC4052. This I.C chip on receiving digital inputs from the control unit passes one of the inputs to the output. The pin diagram of the Multiplexer is shown in the Figure 3.5.

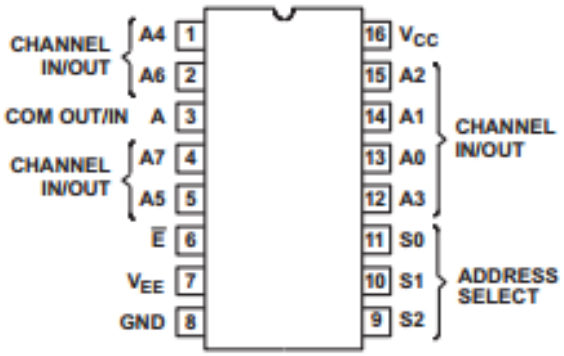

Figure 3.5: Pin configuration of multiplexer [152]

Relation between control signal and the input selection is shown in Table 3.3

Table 3.3: Relation between Control signal and the input selection

S 0	**S1**	**output**
0	0	Input 1
0	1	Input 2
1	0	Input 3
1	1	Input 4

Multiplexer was used as a switch in the following fashion. The supply of the LED was given to one of the inputs of the multiplexer and the other inputs of the multiplexer had no connection. The terminals of the LED were connected at the Multiplexer's output. On providing the control signal (S0,S1) as (0,0) the LED would receive the supply and would turn on. Upon receiving other signals, the supply would be disconnected from the LED and would turn off. The drawback of the multiplexer was that due to its high resistance the

input (constant current) passed onto the output (LED) dropped and LED could not receive required voltage.

To avoid this problem Analog switch from Vishay electronics (Part number: DG 413) was used to switch the LED. These were used as used two single-pole/single-throw (SPST) analog switches. Each Analog switch IC has four individual switches. These switches had a low input resistance thereby causing no voltage drop. Each switch has three pins, one is the input which is the output of constant current source, second is the digital port which was connected to the control unit and third was the output port which was connected to the LED. On receiving high digital signal from the control unit, switch connects the input to the output and upon receiving digital low it is disconnects the output from the input. In this way, LED, can be turned on and off by communicating with the control unit.

The Pin configuration of the Analog switch is shown in the Figure 3.6

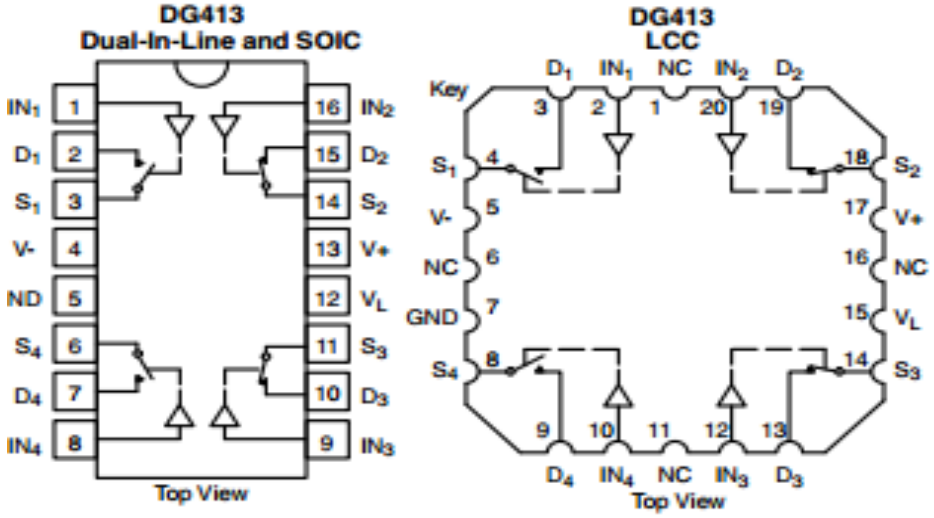

Figure 3.6: Pin configuration of analog switch [153]

Table 3.4: Specifications of the Analog switch

PARAMETER	VALUE
SUPPLY VOLTAGE	Up to 45V
ON RESISTANCE	25 Ohm
SWITCHING TIME	110ns

3.2.2 Detector Source Unit

The detector chosen for the device is OPT 101 from Texas Instruments. It is an 8 pin Dip Packaged I.C chip. The main advantage of this detector is that it has low noise, with good sensitivity in the range of 450nm-800nm which is desirable. It also has a build in amplifier whose gain can be varied by changing the loads resistor values.

The circuit for OPT 101 and its sensitivity is shown in the Figure 3.7,3.8 respectively.

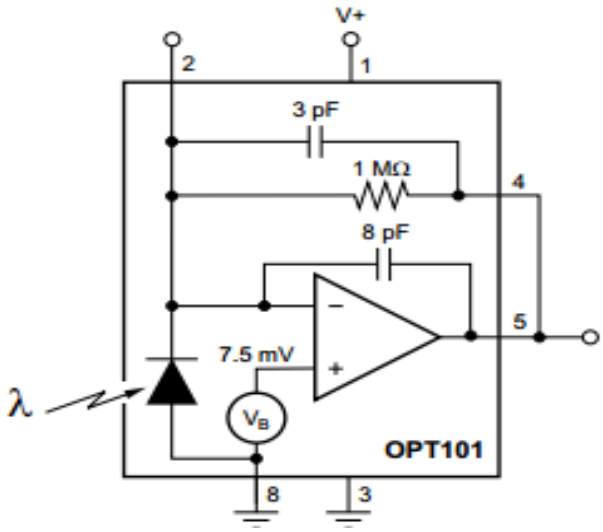

Figure 3.7: Circuit of OPT 101[154]

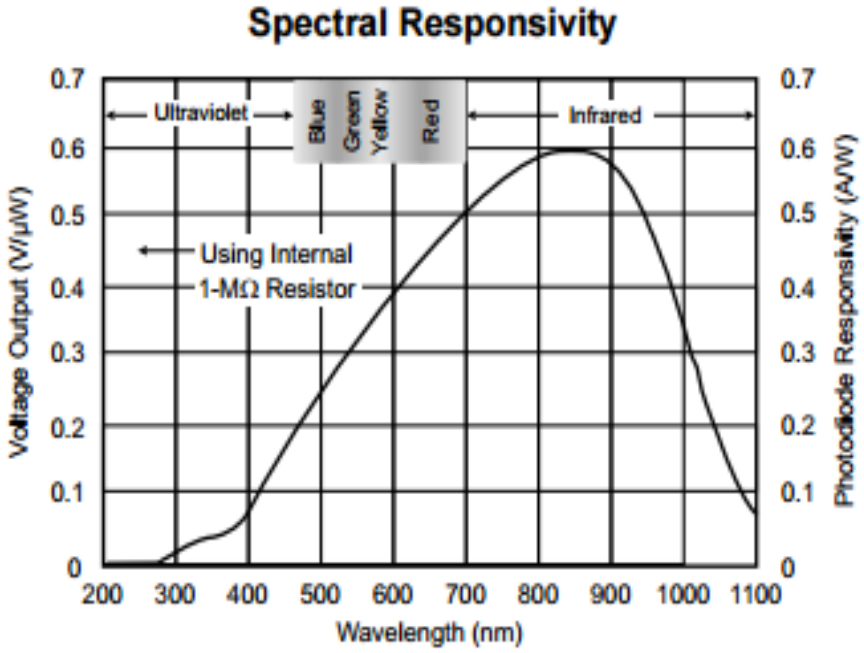

Figure 3.8: Sensitivity curve of OPT 101[154]

The pin configuration of OPT 101 is shown in the Figure 3.9.

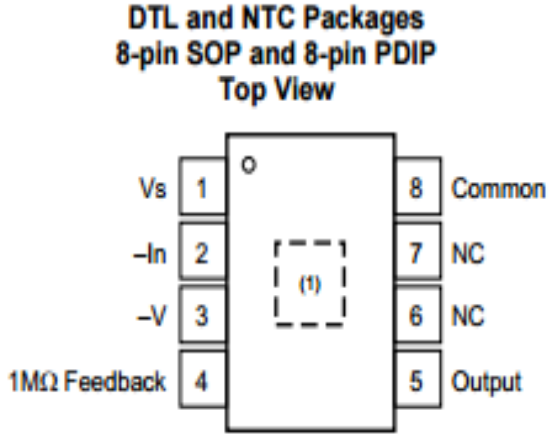

Figure 3.9: Pin configuration of OPT 101[154]

The specifications of the OPT 101 are shown in Table 3.5

Table 3.5: Specifications of Detector-OPT 101

PARAMETER	VALUE
SENSITIVITY AREA	2.2mm x2.2 mm
SENSITIVITY (NADH)	0.4
SENSITIVITY (FAD)	0.22
SUPPLY VOLTAGE (DUAL)	0- +/- 15
MAXIMUM DETECTION	SUPPLY-1.5V

3.2.2.1 Detector Source Unit Testing

The test conducted on the detector to test its sensitivity and stability was the linearity test. In this test the water was taken in a cuvette, LED and detector were placed at right angles that there is a minimal leakage from the light source in the detector unit. The fluorophore used for the linearity test was fluorescein. The excitation wavelength of Fluorophore is anywhere between 360nm-470nm and the emission peak is around 530nm. The fluorescein solution used was taken from amazon. The part number of this product is B00WREOKIU. This solution was taken and the light intensity was measured with no fluorescein, 1 drop, 2 drops and 3 drops of fluorescein. Then the leakage was deducted from the detected signal to give a pure fluorescence signal. To prevent the leakage of light source onto the detector a 500nm long pass filter was used from Thorlabs (Part number: FELH0500)

The setup, fluorescence and the results are shown in the Figures 3.10, 3.11.

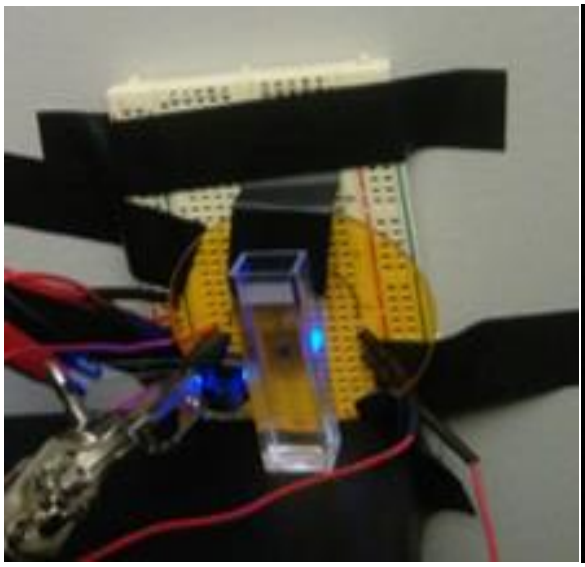

Figure:3.10 Small model setup

Figure 3.11: Fluorescence

The result of linearity test is given in the Table 3.6

Table 3.6: Linearity test (Compact Model)

CONCENTRATION	**INTENSITY**
NO CONCENTRATION	130Mv
1 DROP	620Mv
2 DROP	1170Mv
3 DROP	2260Mv

The Linearity plot is shown in the Figure 3.12

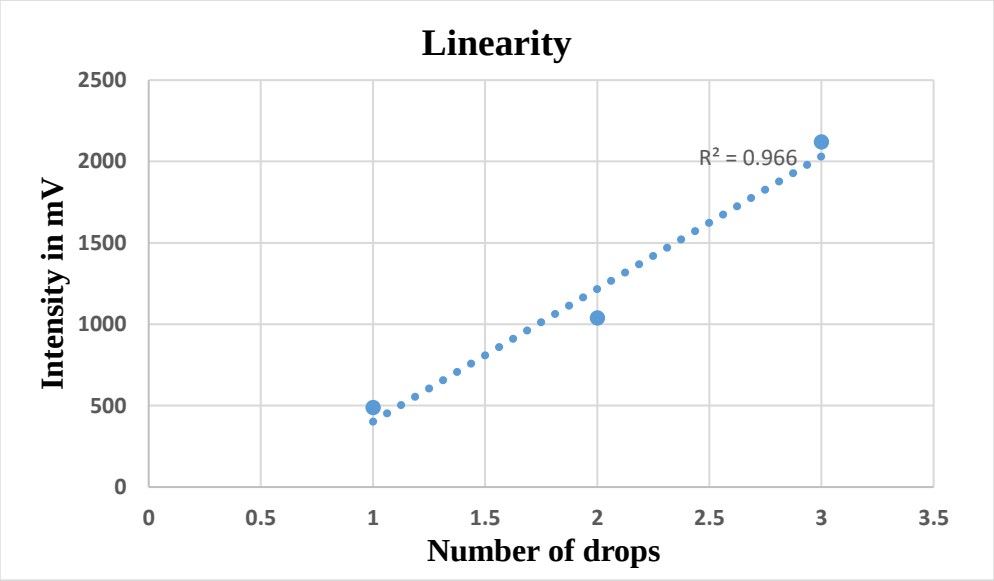

Figure 3.12: The Linearity Plot

3.2.2.2 Amplifier

The detector used in the device could give an amplification of about 1.1 x 10^7. If further amplification was needed, then a post amplifier was used to provide further amplification. The amplifier used in the device was an I.C TL072CP. This I.C chip provided the desired amplification. It was possible to change the amplification provided by the Operational Amplifier (Op-Amp) by slightly varying its circuit components. The pin configuration of the I.C chip used is shown in the Figure.

The block diagram and pin configuration of the Operational amplifier is shown in the Figure 3.13 and 3.14.

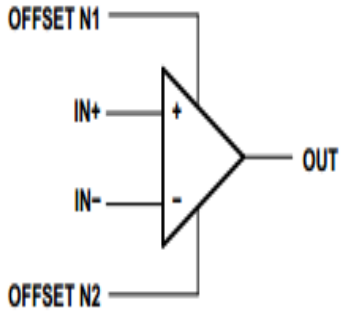

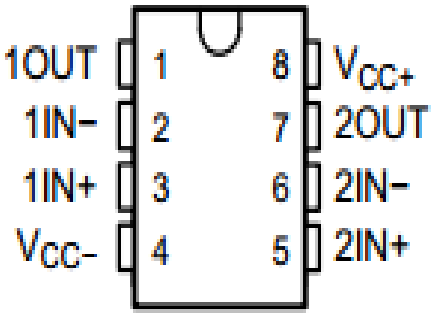

Figure 3.13: Operational Amplifier [155]Figure 3.14: Pin Configuration of Op-Amp[155]

The specifications of the operational amplifier used in the design is shown in the Table 3.7

Table 3.7: Specifications of Operational Amplifier

PARAMETER	VALUE
SUPPLY VOLTAGE (DUAL)	-15 - +15
MAX AMPLIFIED VOLTAGE	+/- SUPPLY
AMPLIFICATION	- Rf/Rin

3.2.2.3 Optical Filters

Filters were used in this setup to separate the signal emitted by NADH and FAD. Gelatin filters form Gam Color were initially used to perform the separation. The part number of the filters used in the device are Gold rush -388(FAD) and Orchid-955(NADH). The pass spectrum of these filters is shown in the Figures 5.13-5.15

The transmission data of Gelatin filters is shown in the Figures 3.15-3.17

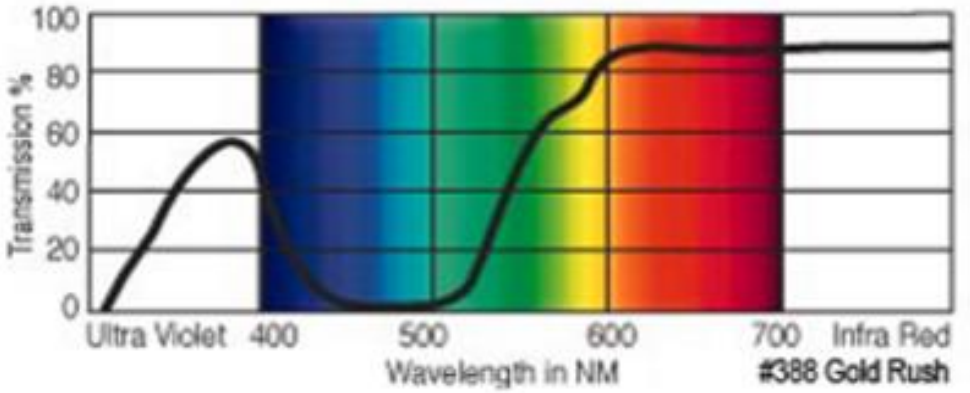

Figure 3.15: Transmission data of Gold rush -388(FAD)[156]

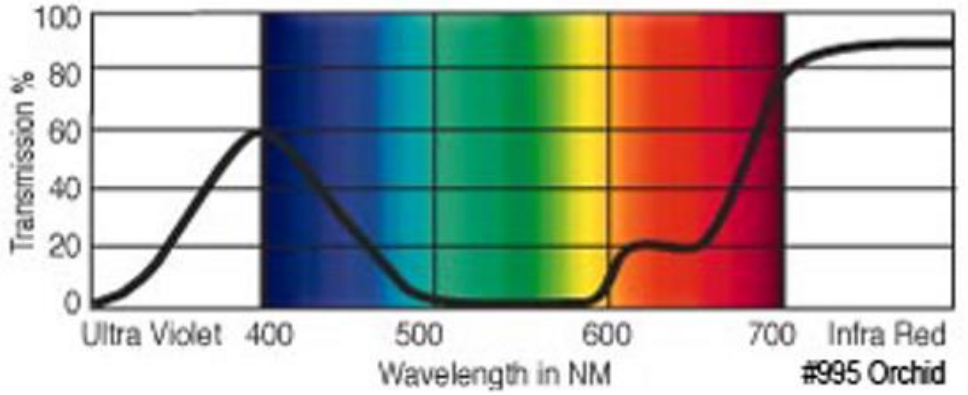

Figure 3.16: Transmission data of Orchid -955(NADH). [156]

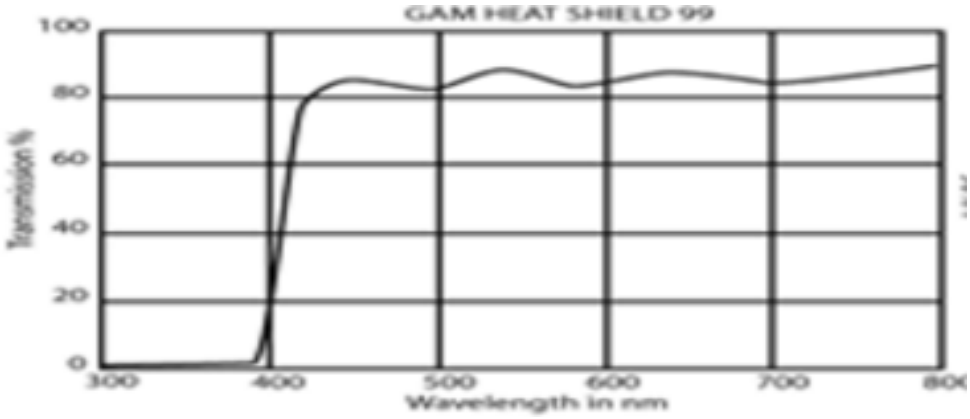

Figure 3.17: Transmission data of Heat Shield [156]

Due to their low efficiency, there were not included in the device as they were not able to efficiently separate the signals (NADH and FAD) and they also included a lot of light from the excitation LED.

To avoid this, glass filters from Edmund optics were used to perform the separation. The diameter of these glass filters was about 11.7mm. One glass filter centered at 460nm was used to pass only the NADH signal to the detector and another filter centered at 520nm was used pass only the FAD signal to the detector. The part number of the filters used are 62-083 (NADH) and 62-095(FAD). To avoid leakage from the source two layers of 400nm long pass gelatin filters were placed on top of glass filters. The part number of this gelatin filter from Gam-color is Heat Shield 99.

The pass spectrum of glass filters and heat shield is shown in the Figures 3.18,3.19.

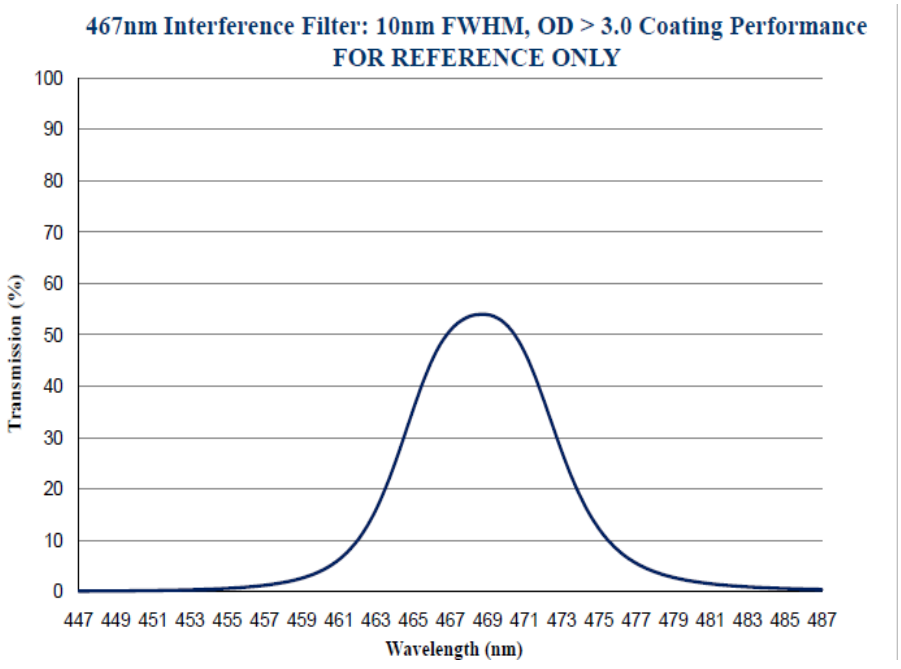

Figure 3.18: Transmission data of 467nm bandpass filter [157]

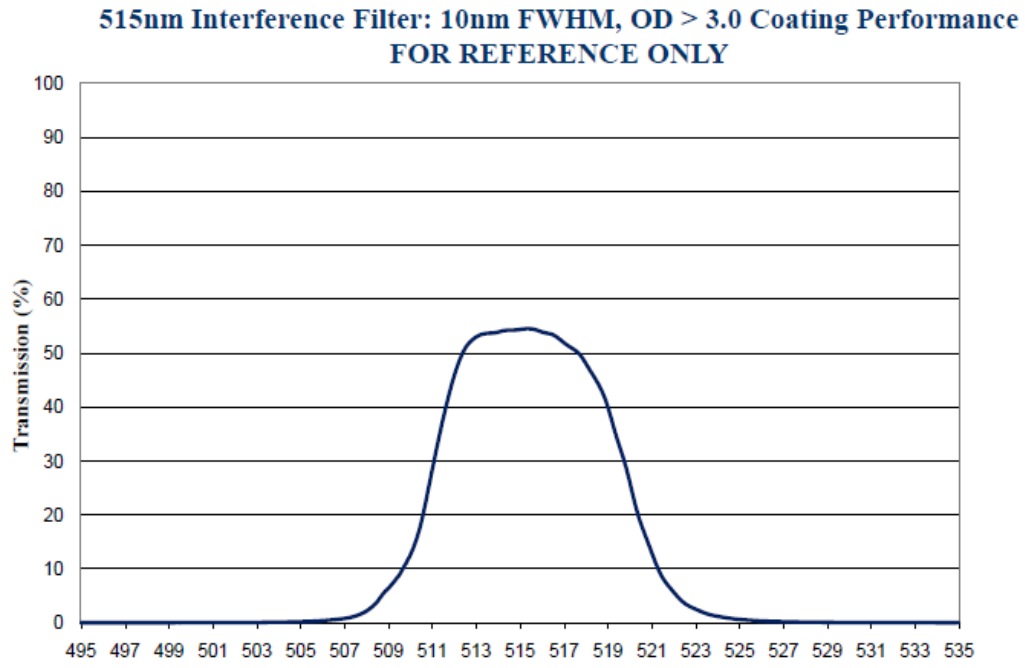

Figure 3.19: Transmission data of 515nm bandpass filter [158]

3.2.3 Control Unit

The control unit used in most of such applications is Data Acquisition Card (DAC) from National Instruments. This is easy to use and has all the functionality of a perfect control unit. The drawback of using a DAC is that it is expensive, has a larger size and would make the device wired which is not desired. So, a microcontroller Atmel-Atmega32P (Arduino) is used in place of a DAC unit. The advantage of using this microcontroller is that it is inexpensive and have a considerable number of analog input, analog output and digital lines sufficient for the application. The specifications of the Microcontroller are shown in the Table 3.8.

Table 3.8: Specifications of the Microcontroller

Microcontroller	**ATmega328P**
Operating Voltage	5V
Input Voltage (recommended)	7-12V
Input Voltage (limit)	6-20V
Digital I/O Pins	14
PWM Digital I/O Pins	6
Analog Input Pins	6
SRAM	2 KB
EEPROM	1 KB
Clock Speed	16 MHz
Length	68.6 mm
Width	53.4 mm
Weight	25 g

To control a microcontroller, a program was written on its software (ARDUINO 1.6.11) and dumped on it. After dumping the code, the microcontroller would perform the desired functionality. It also has transmission and reception ports which can be used for wireless application. Another advantage of using microcontroller is that it has good ADC resolution of about 5mV which is good when compared to the expensive Data Acquisition Card. In addition to that the microcontroller has a regulated 5V and 3.3 V supply which can be used as a power supply to other components in the device.

The Pin configuration of the microcontroller is shown in the Figure 3.20

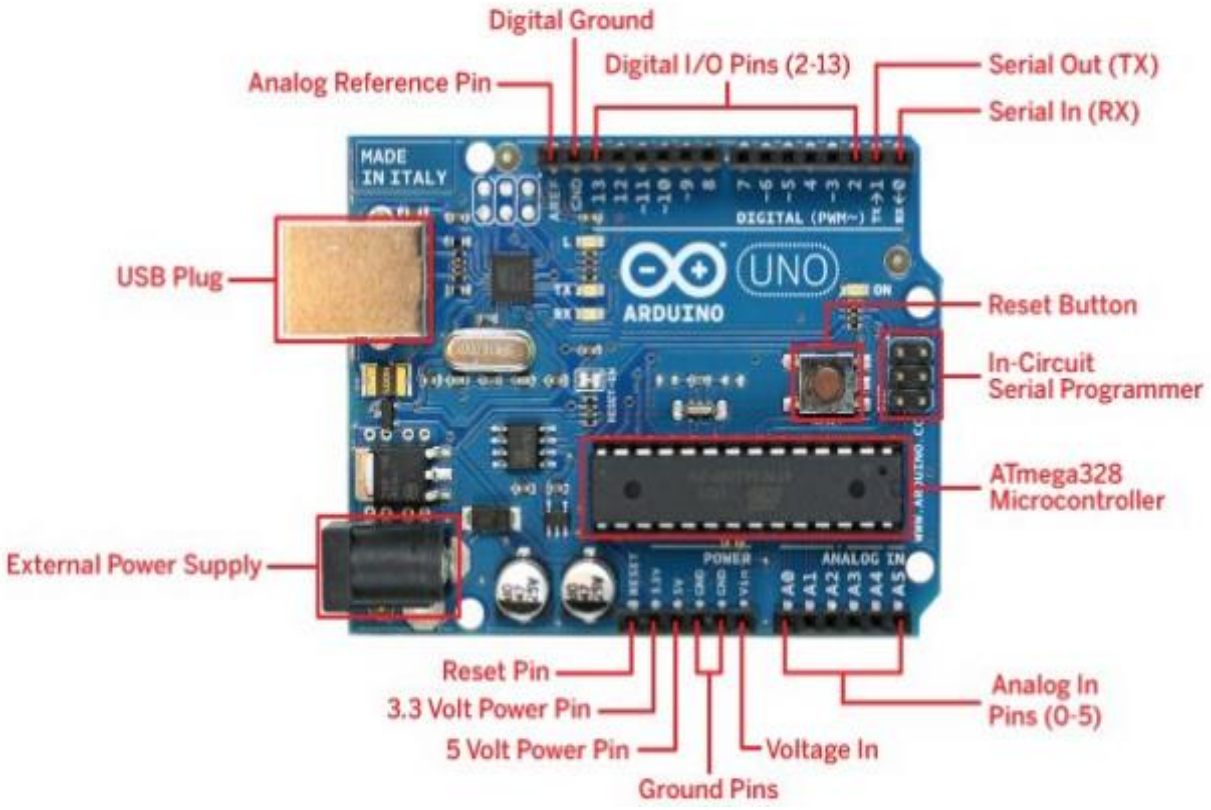

Figure 3.20: Pin configuration of Arduino [159]

3.2.4 Wireless Application

The device was made wireless using a Bluetooth module. The Bluetooth module used in the device is HC-06. This module was chosen for wireless transmission because it is compact and inexpensive. Another advantage of using HC-06 is that it can easily be connected to any device having Bluetooth facility and data can be logged on the PC using a Tera-term serial emulator which is available online for free or an application can be created on android or IOS platform using which two-way communication can be done between the Bluetooth module and a mobile phone. To use the Bluetooth module along

with the microcontroller the program written on the microcontroller had to be modified by including the header files of the Bluetooth module and the way you want wireless communication to take place. The specifications of the HC-06 are shown in the Table 3.9.

Table 3.9: specifications of the HC-06

PARAMETER	**VALUE**
SUPPLY VOLTAGE	3.1-5V
FREQUENCY	2.4GHz
BAUD RATE	9600-38400
SIZE	27mm×13mm×2mm

On using the Bluetooth module with the microcontroller, it was possible to get around 140 digital converted values from a single detector or about 50-70 digital converted values from two detectors which gave sufficient averaging.

The HC-06 is connected to the microcontroller as shown in the Figure 3.21

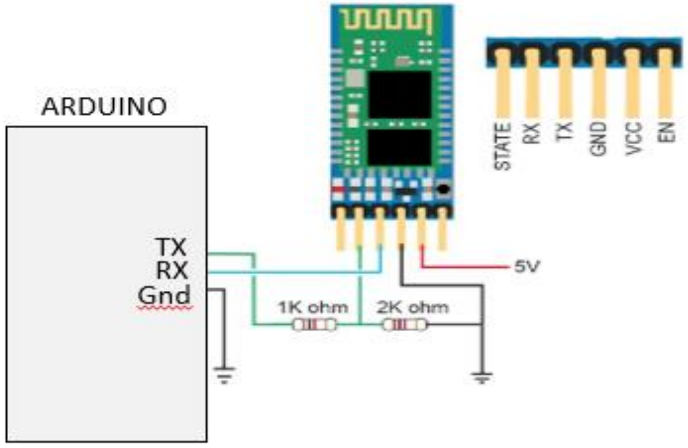

Figure 3.21: Connected of HC-06 with the microcontroller [160]

3.2.5 Power Supply

As the aim was to make the device wireless, wall power supplies were not used to power the device. Instead a couple of Lithium Ion batteries from Adafruit.com (Part number 1317) were used. These Batteries are rechargeable and can be charged to a voltage of 3.7 V. A couple of these batteries were connected in series to give a total voltage of 7.4V which was used as a power supply to the detectors and the microcontroller. Providing a voltage of about +/- 7.4 V DC to the detectors makes a maximum detectable range of the detectors to +/-5V. All the other components in the device were powered using the 5v supply from the Microcontroller. These Lithium Ion batteries were charged using the rechargeable kit from Adafruit.com (Part number 2190).

The Li-ion battery and its charger are shown in Figure 3.22

Figure 3.22: Battery and charger

3.2.6 Display

The following were used to display the values detected by the device.

3.2.6.1 Liquid Crystal Display

Liquid Crystal Display (LCD) was initially used to display the results obtained from the device. The idea was not to use wireless communication and directly display the digital values converted by the microcontroller onto the LCD screen. The LCD screen selected for this was taken from Adafruit.com (Part no: 198) and was 20 X 4 LCD screen. To use the LCD, the program written onto the microcontroller was modified by adding specific details and headers of the LCD screen. Next the way results are to be displayed was also include in the program.

The connection between the LCD and microcontroller is shown in the Figure 3.23

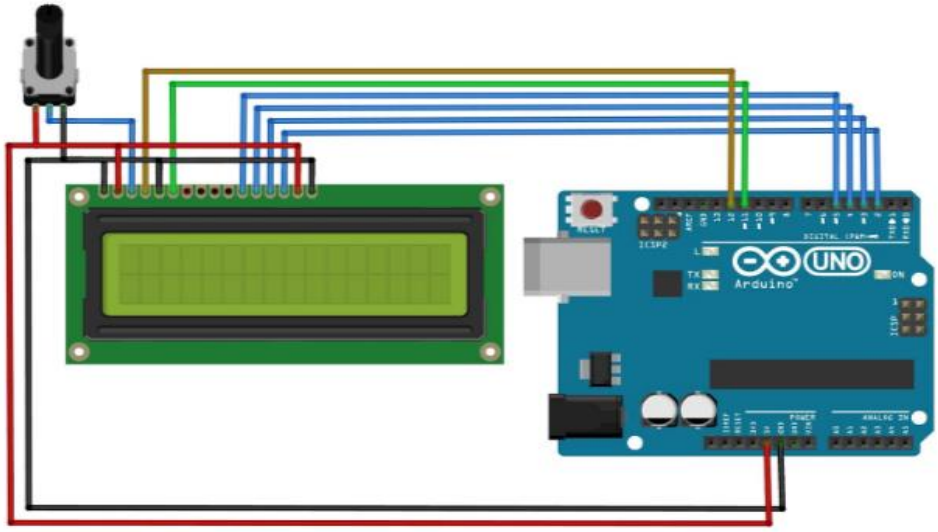

Figure 3.23: Connection between LCD and microcontroller [161]

The results obtained and dis-played on the LCD screen is shown in the Figure 3.24

Figure 3.24: Display on LCD screen

3.2.6.2 Wireless Bluetooth Display

Using a Bluetooth module with the device made possible to connect it to any device having Bluetooth facility.

3.2.6.2.1 Tera-Term

On a personal computer, downloading a Tera-Term terminal made it easy to communicate with the device. It was possible to give instructions to the device and to take results from the device. The panel of Tera-Term emulator is shown in the Figure 3.25.

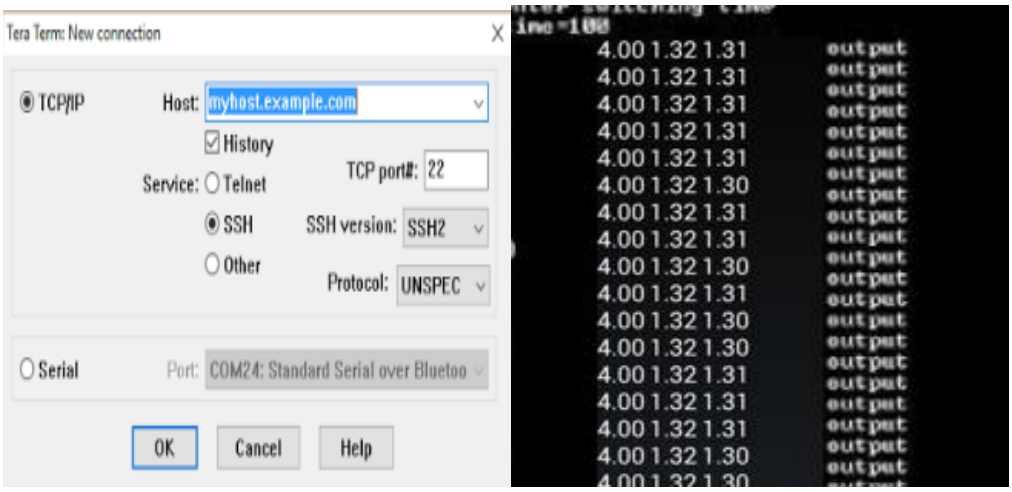

Figure 3.25: Tera Term terminal

3.2.6.2.2 LABVIW

A Lab-view code was also written to get the values form Bluetooth and display the real-time values. The front panel of the Lab-view code is shown in the Figure 3.26

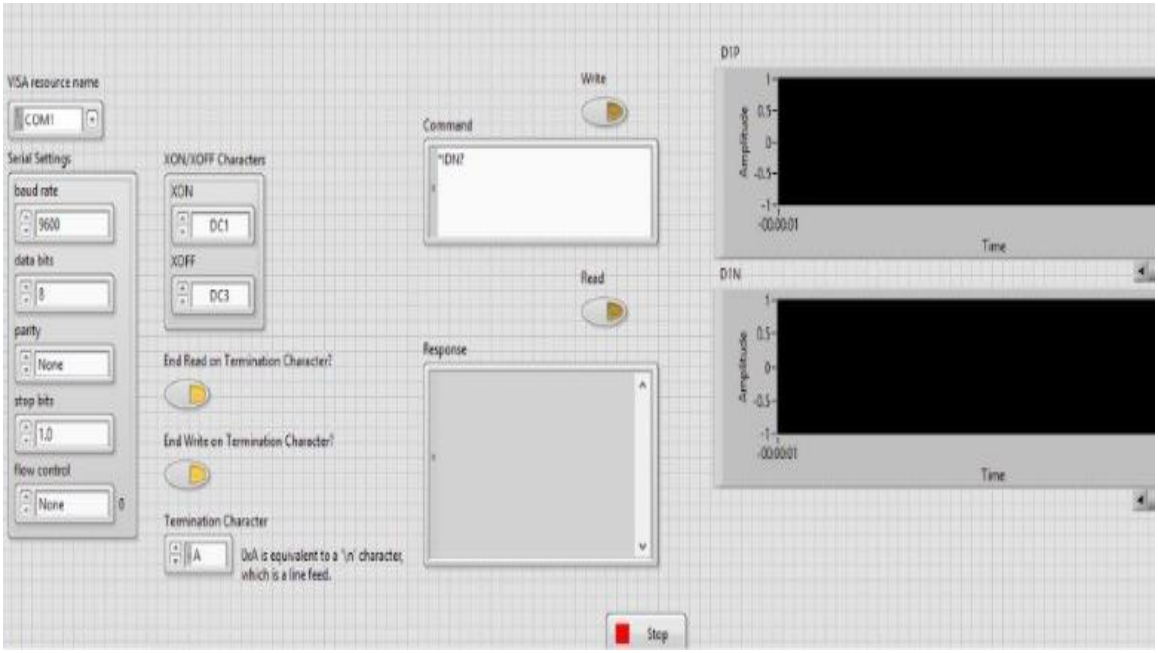

Figure 3.26: Lab-view front panel

3.2.6.2.3 Mobile Application

As the device, could send the data wirelessly to any device having Bluetooth, a mobile application on Android platform was used to avoid the usage of P.C, give commands and record the measurements on a mobile phone. The mobile application was user friendly and the user only had to decide the acquisition time and the detected data would be saved as a text file on the mobile phone indicating the results. The mobile application used is the Bluetooth serial controller available on Android platform for free. The panel of this application is shown in the Figure 3.27

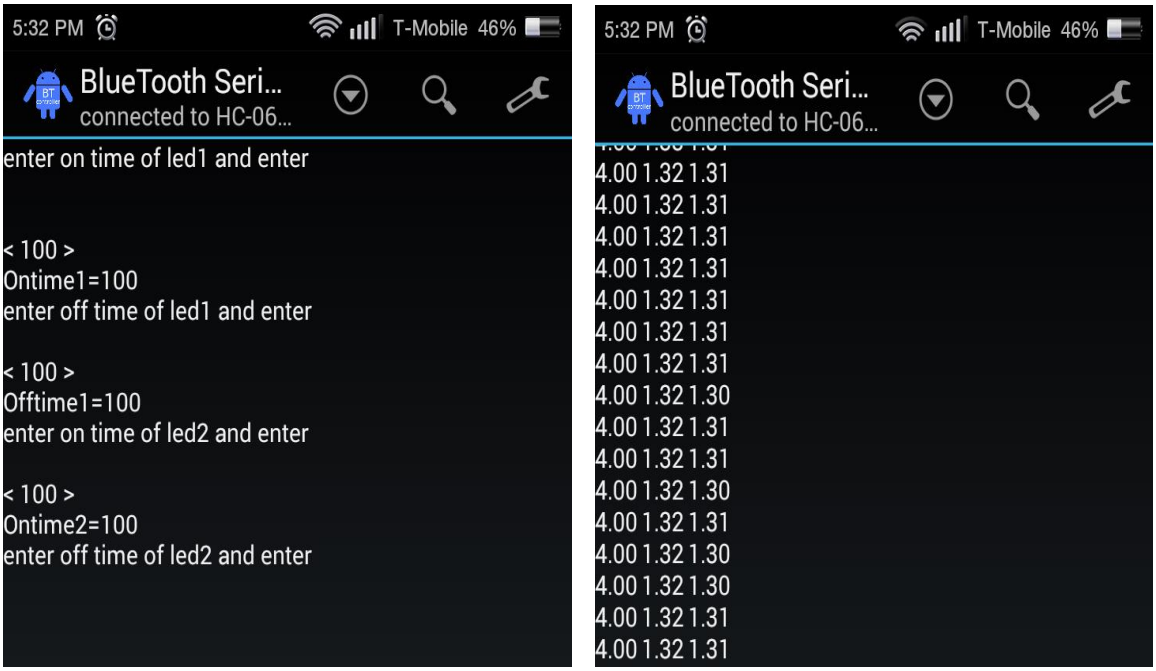

Figure 3.27: Mobile application

3.2.7 Post Processing

In this application, a lot of post processing was not used as the results directly indicated the fluorescence values detected by the detector. When Lab-view code was used, the program included the post processing section which gave the average of detected values.

In the case of results obtained from Mobile application and Tera-term emulator, they were stored as an Xcel file and the average of results was taken either in Excel directly or MATLAB.

3.3 Block Diagram

The block diagram of the complete setup is shown in the Figure 3.28

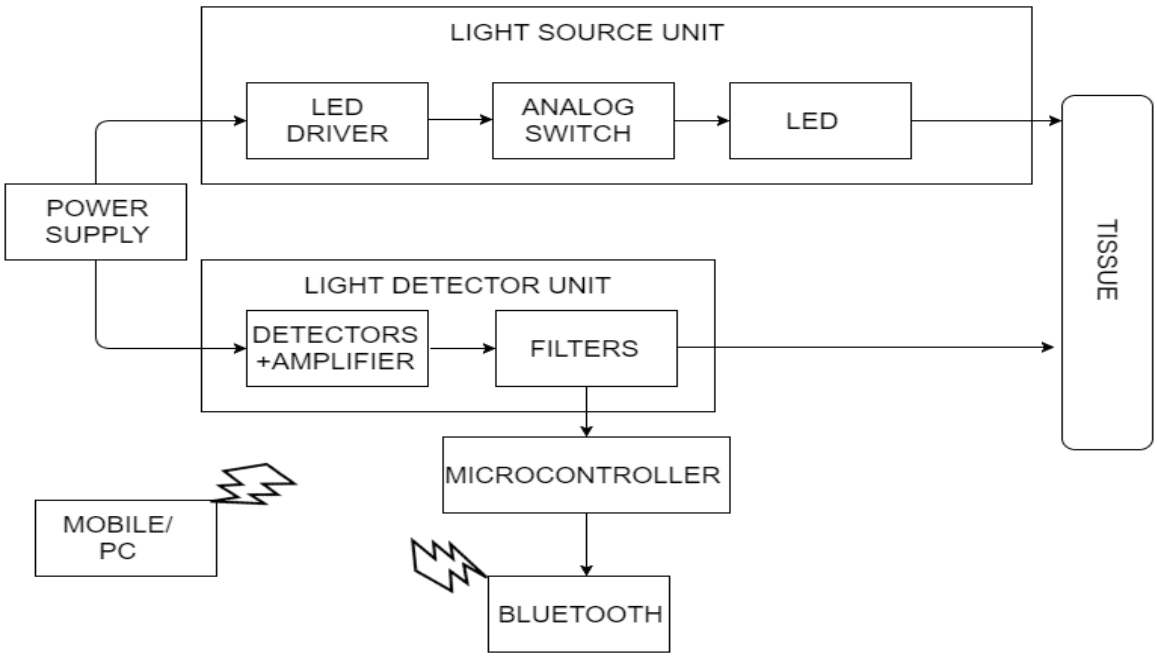

Figure 3.28: Block diagram of compact model

3.4 3d Printed Patch

The patch used to hold the source and detectors was designed using Fee-Cad software and printed using a 3D printer. The patch was designed such that it had outlets for the source (LED) and detector coupled with filter. The patch has straps on either side which can be firmly attached to the detecting surface and thereby avoiding any stray light getting into the detectors. Due to size restrictions, the source-detector separation no less than 1 cm was obtained. The 3D printed patch is shown in the Figure 3.29

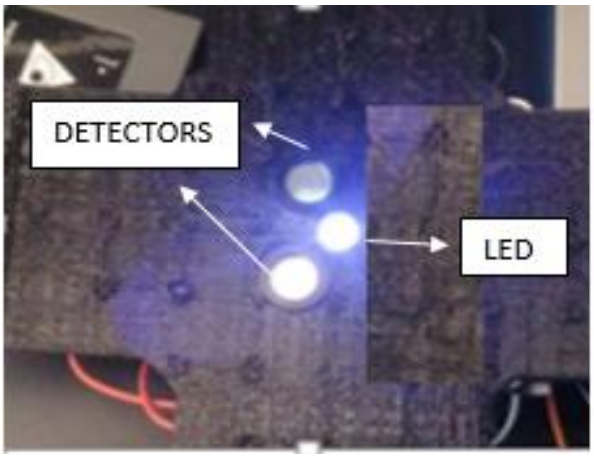

Figure 3.29: Patch

3.5 Experiment and Result

The efficiency of the device was tested by its ability to differentiate the concentrations of NADH and FAD in normal tissue to that of cancer tissue as shown in the paper [132]. Per this, a normal tissue has a mean concentration of NADH and FAD as 84um and 83um respectively. Whereas a normal tissue has a mean concentration of NADH and FAD is 308um and 217um respectively. For these concentrations, FAD redox ratio which is the ratio of FAD fluorescence intensity to the sum of FAD and NADH fluorescence intensity was calculated. For normal tissue a mean redox ratio value of 0.44 was obtained and for a cancer tissue a redox ratio value of 0.56 was obtained.

To perform a similar study Tonic water (Quinine) was used in place of NADH which has similar excitation-emission wavelength to NADH. Similarly, Fluorescein was used in place of FAD because of its similar fluorescence properties. Fluorescein also gets excited at a couple of wavelengths 365nm, 450nm and has an emission peak at 530nm. These

fluorophores were used for preliminary testing as NADH and FAD are expensive drugs. On the contrary fluorescein and quinine have different molar excitation coefficient and quantum yield compared to NADH and FAD. To make them comparable for the experiment the concentration of fluorescein and quinine were reduced to mimic the molar excitation coefficient and quantum yield of FAD and NADH respectively.

After making the parameters of fluorescein and quinine equivalent to NADH and FAD, concentration of quinine and fluorescein in normal tissue was 6um and 14um respectively. Whereas for a cancer tissue the concentration of quinine and fluorescein in normal tissue was 14um and 52um respectively. These concentrations were added to the prepared phantom and the fluorescence emitted by them was recorded.

In this experiment phantom used had optical properties us' as 10cm-1 and absorption coefficient as 0.1cm-1. Scattering was introduced into the phantom by adding 20% intra-lipid solution and absorption was introduced by adding Indian ink to the water. After phantom of desired optical properties was made, the required concentration of quinine and fluorescein were added and fluorescence was detected by the detectors. The detector coupled with a 460nm Band Pass Filter detected quinine and the detector coupled with a 580nm Band Pass Filter detected fluorescein. The acquisition time was set to 2000ms and the detected value was averaged to give the net fluorescence value. Finally, the fluorescence detected by the device at normal concentration to cancer conditions were compared and R.R was calculated.

The setup used in the experiment is shown in the Figure 3.30

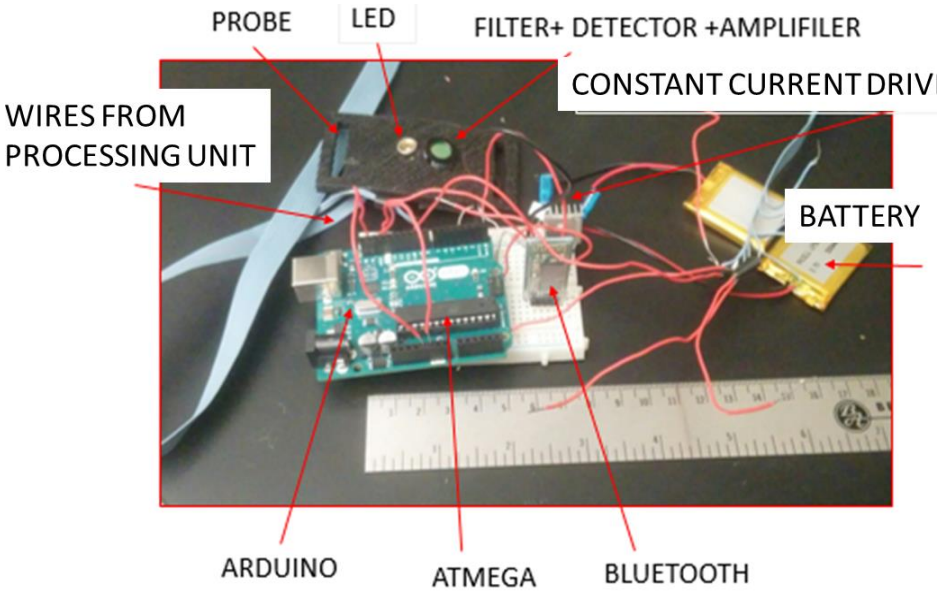

Figure 3.30: Setup of compact model

The complete setup is shown in the figure 3.31

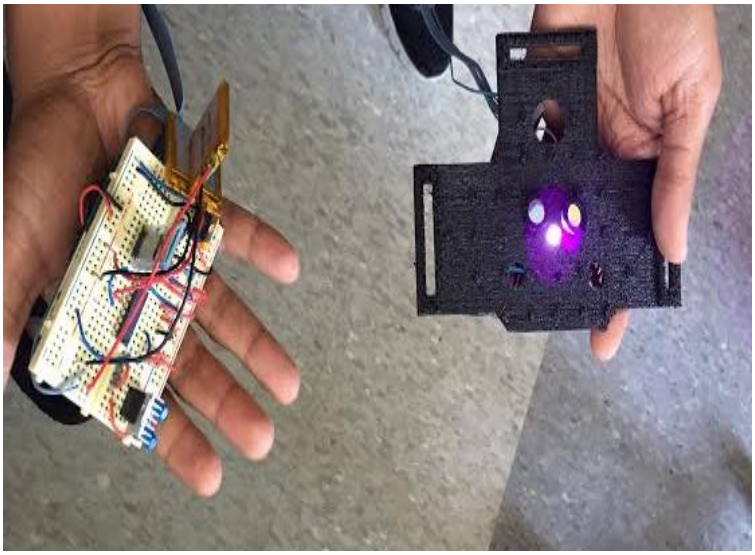

Figure 3.31: Compact Device

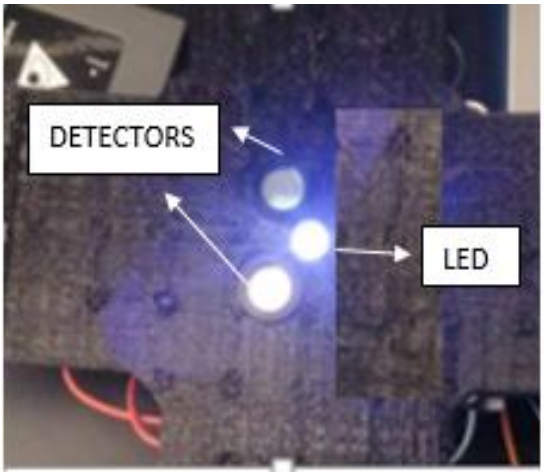

Figure 3.32: Patch

Figure: 3.33: Fluorescence

Finally, the detected fluorescence shown in the Figure 5.30 was corrected for peak and sensitivity. So, the resultant redox ratio for a normal tissue and cancer tissue was 0.515 and 0.617 respectively. Per previous study the mean value of redox ratio normal tissue and cancer tissue was 0.44 and 0.56 respectively [132]. The results obtained by the device are off by 9-15% but is still within the standard deviation of the study. The comparison is shown in Table 3.10.

Table 3.10: Results from compact model

TISSUE (R.R)	**PAPER [132]**	**COMPACT MODEL**	**% ERROR**
NORMAL	0.44	0.515	14
CANCER	0.56	0.617	9

3.6 Conclusion

The designed explained in this chapter is wireless, compact and inexpensive. The design is also accurate and can detect concentrations to about 4µM. The limitation of this compact model was the large source-detector separation distance. The presence of glass filters restricted the source-detector separation distance not less than 1 cm which prevented the device from measuring very low concentrations. Even if the glass filters were removed and cut to exactly fit onto the detector surface then the source-detector separation would be around 6mm which is not a huge difference. The minimum concentration that could be detected by the compact device was around 6µM of NADH. To detect even lower concentrations a third design was used which will be explained in the next chapter.

Instrumentation and Results of Spectrometer Based Model

4.1 Introduction

To overcome the problems of large source detector separation distance and small concentration measurement in the compact module an alternative devised using a spectrometer which could possibly overcome all the drawbacks of the compact model discussed in the previous chapter.

The study of the interaction of matter with electromagnetic radiation is known as Spectroscopy [162-163]. Biomedical spectroscopy is done by measuring the interaction between light and tissue, which provides a variety of information of the tissue [164].

4.2 Instrumentation

In this section, all the components used for the instrumentation of the modified small fluorescence model will be mentioned

4.2.1 Light Source Unit

The LED used for the modified design was a fiber coupled LED from Mightex Inc. The part number of this LED is FCS-0365-000. The wavelength chosen for this model was a 365nm as both NADH and FAD could be excited using this and would eliminate the use a second source unit. The main advantage of using this LED was that it was compact, fiber coupled and not very expensive

The specifications of the LED are shown in the Table 4.1 and spectrum in Figure 4.1.

Table 4.1: Specifications of the LED (Spectrometer model)

PARAMETER	**VALUE**
WAVELENGTH	365nm
SUPPLY VOLTAGE	3.7 V
SUPPLY CURRENT	500mA
OPTICAL POWER	18mW

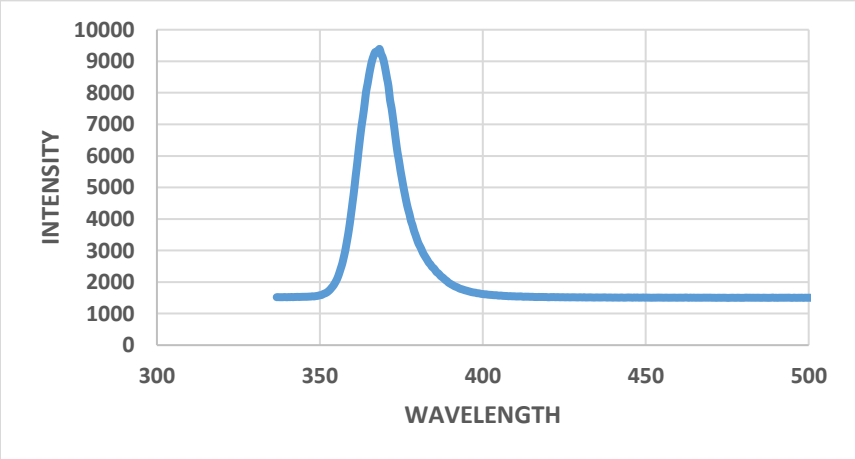

Figure 4.1: LED spectrum

4.2.1.1 LED Driver

The driver used to run the LED was constant current source and was taken form Digi-key (part number 945-1122-ND). This supply gave a constant current to the LED of 500mA.The Specifications of the constant current driver is shown in the Table 4.2

Table 4.2: Specifications of the LED driver (Spectrometer model)

PARAMETER	VALUE
WAVELENGTH	365nm
SUPPLY VOLTAGE	4.5-36V
OUTPUT VOLTAGE MAX	500mA
OUTPUT VOLTAGE MAX	2-35V

The pin configuration of LED driver is shown in the Figure 4.2

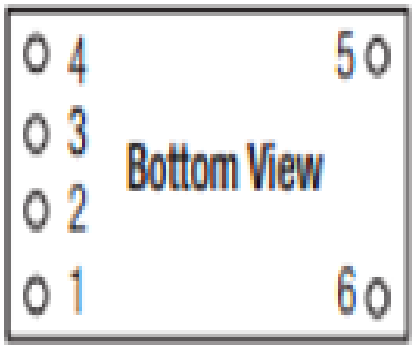

Pin Connections RCD-24 Series

Pin #	Out	Comments
1	+Vin	DC Supply
2	Analogue Dimming	Leave open if not used
3	PWM/ON/OFF	Leave open if not used
(3	Vref	Vref Version only)
4	GND	Do not connect to -Vout
5	-Vout	LED Cathode Connection
6	+Vout	LED Anode Connection

Figure 4.2: Pin configuration of led driver [165]

The connection from the LED driver to the LED is shown in the Figure 4.3.

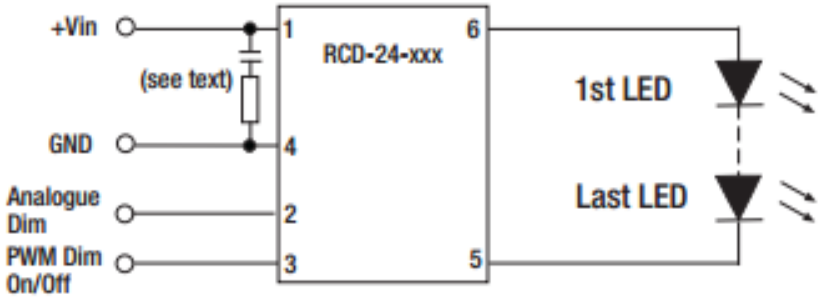

Figure 4.3: Connection from LED driver to the LED [165]

4.2.1.2 Light Source Unit Testing

The most important testing of the source used for optical applications is its power or stability testing. It is very important for the source to be very stable as variation its power can lead to false positives during diagnosis. Thus, it is very important that the source should be highly stable. The result is shown in the Figure 4.4 and Table 4.3.

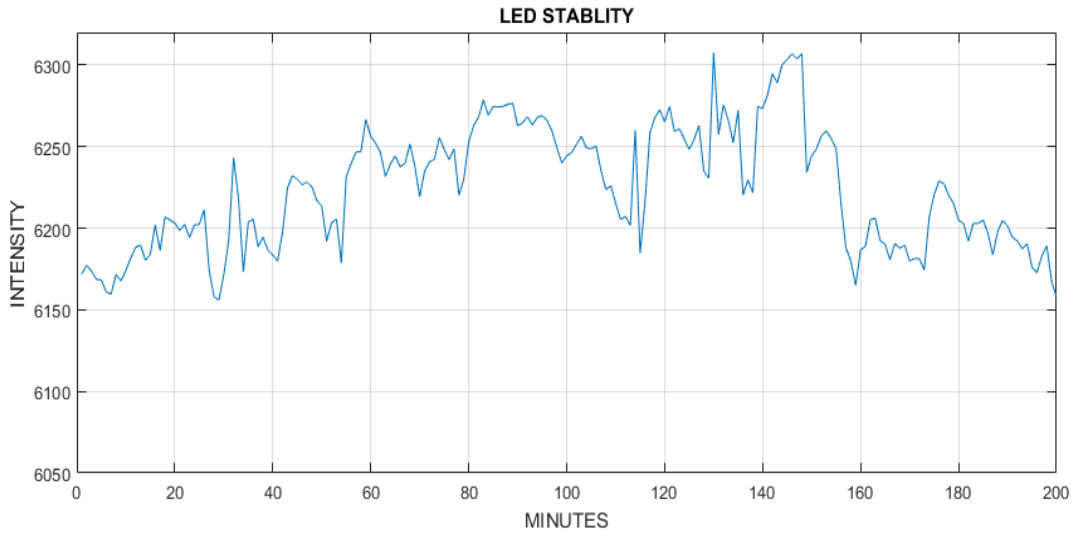

Figure 4.4: LED stability test (Spectrometer model)

Table 4.3: Stability test of LED (Spectrometer model)

PARAMETER	VALUE
MEAN	6223counts
STANDARD DIVIATION	36.9 counts
% ERROR	0.5

4.2.1.3 Switch

The switch used in this version is the same switch (Vishay: DG-413) used for the compact model explained in section 3.2.1.3. The input of the switch was the LED driver. As each switch has three pins, one is the input which is the output of LED driver, second is the digital port which was connected to the control unit and third was the output port which was connected to the LED. In this way LED, can be turned on and off by communicating with the control unit.

4.2.2 Detector Source Unit

The detector used for this design was STS spectrometer from Ocean Optics. The advantage of using a spectrometer is that it is very sensitive, fiber based and ultra-compact. The only disadvantage of spectrometer was that it was a little expensive. The specifications of the spectrometer are shown in the Table. Sensitivity solves the problem of lower concentration detection and fiber based solved the problem of large source-detector separation. The specifications of the STS spectrometer are shown in Table 4.4.

Table 4.4: Specifications of the Spectrometer

PARAMETER	VALUE
WAVELENGTH RANGE	350-800nm
OPTICAL RESOLUTION	12nm
DYBAMIC RANGE	5×10^9
INTEGRATION TIME	10 µs to 10 s
ADC RESOLUTION	14 bits

The sensitivity curve of the spectrometer is shown in the Figure 4.5

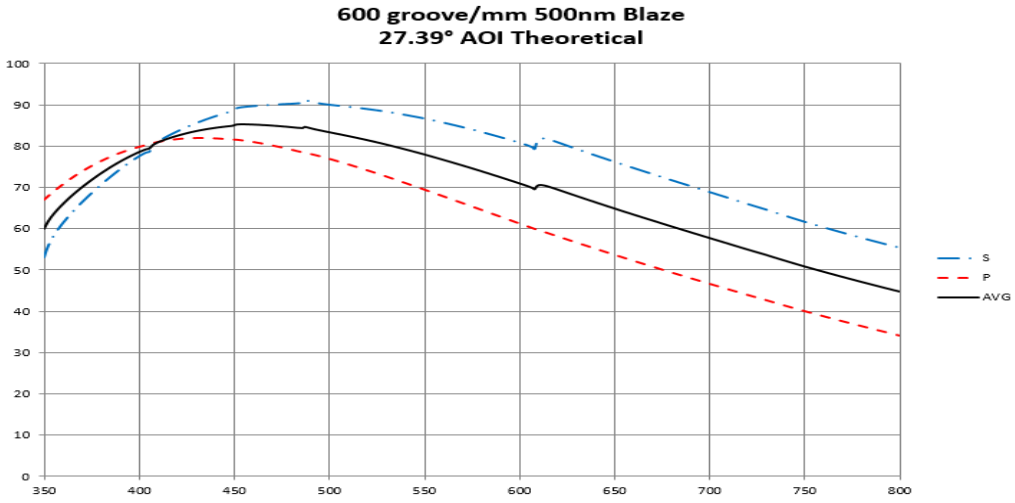

Figure 4.5: Sensitivity curve of spectrometer- oceanoptics.com

4.2.2.1 Detector Unit Testing

The spectrometer was tested to see the minimum detectable concentration it could measure. This experiment was done by measuring the fluorescence emitted by fluorescein. A stock solution of fluorescein was made using its powdered form (Sigma Aldrich: 518-47-8). This

was further diluted to make lower concentrations. The prepared solution was excited using the 365nm LED and the fluorescence emitted by it was measured on the spectrometer. The experiment setup is shown in the Figure 4.6.

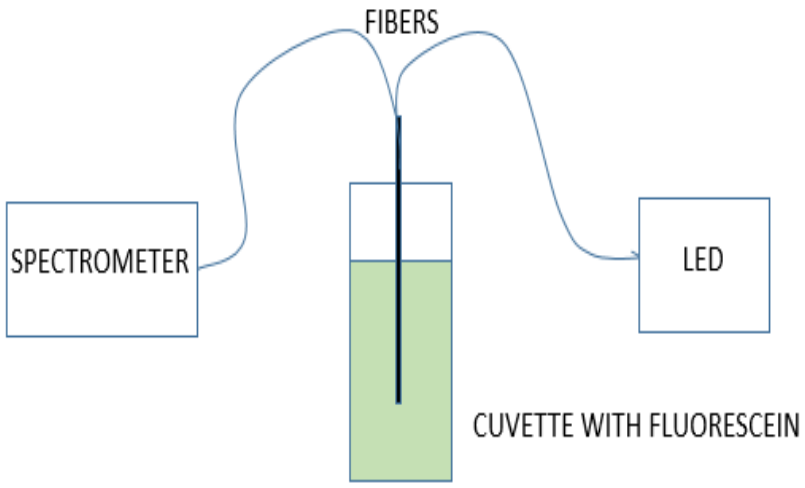

Figure 4.6: Experimental Setup of spectrometer based model

The experiment started with the fluorophore concentration in micro molar range and the concentration was reduced to Nano molar range. The instrument could measure up to 5uM with an integration time of 100ms. An integration time of 1 second was used to measure the concentration in Nano molar range and the instrument could measure a concentration of 2nM. It is possible to set the integration time of spectrometer up to 10 seconds and take the measurements. So, experiment was stopped at this point as from the data obtained it was clear that the device could measure concentration lower than 2nM.

The results obtained from the experiment is shown in Figure 4.7.

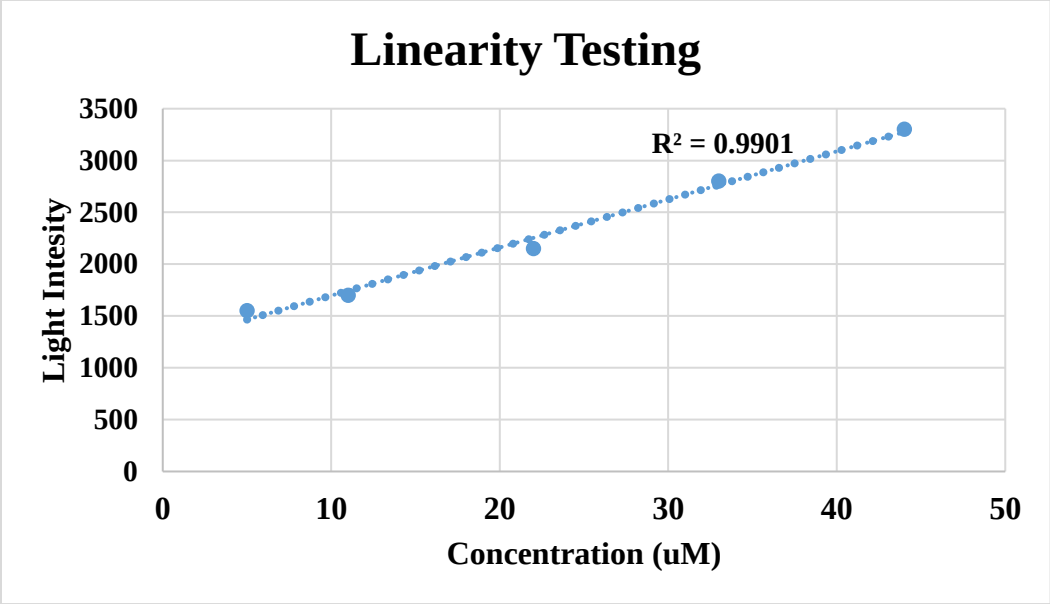

Figure 4.7: Linearity in Micro molar range with integration time 100ms

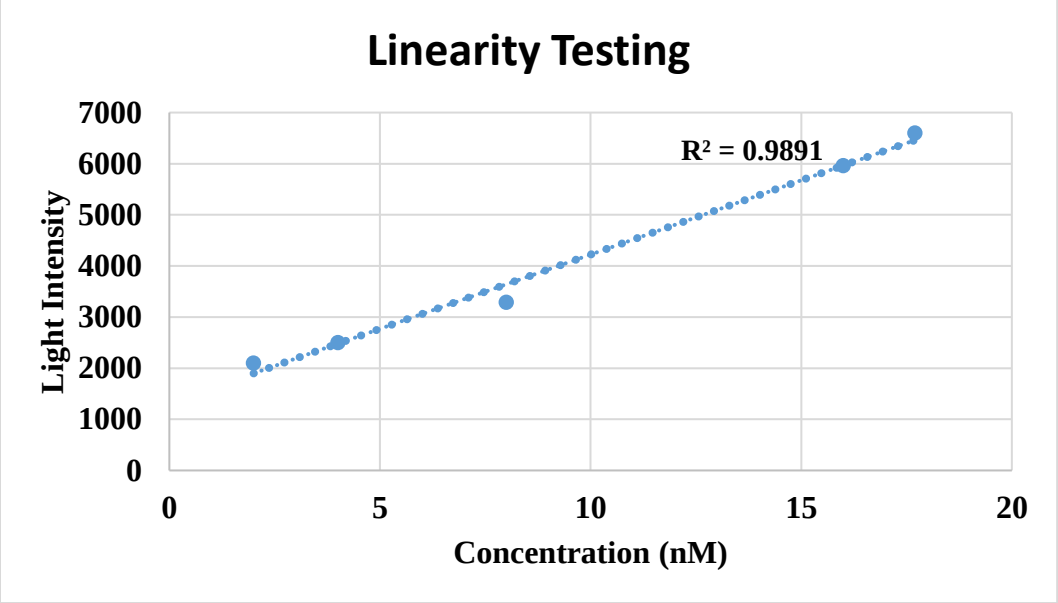

Figure 4.8: Linearity in Nano molar range with integration time 1s

4.2.3 Wireless Application

The following components were used for the wireless transmission of data from the spectrometer to the P.C / Laptop / Mobile device.

4.2.3.1 Raspberry Pi

The control unit used for transmitting the signal from the spectrometer to the P.C and giving digital signal to the analog switch is a Raspberry Pi. This is a smallest form of processing unit available which works on Linux operating system. The specifications of the Raspberry Pi are shown in the Table 4.5

Table 4.5: Specifications of the Raspberry Pi

PARAMETER	VALUE
RAM	1GB
PROCESSOR	900MHz
USB PORTS	4
GPIO PINS	40
MIN SUPPLY CURRENT	700mA

A spectrometer and WIFI dongle were connected to the USB ports of Raspberry Pi and the one of the general-purpose input/output (GPIO) pin of the Pi was given to the analog switch to turn on and off the LED.

4.2.3.2 WIFI

A WIFI dongle was attached to one of the ports of the Raspberry pi to transmit the data wirelessly from the Raspberry Pi to the control device and vice versa. The WIFI dongle used had a speed of 150Mbps. This enabled to control the design with any device having WIFI facility. To control the spectrometer and LED from the control device a program was written in .HTML and two webpages were created which are shown in Figure 6.8 and 6.9.

One webpage was used to control the spectrometer and this program was taken from ocean optics. The other webpage was used to turn on and off the LED. A screenshot of the webpages used to control the Spectrometer and LED are shown in the Figure 49,4.10

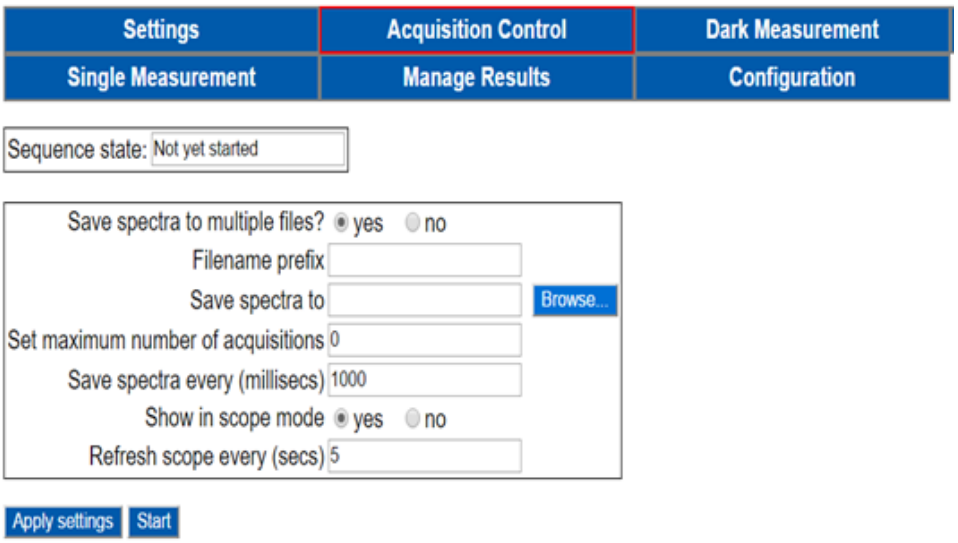

Figure 4.9: Screensoot of Spetrometer webpage (Ocean Optics)

Figure 4.10: Screensoot of LED webpage

4.2.4 Power Supply

The power supply initially used to power the device was a portable power supply form Ocean-optics (Part: CM-5095-WE). The specifications of the power supply are shown in Table 4.6.

Table 4.6: Specifications of the Power supply from Ocean Optics

PARAMETER	VALUE
VOLTAGE	5V
CURRENT	1A
CAPACITY	3000mAh

This power supply was given to the Raspberry Pi and the Spectrometer, WIFI dongle received power from its USB ports and the power supply could power all of them without any problem. When the 5V supply of Raspberry Pi was given to the LED driver to run the LED but the power supply did not have sufficient current to power up all the components. To overcome the problem of current deficiency this power supply was replaced by another

Jackery power supply taken from Amazon.com (Part number: B00AANMVNQ). This solved the problem of insufficient current. The specification of the power supply form Jackery is shown in the Table 4.7.

Table 4.7: Specifications of the Power supply from Jackery

PARAMETER	**VALUE**
VOLTAGE	5V
CURRENT	2A
CAPACITY	6000mAh

Two paths were taken from the output of the supply and one was given to Raspberry Pi and the other was given to the LED driver.

4.3 Block Diagram

The block diagram of the complete setup is shown in the Figure 4.11.

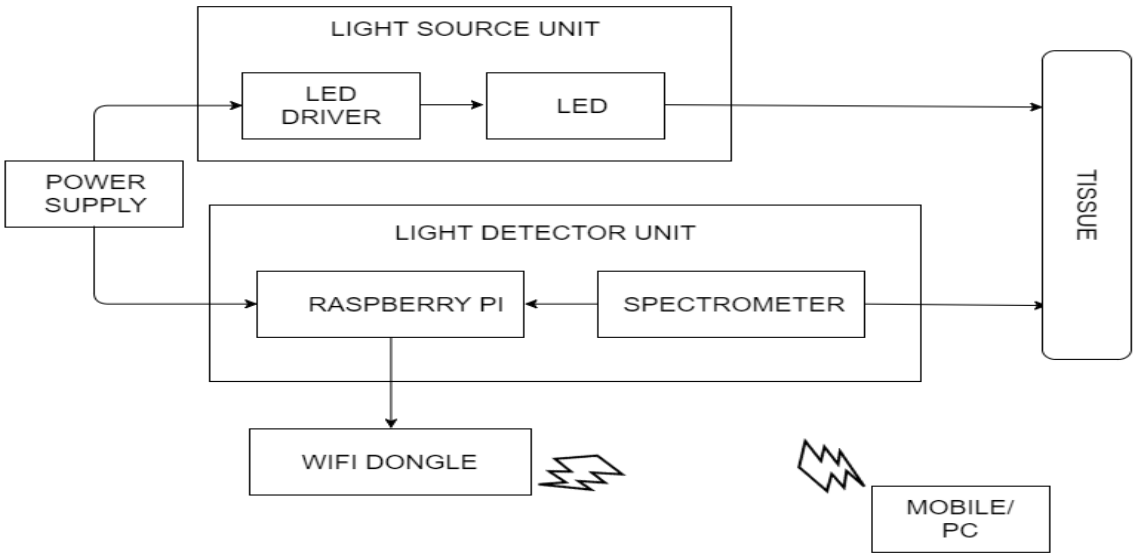

Figure 4.11: Block diagram of spectrometer model

4.4 3D Printed Module

A module was designed using AutoCAD software and 3D printed to fit all the components of the spectrometer model in a small box. The box also had openings for spectrometer and LED using which fibers of different diameters can be attached before taking the measurements. It also had slits to turn on the module, charge the battery, show the charge of the battery and for cooling purpose.

Figure 4.12: Front and side view of the spectrometer module

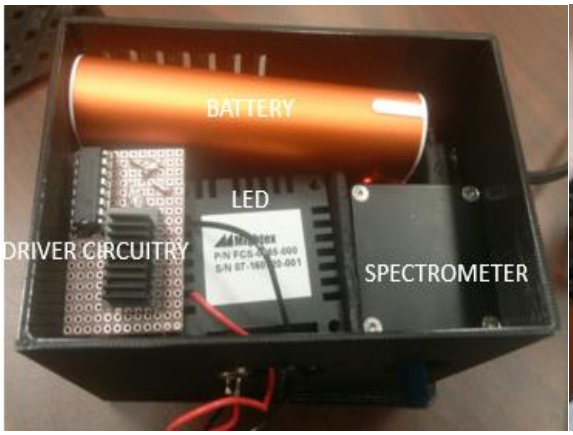

Figure 4.13: Top view of spectrometer module

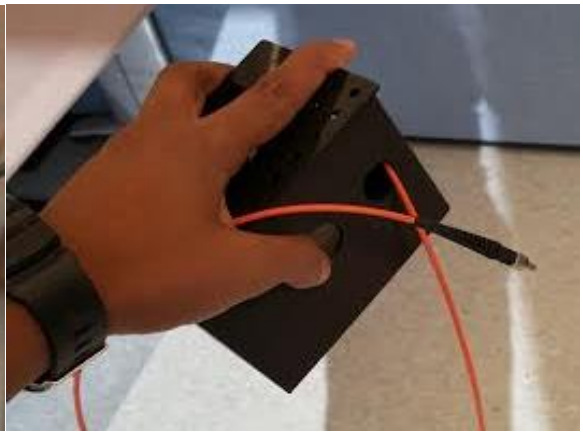

Figure 4.14: Handheld device

4.5 Ex-Vivo Experiment

In this section the experiments performed ex-vivo on mice placenta and cancer cells will be discussed.

4.5.1 Measurement 0f Redox Ratio in Placenta

In this experiment, mice placentas were used to detect FAD redox ratio. The setup used in the experiment is shown in the Figure

Experiment was performed on three placentas numbered 7-9 which is showed in the Figure 4.15.

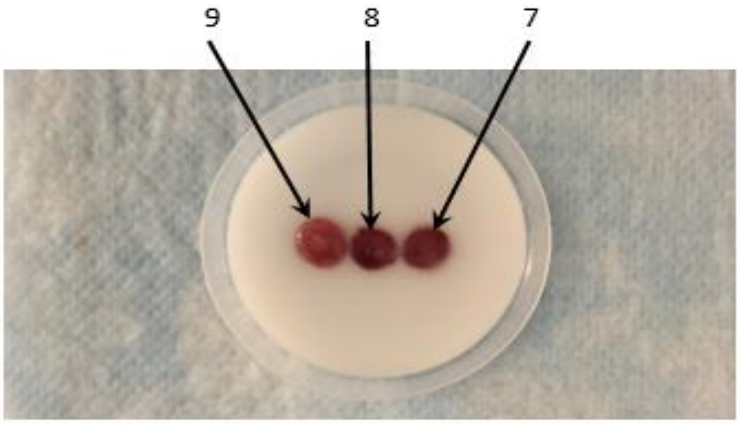

Figure 4.15: Placenta

4.5.1.1 Results

Several measurements were performed on each placenta and average of these readings were divided by LED leakage to obtain the spectra for each placenta. This spectrum was used to extract the NADH (460nm) and FAD (520nm) excitation band. The results are shown in Figure 4.16,4.17.

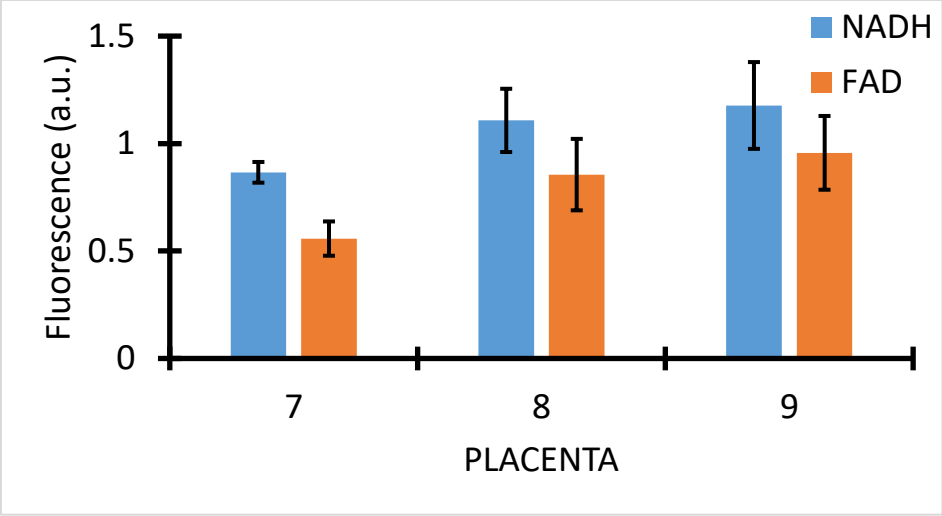

Figure 4.16: Extracted values of NADH and FAD

The extracted NADH and FAD values were used to obtain the FAD redox ratio which is given as shown below

$$\text{FAD REDOX RATIO} = \frac{\text{FAD}}{\text{FAD+NADH}}$$

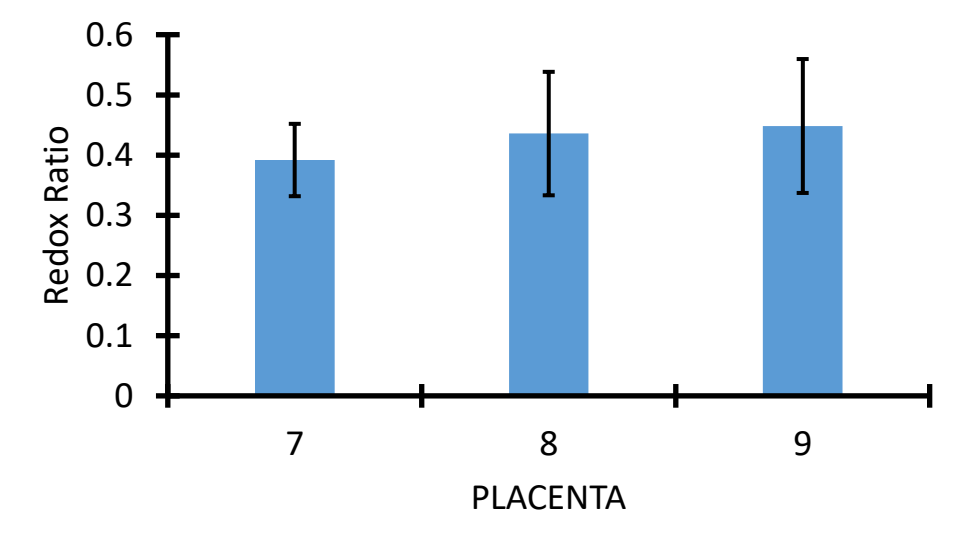

Figure 4.17: Redox ratio of each sample

These results are like camera based model which shows placenta 9 had maximum fluorescence since it has less blood comparatively to placenta 7 and 8. Presence of blood increases reduces fluorescence intensity. Whereas the fluorescence intensity from placenta 7 and 8 are close to each other.

4.5.2 Brain Cancer Cells

In this experiment cancer cells from brain were used to obtain the FAD redox ratio. The setup used in the experiment is like Figure 4.9,410. Brain cancer cells is shown in the Figure 4.18.

Figure 4.18: Cancer cells

4.5.2.1 Results

Several measurements were performed on cancer cells and the medium in which they were grown and their average was divided to remove the any auto fluorescence from the medium. This ratio gave the final spectrum. This final spectrum was used to extract the

NADH (460nm) and FAD (520nm) excitation band. The results are shown in the Figures 4.19,4.20.

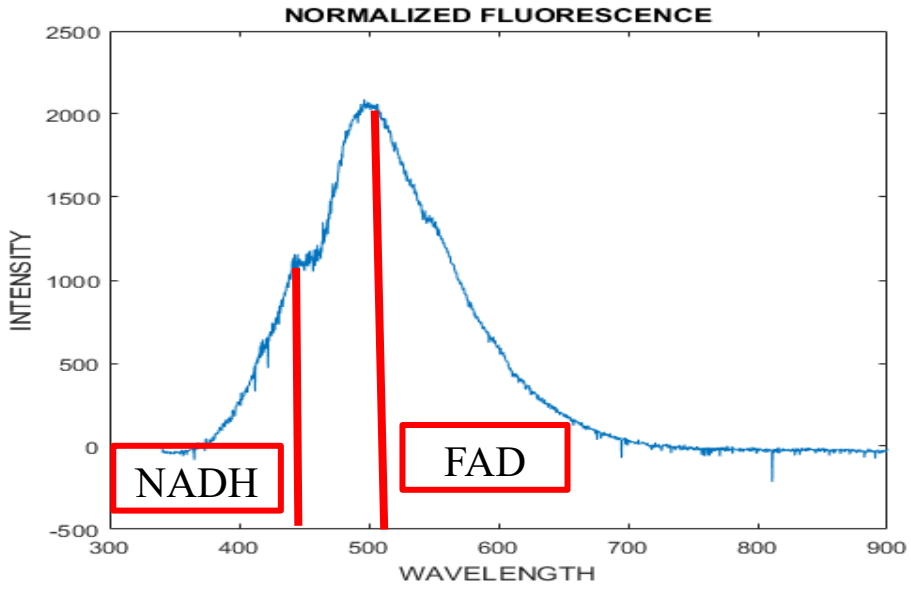

Figure 4.19: Normalized fluorescence signal-Cancer cells

The extracted values of NADH and FAD is shown in the Figure 4.18

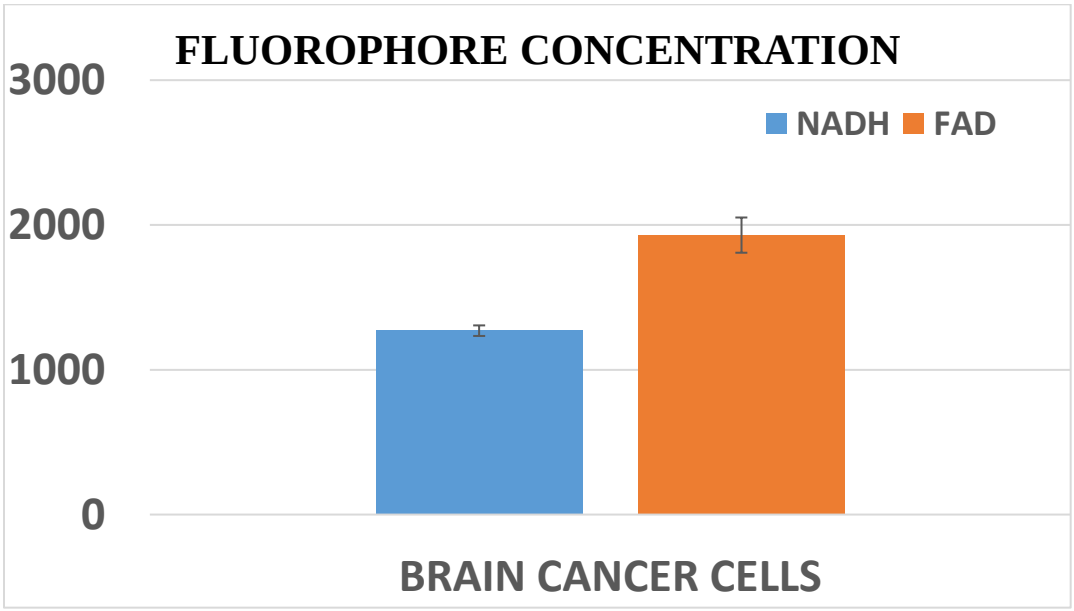

Figure 4.20: Extracted NADH and FAD- Cancer cells

$$\text{FAD REDOX RATIO} = \frac{\text{FAD}}{\text{FAD+NADH}}$$

Table 4.8: Mean and standard deviation of redox ratio – Cancer cells

REDOX RATIO	VALUE
MEAN	0.6116
STD	0.0183

These values are very like the camera based model and literature [132].

4.5.3 Brain Normal Cells

A similar process was performed like section 4.5.3 and FAD redox ratio of normal cells was calculated

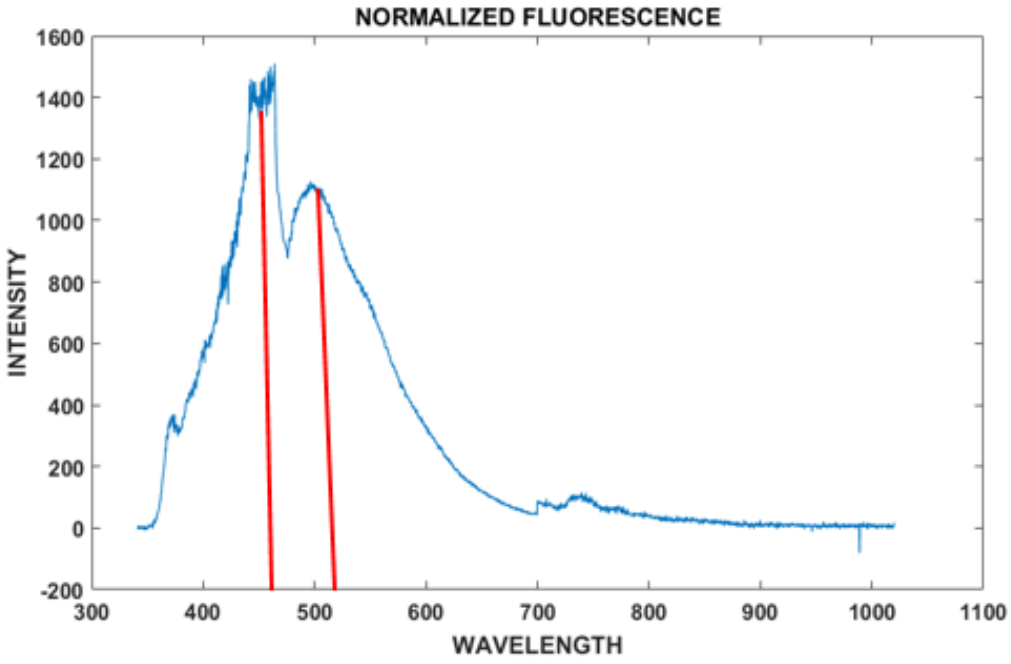

Figure 4.21: Normalized fluorescence signal-Normal cells

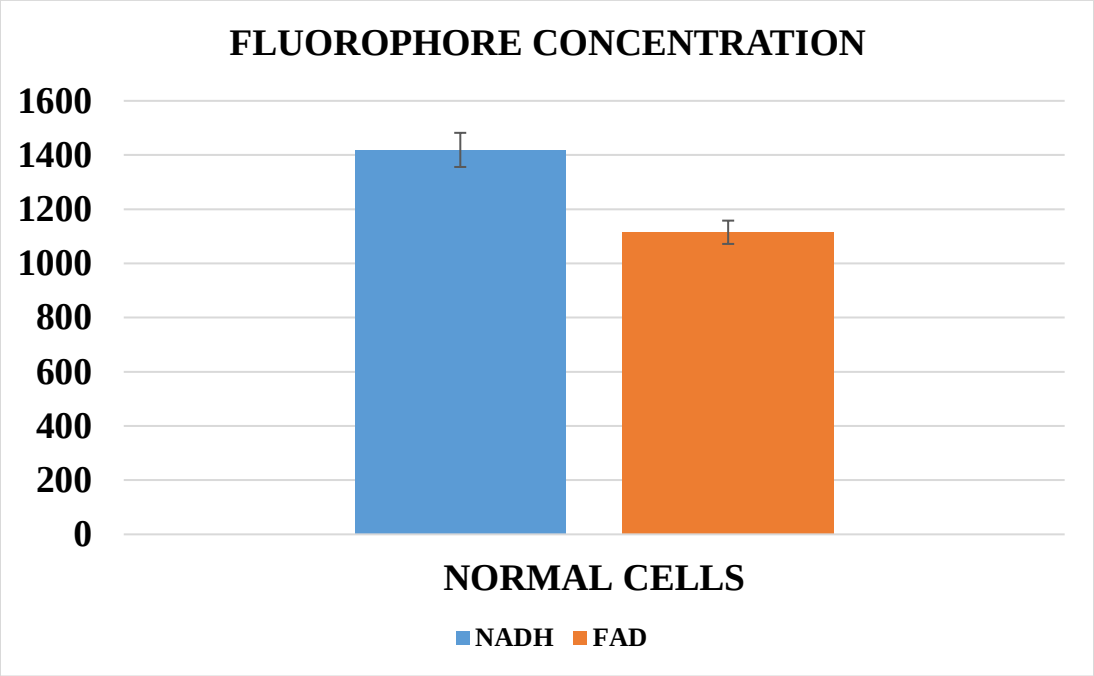

Figure 4.22: Extracted NADH and FAD- Normal cells

Table 4.9: Mean and standard deviation of redox ratio -Normal Cells

REDOX RATIO	VALUE
MEAN	0.44001
STD	0.022

These values are very like the camera based model and literature [132].

4.5.4 Comparison of Camera Model and Spectrometer Model

The results obtained from both the instruments are shown in Table 4.10

Table 4.10: Redox ratio comparison

CELLS	CAMERA MODEL	SPECTROMETER MODEL
CANCER	0.6297± 0.0016	0.6116± 0.0183
NORMAL	0.4414± 0.0019	0.4400± 0.022

The Figure 4.23 below shows the comparison of camera based model and compact model

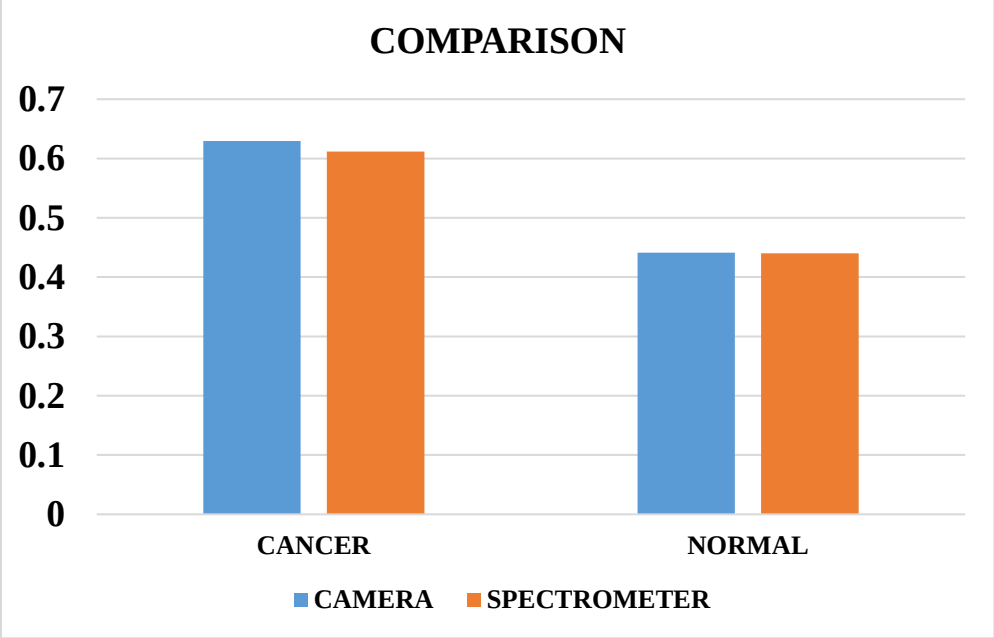

Figure 4.23: Comparison between camera system and compact spectrometer system

As it is seen from the plot the values of the redox ratio obtained with camera based system and compact spectrometer system are very similar.

4.6 Conclusion

The spectrometer model is slightly larger in size but a lot more sensitive compared to the compact model explained in previous chapter. This design can detect low fluorophore concentration unlike the compact model. The sensitivity of the of the spectrometer model is in comparison to the camera model which is evident from the close redox ratio obtained from the brain cells.

4.7 Comparison of Three Systems

The Table 4.11 shows the comparison of all the three models used.

Table 4.11: Comparison of modalities

PARAMETER	**CAMERA BASED SYSTEM**	**COMPACT MODEL**	**SPECTROMETER MODEL**
SENSITIVITY	VERY HIGH	MODERATE	HIGH
PORTABLITY	NO PORTABILITY	HIGH PORTABILITY	HIGH PORTABILITY
COST	VERY HIGH	VERY LOW	LOW

Bibliography

1. Mayevsky, A. (2009). Mitochondrial function and energy metabolism in cancer cells: past overview and future perspectives. *Mitochondrion*, *9*(3), 165-179.
2. Mayevsky, A., & Barbiro-Michaely, E. (2009). Use of NADH fluorescence to determine mitochondrial function in vivo. *The international journal of biochemistry & cell biology*, *41*(10), 1977-1988.
3. Warburg. The metabolism of tumors. Constable & CO LTD., London (1930)
4. N.J. Linford, S.E. Schriner, P.S. Rabinovitch. Oxidative damage and aging: spotlight on mitochondria. Cancer Res., 66 (2006), pp. 2497–2499
5. A. Navarro, A. Boveris. The mitochondrial energy transduction system and the aging process. Am. J. Physiol. Cell Physiol., 292 (2007), pp. C670–C686
6. P. Kermer, J. Liman, J.H. Weishaupt, M. Bahr. Neuronal apoptosis in neurodegenerative diseases: from basic research to clinical application. Neurodegener. Dis., 1 (2004), pp. 9–19
7. M.T. Lin, M.F. Beal. Mitochondrial dysfunction and oxidative stress in neurodegenerative diseases. Nature, 443 (2006), pp. 787–795
8. W.G. Tatton, C.W. Olanow. Apoptosis in neurodegenerative diseases: the role of mitochondria Biochim. Biophys. Acta, 1410 (1999), pp. 195–213.

9. N.R. Sims, M.F. Anderson. Mitochondrial contributions to tissue damage in stroke. Neurochem. Int., 40 (2002), pp. 511–526
10. P.G. Sullivan, S. Krishnamurthy, S.P. Patel, J.D. Pandya, A.G. Rabchevsky. Temporal characterization of mitochondrial bioenergetics after spinal cord injury. J. Neurotraum., 24 (2007), pp. 991–999
11. S.W. Ballinger. Mitochondrial dysfunction in cardiovascular disease. Free Rad. Biol. Med., 38 (2005), pp. 1278–1295
12. F. Porta, J. Takala, C. Weikert, H. Bracht, A. Kolarova, B.H. Lauterburg, E. Borotto, S.M. Jakob. Effects of prolonged endotoxemia on liver, skeletal muscle and kidney mitochondrial function. Crit. Care, 10 (2006), p. R118
13. A. Rotig. Renal disease and mitochondrial genetics. J. Nephrol., 16 (2003), pp. 286–292
14. C.D. Berdanier. Diabetes and nutrition: the mitochondrial part. J. Nutr., 131 (2001), pp. 344S–353S
15. M.R. Duchen. Roles of mitochondria in health and disease. Diabetes, 53 (1) (2004), pp. S96–102
16. E. Gottlieb, S.M. Armour, C.B. Thompson. Mitochondrial respiratory control is lost during growth factor deprivation. Proc. Natl. Acad. Sci. USA, 99 (2002), pp. 12801–12806
17. R. Moreno-Sanchez, S. Rodriguez-Enriquez, A. Marin-Hernandez, E. Saavedra. Energy metabolism in tumor cells. FEBS J., 274 (2007), pp. 1393–1418
18. E. Alirol, J.C. Martinou. Mitochondria and cancer: is there a morphological connection? Oncogene, 25 (2006), pp. 4706–4716

19. J.M. Cuezva, M. Krajewska, M.L. de Heredia, S. Krajewski, G. Santamaria, H. Kim, J.M. Zapata, H. Marusawa, M. Chamorro, J.C. Reed. The bioenergetic signature of cancer: a marker of tumor progression. Cancer Res., 62 (2002), pp. 6674–6681
20. K. Smallbone, R.A. Gatenby, R.J. Gillies, P.K. Maini, D.J. Gavaghan. Metabolic changes during carcinogenesis: potential impact on invasiveness. J. Theor. Biol., 244 (2007), pp. 703–713
21. M. Wu, A. Neilson, A.L. Swift, R. Moran, J. Tamagnine, D. Parslow, S. Armistead, K. Lemire, J. Orrell, J. Teich, S. Chomicz, D.A. Ferrick. Multiparameter metabolic analysis reveals a close link between attenuated mitochondrial bioenergetic function and enhanced glycolysis dependency in human tumor cells. Am. J. Physiol. Cell Physiol., 292 (2007), pp. C125–C136
22. R.H. Xu, H. Pelicano, Y. Zhou, J.S. Carew, L. Feng, K.N. Bhalla, M.J. Keating, P. Huang. Inhibition of glycolysis in cancer cells: a novel strategy to overcome drug resistance associated with mitochondrial respiratory defect and hypoxia. Cancer Res., 65 (2005), pp. 613–621
23. W. Assaily, S. Benchimol. Differential utilization of two ATP-generating pathways is regulated by p53. Cancer Cell, 10 (2006), pp. 4–6
24. D.R. Green. At the gates of death. Cancer Cell, 9 (2006), pp. 328–330
25. J.P. Kruse, W. Gu. P53 aerobics: the major tumor suppressor fuels your workout. Cell Metab., 4 (2006), pp. 1–3
26. B. Chance. Spectrophotometry of intracellular respiratory pigments. Science, 120 (1954), pp. 767–775

27. B. Chance. Spectra and reaction kinetics of respiratory pigments of homogenized and intact cells. Nature, 169 (1952), pp. 215–221
28. B. Chance, V. Legallias. Rapid and sensitive spectrophotometry. A stopped-flow attachment for a stabilized quartz spectrophotometer. Rev. Sci. Instr., 22 (1951), pp. 627–638
29. A. Mayevsky, B. Chance. Oxidation–reduction states of NADH *in vivo*: from animals to clinical use. Mitochondrion, 7 (5) (2007), pp. 330–339
30. A. Mayevsky, G.G. Rogatsky. Mitochondrial function in vivo evaluated by NADH fluorescence. from animal models to human studies
31. WebMD. Cancer Health Center. Retrieved from: http://www.webmd.com/cancer/default.htm
32. Centers for Disease Control and Prevention. Global Cancer Statistics. Retrieved from: https://www.cdc.gov/cancer/international/statistics.htm
33. WebMD. Brain Cancer Health Center. Retrieved from: http://www.webmd.com/cancer/brain-cancer/brain-cancer
34. National Cancer Institute. SEER Stat Fact Sheets: Brain and Other Nervous system Cancer. Retrieved from: https://seer.cancer.gov/statfacts/html/brain.html
35. Dana-Farber. June 27, 2014. "Which Countries Have the Highest and Lowest Cancer Rates?". Retrieved from: http://blog.dana-farber.org/insight/2014/06/which-countries-have-the-highest-and-lowest-cancer-rates/

36. National Cancer Institute. Adult Central Nervous System Tumors Treatment (PDQ®)–Health Professional Version. Retrieved from: https://www.cancer.gov/types/brain/hp/adult-brain-treatment-pdq

37. Siegel, R. L., Miller, K. D. and Jemal, A. (2016), Cancer statistics, 2016. CA: A Cancer Journal for Clinicians, 66: 7–30. doi:10.3322/caac.21332.

38. Ward, P. S., & Thompson, C. B. (2012). Metabolic reprogramming: a cancer hallmark even warburg did not anticipate. *Cancer cell*, *21*(3), 297-308.

39. Hanahan, D., & Weinberg, R. A. (2011). Hallmarks of cancer: the next generation. *cell*, *144*(5), 646-674

40. WARBURG O .(1956) On the origin of cancer cells. Science Science 123,309-314.

41. J. R. Lakowicz, Principles of Fluorescence spectroscopy. New York: plenumpress, 1985.

42. B. R. Masters and B. chance, Fluorescence and Luminescent probes for Biological Activity. London: Academic Press, 1993.

43. Natacha Bochud-Allemann and André Schneider. Mitochondrial Substrate Level Phosphorylation Is Essential for Growth of Procyclic Trypanosoma brucei J. Biol. Chem. 2002 277: 32849-. doi:10.1074/jbc.M205776200

44. Mark van der Giezen. Mitochondria and the Rise of Eukaryotes BioScience (2011) 61 (8): 594-601 doi:10.1525/bio.2011.61.8.5.

45. Spriet, L. L. (2014). New Insights into the Interaction of Carbohydrate and Fat Metabolism During Exercise. Sports Medicine (Auckland, N.z.), 44(Suppl 1), 87–96. http://doi.org/10.1007/s40279-014-0154-1

46. Deborah Fields. September 2, 2016. What are Mitochondria? Retrieved from: http://www.news-medical.net/life-sciences/What-are-Mitochondria.aspx

47. Dr S Venugopal. Biology-vol-II. Saraswati House Pvt Ltd. ISBN 8173358710, 9788173358715

48. Stephen W. G. Tait, Douglas R. Green, “Mitochondria and cell signaling”. J Cell Sci 2012 125: 807-815; doi: 10.1242/jcs.099234.

49. C. N. A. B. W. R. J. Heyden, Biology: Exploring Life. Boston: Pearson Prentice Hall, 2006.

50. J. L. Spees, et al., "Mitochondrial transfer between cells can rescue aerobic respiration," Proc Natl Acad Sci U S A, vol. 103, pp. 1283-8, Jan 31 2006.

51. Pramanik KC, Boreddy SR, Srivastava SK (2011) Role of Mitochondrial Electron Transport Chain Complexes in Capsaicin Mediated Oxidative Stress Leading to Apoptosis in Pancreatic Cancer Cells. PLoS ONE 6(5): e20151. doi: 10.1371/journal.pone.0020151

52. Lorenzo Galluzzi, Oliver Kepp, Christina Trojel-Hansen, and Guido Kroemer. Mitochondrial Control of Cellular Life, Stress, and Death. Circ Res. 2012; 111:1198-1207, doi:10.1161/CIRCRESAHA.112.268946.

53. Michael R. Duchen. “Roles of Mitochondria in Health and Disease”. Diabetes Feb 2004, 53 (suppl 1) S96-S102; DOI: 10.2337/diabetes.53.2007.S96

54. Sepideh Maleki, “Optical Cryoimaging of Celular Redox in Kidneys from Diabetic Mice”, Master thesis (2012), The University of Wisconsin-Milwaukee.

55. (2010). The Electron Transfer Chain. Retrieved from: http://inoxx.net/?tag=electrontransport-chain

56. Trüeb, R. M. (2015), The impact of oxidative stress on hair. Int J Cosmet Sci, 37: 25–30. doi:10.1111/ics.12286

57. Bind, Marie-Abele et al. “A Novel Genetic Score Approach Using Instruments to Investigate Interactions between Pathways and Environment: Application to Air Pollution.” Ed. Hugo ten Cate. PLoS ONE 9.4 (2014): e96000. PMC. Web. 7 Sept. 2016.

58. J. M. M. a. F. M. Sanchez-Jimenez, "Role of reactive oxygen species in apoptosis: implications for cancer therapy," Int J Biochem Cell Biol, vol. 32, pp. 157-70, Feb 2000.

59. B. H. a. J. M. C. Gutteridge, Free radicals in biology and medicine vol. 4th ed.New York: Oxford University Press, 2007.

60. G. Lenaz, et al., "Mitochondria, oxidative stress, and antioxidant defences," Acta Biochim Pol, vol. 46, pp. 1-21, 1999.

61. Sepehr R, Staniszewski K, Maleki S, Jacobs ER, Audi S, Ranji M; Optical imaging of tissue mitochondrial redox state in intact rat lungs in two models of pulmonary

oxidative stress. J. Biomed. Opt. 0001;17(4):046010-1-046010-7. doi: 10.1117/1.JBO.17.4.046010.

62. James E. Klaunig, Lisa M. Kamendulis, and Barbara A. Hocevar. Oxidative Stress and Oxidative Damage in Carcinogenesis. Toxicol Pathol January 2010 38: 96-109, first published on December 17, 2009 doi:10.1177/0192623309356453

63. W. L. Yen and D. J. Klionsky, "How to live long and prosper: autophagy, mitochondria, and aging," Physiology (Bethesda), vol. 23, pp. 248-62, Oct 2008.

64. Barber, S. C., & Shaw, P. J. (2010). Oxidative stress in ALS: key role in motor neuron injury and therapeutic target. Free Radical Biology and Medicine, 48(5), 629-641.

65. Jenner, P. (2003). Oxidative stress in Parkinson's disease. Annals of neurology, 53(S3), S26-S38.

66. Smith, M. A., Rottkamp, C. A., Nunomura, A., Raina, A. K., & Perry, G. (2000). Oxidative stress in Alzheimer's disease. Biochimica et Biophysica Acta (BBA)-Molecular Basis of Disease, 1502(1), 139-144.

67. Browne, S. E., Ferrante, R. J., & Beal, M. F. (1999). Oxidative stress in Huntington's disease. Brain pathology, 9(1), 147-163.

68. Lukas Haider, Marie T. Fischer, Josa M. Frischer, Jan Bauer, Romana Höftberger, Gergö Botond, Harald Esterbauer, Christoph J. Binder, Joseph L. Witztum, Hans Lassmann. Oxidative damage in multiple sclerosis lesions. Brain Jul 2011, 134 (7) 1914-1924; DOI: 10.1093/brain/awr128.

69. Patel VP, Chu CT. (2011). "Nuclear transport, oxidative stress, and neurodegeneration.". Int J Clin Exp Pathol. 4 (3): 215–29.

70. T. M. Buttke and P. A. Sandstrom, "Oxidative stress as a mediator of apoptosis," Immunol Today, vol. 15, pp. 7-10, Jan 1994.

71. Denk, W., Delaney, K. R., Gelperin, A., Kleinfeld, D., Strowbridge, B. W., Tank, D. W., & Yuste, R. (1994). Anatomical and functional imaging of neurons using 2-photon laser scanning microscopy. Journal of neuroscience methods, 54(2), 151-162.

72. Ntziachristos, V., & Chance, B. (2000). Breast imaging technology: Probing physiology and molecular function using optical imaging-applications to breast cancer. Breast Cancer Research, 3(1), 1.

73. Piston, D. W., Masters, B. R., & Webb, W. W. (1995). Three-dimensionally resolved NAD (P) H cellular metabolic redox imaging of the in situ cornea with two-photon excitation laser scanning microscopy. Journal of microscopy, 178(1), 20-27.

74. Ntziachristos, V., Bremer, C., & Weissleder, R. (2003). Fluorescence imaging with near-infrared light: new technological advances that enable in vivo molecular imaging. European radiology, 13(1), 195-208.

75. T. Vo-Dinh, Biomedical photonics handbook. Boca Raton, Fla: CRC Press, 2003.

76. Panet M.-F., Mikhaylova, M., Li, C., Krishnamachary, B., Glunde, K., Pathak, A. P., & Bhujwalla, Z. M. (2010). Applications of molecular MRI and optical imaging in cancer. Future Medicinal Chemistry, 2(6), 975–988.

77. M. Papademetriou, “Multichannel Near Infrared Spectroscopy to monitor cerebral oxygenation in infants and children supported in extracorporeal membrane oxygenation (ECMO)”, PhD. Thesis, University College of London, 2011

78. P. Rolfe. “In vivo near-infrared spectroscopy”. Annu. Rev. Biomed. Eng. 2(1), pp. 715-754, 2000.

79. YOUNG, P. A., CLENDENON, S. G., BYARS, J. M., & DUNN, K. W. (2011). The effects of refractive index heterogeneity within kidney tissue on multiphoton fluorescence excitation microscopy. Journal of Microscopy,242(2), 148–156. http://doi.org/10.1111/j.1365-2818.2010.03448.x

80. M. Cope, “The Application of Near Infrared Spectroscopy to Non Invasive Monitoring of Cerebral Oxygenation in the Newborn Infant”, PhD Thesis, Department of Medical Physics and Bioengineering, University College London, 1991

81. G. Brant, “Studies on lipids in the nervous system with special reference to quantitative chemical determination and topical distribution”, Acta. Physiol. Scand. Suppl., 18 Suppl 63, 1949.

82. Mourant, J. R., Hielscher, A. H., Eick, A. A., Johnson, T. M., & Freyer, J. P. (1998). Evidence of intrinsic differences in the light scattering properties of tumorigenic and nontumorigenic cells. *Cancer Cytopathology, 84*(6), 366-374

83. S. Wan, et al., "Transmittance of nonionizing radiation in human tissues," Photochem Photobiol, vol. 34, pp. 679-81, Dec 1981.

84. J. Lee, et al., "Noninvasive in vivo monitoring of cyanide toxicity and treatment using diffuse optical spectroscopy in a rabbit model," Mil Med, vol. 174, pp. 615-21, Jun 2009.

85. O. Coquoz, et al., "Optical property measurements of turbid media in a smallvolume cuvette with frequency-domain photon migration," Appl Opt, vol. 40, pp. 6281-91, Dec 1 2001.

86. Body-Monitoring and Health Supervision by Means of Optical Fiber-Based Sensing Systems in Medical Textiles - Scientific Figure on ResearchGate. Available from: https://www.researchgate.net/267628092_fig13_Figure-6-For-postmortem-examinations-upper-left-Optical-penetration-depth-d-of-light [accessed 23 Aug, 2016].

87. Jan Hein Hooijschuur. Flurorescence Spectroscopy. Retrieved from: http://www.chromedia.org/chromedia?waxtrapp=mkqjtbEsHonOvmOlIEcCArB&subNav=cczbdbEsHonOvmOlIEcCArBP

88. (2012). Basic Concepts in Fluorescence. Retrieved from: http://micro.magnet.fsu.edu/primer/techniques/fluorescence/fluorescenceintro.htm

89. (2011). Stokes Shift. Retrieved from: https://upload.wikimedia.org/wikipedia/commons/thumb/2/28/Stokes-Verschiebung.svg/430px-Stokes-Verschiebung.svg.png.

90. Mayevsky, A., & Chance, B. (1982). Intracellular oxidation-reduction state measured in situ by a multichannel fiber-optic surface fluorometer. Science,217(4559), 537-540.

91. A. Mayevsky, S. Labordious, B. Chance, J.Neurosci. Res. 5, 173 (1980).

92. A. Mayevsky and N. Zarchm, Bram Res. 206, 155. (1981).

93. X. Aubert, B. Chance, R. D. Keynes, Proc. R. Soc. London Ser. B 160, 21 1 (1963).

94. F. Jobsis, M. O'Connor, A. Vitale, H. Verman, J. Neurophysiol. 34, 735 (1971).

95. A. Harden, W. Young Alcoholic ferment of yeast-juice Part II. Co-ferment of yeast-juice Proc. Roy Soc., B78 (1906), pp. 369–375

96. O. Warburg, W. Christian, A. Griese, Biochem. Zeitschrift, 282 (1935), p. 157

97. O. Warburg, T.A. Lawson (Ed.), Heavy Metal Prosthetic Groups and Enzyme Action, Clarendon Press, Oxford (1949)

98. H. Theorell, R. Bonnichsen Studies on liver alcohol dehydrogenase. I. Equilibria and initial reaction velocities Acta Chem. Scand., 5 (1951), pp. 1105–1126

99. B. Chance, Spectrophotometry of intracellular respiratory pigments, Science, 120 (1954), pp. 767–775

100. D. Keilin, The History of Cell Respiration and Cytochrome, Cambridge University Press, Cambridge, UK (1966)

101. L.N.M. Duysens, J. Amesz, Fluorescence spectrophotometry of reduced phosphopyridine nucleotide in intact cells in the near-ultraviolet and visible region, Biochim. Biophys. Acta, 24 (1957), pp. 19–26

102. B. Chance, H. Baltscheffsky, Respiratory enzymes in oxidative phosphorylation (VII – Binding of intramitochondrial reduced pyridine nucleotide), J. Biol. Chem., 233 (1958), pp. 736–739

103. B. Chance, F. Jobsis, Changes in fluorescence in a frog sartorius muscle following a twitch Nature, 184 (1959), pp. 195–196

104. B. Chance, P. Cohen, F. Jobsis, B. Schoener, Intracellular oxidation–reduction states in vivo Science, 137 (1962), pp. 499–508

105. B. Chance, N. Oshino, T. Sugano, A. Mayevsky, Basic principles of tissue oxygen determination from mitochondrial signals, H.I. Bicher, D.F. Bruley (Eds.), International Symposium on Oxygen Transport to Tissue, Adv. Exp. Med. Biol., Plenum Publishing Corporation, New York (1973), pp. 277–292.

106. B. Chance, et al., "Oxidation-reduction ratio studies of mitochondria in freeze trapped samples. NADH and flavoprotein fluorescence signals," J Biol Chem, vol. 254, pp. 4764-71, Jun 10 1979.

107. Sepehr R, Staniszewski K, Maleki S, Jacobs ER, Audi S, Ranji M; Optical imaging of tissue mitochondrial redox state in intact rat lungs in two models of pulmonary oxidative stress. J. Biomed. Opt. 0001;17(4):046010-1-046010-7. doi: 10.1117/1.JBO.17.4.046010.

108. M. Ranji, et al., "Fluorescence spectroscopy and imaging of myocardial apoptosis," J Biomed Opt, vol. 11, p. 064036, Nov-Dec 2006.

109. M. Ranji, et al., "Quantifying acute myocardial injury using ratiometric fluorometry," IEEE Trans Biomed Eng, vol. 56, pp. 1556-63, May 2009.

110. J. M. Christie, et al., "LOV (light, oxygen, or voltage) domains of the blue-light photoreceptor phototropin (nph1): binding sites for the chromophore flavin mononucleotide," Proc Natl Acad Sci U S A, vol. 96, pp. 8779-83, Jul 20 1999.

111. G. H. Patterson, et al., "Separation of the glucose-stimulated cytoplasmic and mitochondrial NAD(P)H responses in pancreatic islet beta cells," Proc Natl Acad Sci U S A, vol. 97, pp. 5203-7, May 9 2000.

112. G. A. Wagnieres, et al., "In vivo fluorescence spectroscopy and imaging for oncological applications," Photochem Photobiol, vol. 68, pp. 603-32, Nov 1998.

113. S. Andersson-Engels, et al., "In vivo fluorescence imaging for tissue diagnostics," Phys Med Biol, vol. 42, pp. 815-24, May 1997.

114. J. M. Maarek, et al., "Time-resolved fluorescence spectra of arterial fluorescent compounds: reconstruction with the Laguerre expansion technique," Photochem Photobiol, vol. 71, pp. 178-87, Feb 2000.

115. C. H. Barlow, et al., "Fluorescence mapping of mitochondrial redox changes in heart and brain," Crit Care Med, vol. 7, pp. 402-6, Sep 1979

116. R. S. Balaban and L. J. Mandel, "Coupling of aerobic metabolism to active ion transport in the kidney," J Physiol, vol. 304, pp. 331-48, Jul 1980.

117. S. Maleki, et al., "Mitochondrial redox studies of oxidative stress in kidneys from diabetic mice," Biomed Opt Express, vol. 3, pp. 273-81, Feb 1 2012.

118. B. Vollmar, et al., "A correlation of intravital microscopically assessed NADH fluorescence, tissue oxygenation, and organ function during shock and resuscitation of the rat liver," Adv Exp Med Biol, vol. 454, pp. 95-101, 1998.

119. S. Nioka, et al., "Simulation of Mb/Hb in NIRS and oxygen gradient in the human and canine skeletal muscles using H-NMR and NIRS," Adv Exp Med Biol, vol. 578, pp. 223-8, 2006.

120. N. Ramanujam, et al., "In vivo diagnosis of cervical intraepithelial neoplasia using 337-nm-excited laser-induced fluorescence," Proc Natl Acad Sci U S A, vol. 91, pp. 10193-7, Oct 11 1994.

121. E. Meirovithz, et al., "Effect of hyperbaric oxygenation on brain hemodynamics, hemoglobin oxygenation and mitochondrial NADH," Brain Res Rev, vol. 54, pp. 294-304, Jun 2007.

122. A. Mayevsky, B. Chance. Intracellular oxidation–reduction state measured in situ by a multicannel fiber-optic surface fluorometer. Science, 217 (1982), pp. 537–540

123. A. Mayevsky, A. Deutsch, N. Dekel, E. Pevzner, A. Jaronkin. A new biomedical device for in vivo multiparametric evaluation of tissue vitality in critical care medicine. Proc. SPIE, 5692 (2005), pp. 60–70

124. A. Mayevsky, A. Doron, T. Manor, S. Meilin, N. Zarchin, G.E. Ouaknine. Cortical spreading depression recorded from the human brain using a multiparametric monitoring system. Brain Res., 740 (1996), pp. 268–274

125. William H. Schuette ; Boris A. Vern ; Willard C. Whitehouse; A Low-Light Television System For The In Vivo Measurement Of Oxidative Metabolism As Indicated By NADH Fluorescence. Proc. SPIE 0089, Applications of Optics in Medicine and Biology, 47 (January 20, 1977); doi:10.1117/12.955031.

126. V. Masilamani ; B. B. Das ; J. Secor ; M. AlSalhi ; S. B. Amer ; K. Farhat ; D. Rabah ; R. R. Alfano; Time resolved optical biopsy spectroscopy of normal, benign and malignant tissues from NADH and FAD changes. Proc. SPIE 8220, Optical Biopsy X, 822009 (February 9, 2012); doi:10.1117/12.906913.

127. Liu Q, Grant G, Li J, et al; Compact point-detection fluorescence spectroscopy system for quantifying intrinsic fluorescence redox ratio in brain cancer diagnostics. J. Biomed. Opt. 0001;16(3):037004-037004-11. doi:10.1117/1.3558840.

128. A. Rück ; C. Hauser ; S. Lorenz ; S. Mosch ; S. Rotte ; M. Kessler ; S. Kalinina; Cell metabolism, tumor diagnosis and multispectral FLIM , Proc. SPIE 8588, Multiphoton Microscopy in the Biomedical Sciences XIII, 85880U (February 22, 2013); doi:10.1117/12.2003729.

129. Lane PM, Gilhuly T, Whitehead P, et al; Simple device for the direct visualization of oral-cavity tissue fluorescence. J. Biomed. Opt. 0001;11(2):024006-024006-7.

130. Sivabalan S, Vedeswari C, Jayachandran S, et al; In vivo native fluorescence spectroscopy and nicotinamide adinine dinucleotide/flavin adenine dinucleotide reduction and oxidation states of oral submucous fibrosis for chemopreventive drug monitoring. J. Biomed. Opt. 0001;15(1):017010-017010-11.

131. Romana Pauli ; Christian Betz ; Miriam Havel ; Ronald Sroka ; Herbert Stepp ; Andreas Leunig ; Walter Assmann; Multiple fluorophore-analysis (MFA) for qualitative tissue diagnosis in the oral cavity. Proc. SPIE 6628, Diagnostic Optical Spectroscopy in Biomedicine IV, 66280D (July 06, 2007); doi:10.1117/12.728332.

132. He N. Xu ; Julia Tchou ; Min Feng ; Huaqing Zhao ; Lin Z. Li; Differentiating cancerous from normal breast tissue by redox imaging. Proc. SPIE 9303, Photonic Therapeutics and Diagnostics XI, 93032R (February 26, 2015); doi:10.1117/12.2079930.

133. Xu HN, Nioka S, Glickson JD, Chance B, Li LZ; Quantitative mitochondrial redox imaging of breast cancer metastatic potential. J. Biomed. Opt. 0001;15(3):036010-036010-10.

134. Zhang L, Pu Y, Xue J, et al; Tryptophan as the fingerprint for distinguishing aggressiveness among breast cancer cell lines using native fluorescence spectroscopy. J. Biomed. Opt. 0001;19(3):037005. doi: 10.1117/1.JBO.19.3.037005

135. R. Sepehr ; K. Staniszewski ; E. R. Jacobs ; S. Audi ; M. Ranji; Optical studies of tissue mitochondrial redox in isolated perfused rat lungs. Proc. SPIE

8207, Photonic Therapeutics and Diagnostics VIII, 82073Q (February 3, 2012); doi:10.1117/12.909474.

136. R. Sepehr ; K. Staniszewski ; E. R. Jacobs ; S. Audi ; Mahsa Ranji; Fluorometry of ischemia reperfusion injury in rat lungs in vivo. Proc. SPIE 8580, Dynamics and Fluctuations in Biomedical Photonics X, 85800W (February 28, 2013); doi:10.1117/12.2002094.

137. V. Masilamani ; B. B. Das ; J. Secor ; M. AlSalhi ; S. B. Amer ; K. Farhat ; D. Rabah ; R. R. Alfano; Time resolved optical biopsy spectroscopy of normal, benign and malignant tissues from NADH and FAD changes. Proc. SPIE 8220, Optical Biopsy X, 822009 (February 9, 2012); doi:10.1117/12.906913.

138. Binlin Wu ; S. K. Gayen ; M. Xu; Fluorescence spectroscopy using excitation and emission matrix for quantification of tissue native fluorophores and cancer diagnosis. Proc. SPIE 8926, Photonic Therapeutics and Diagnostics X, 89261M (March 4, 2014); doi:10.1117/12.2040985.

139. Maleki S, Gopalakrishnan S, Ghanian Z, et al; Optical imaging of mitochondrial redox state in rodent model of retinitis pigmentosa. J. Biomed. Opt. 0001;18(1):016004-016004. doi:10.1117/1.JBO.18.1.016004.

140. F. Salehpour ; C. Yang ; T. Kurth ; A. W. Cowley ; M. Ranji; Optical cryoimaging of rat kidney and the effective role of chromosome 13 in salt-induced hypertension. Proc. SPIE 9321, Optical Interactions with Tissue and Cells XXVI, 932113 (March 5, 2015); doi:10.1117/12.2079549.

141. Volkmar Betz ; Herbert Schneckenburger ; H. P. Alleroeder ; Gerhard W. Sybrecht ; Joerg-Uwe Meyer; Evaluation of changes in the NADH level between carcinogenic and normal tissue samples by use of fluorescence spectroscopy. Proc. SPIE 2324, Optical Biopsy and Fluorescence Spectroscopy and Imaging, 284 (January 4, 1995); doi:10.1117/12.198733.

142. Camila de Paula D´Almeida ; Carolina Campos ; Marcelo Saito Nogueira ; Sebastião Pratavieira ; Cristina Kurachi; Time-resolved and steady-state fluorescence spectroscopy for the assessment of skin photoaging process. Proc. SPIE 9531, Biophotonics South America, 953146 (June 19, 2015); doi:10.1117/12.2180975.

143. S. Palmer ; K. Litvinova ; E. U. Rafailov ; G. Nabi; Discrimination of healthy and cancer cells of the bladder by metabolic state, based on autofluorescence, Proc. SPIE 9303, Photonic Therapeutics and Diagnostics XI, 93030T (February 26, 2015); doi:10.1117/12.2077218.

144. Andrew M. Siegel, “Investigating the Temporal Evolution Of The Cerebral Hemodynamic Response Using Diffuse Optical Tomography”, Ph.D. thesis (2004), Tuffs University.

145. Tao Ao, L. Zhou and B. Chance, "Miniature fluorescent metabolometer," (CLEO). Conference on Lasers and Electro-Optics, 2005., 2005, pp. 2230-2232 Vol. 3. doi: 10.1109/CLEO.2005.202426.

146. Dmitriy V. Kornilin ; Vladimir N. Grishanov; Portable fluorescence meter for medical applications. Proc. SPIE 9887, Biophotonics: Photonic Solutions for Better Health Care V, 98871N (April 27, 2016); doi:10.1117/12.2227392

147. Nemiroski A, Ryou M, Thompson CC, Westervelt RM. Swallowable fluorometric capsule for wireless triage of gastrointestinal bleeding. Lab Chip. 2015 Dec 7; 15(23):4479-87.

148. E. Jovanov, D. Raskovic, J. Price, A. Krishnamurthy, J. Chapman and A. Moore. “Patient monitoring using personal area networks of wireless intelligent sensors”. Biomed. Sci. Instrum. 37pp. 373-378, 2001.

149. N. Golmie, D. Cypher and O. Rbala. “Performance analysis of low rate wireless technologies for medical applications”. Comput. Commun. 28(10), pp. 1266-1275, 2005.

150. T. Muehlemann, D. Haensse and M. Wolf. “Wireless miniaturized in-vivo near infrared imaging”. Optics Express, 16(14), pp. 10323-10330, 2008.

151. Specification sheet of Ultraviolet Emitter MTE3650L2-UV-HP. Manufactured by Marktech Optoelectronics. 2015-02-02.

152. Specification sheet of I.C CD54HC4052.” CDx4HC405x, CDx4HCT405x High-Speed CMOS Logic Analog Multiplexers and Demultiplexers”. Manufactured by Texas Instruments”. SCHS122K –NOVEMBER 1997– REVISED SEPTEMBER 2015.

153. Datasheet for DG411, DG412, DG413, “Precision Monolithic Quad SPST CMOS Analog Switches”, manufactured by Vishay Siliconix, Document Number: 70050, S11-1185-Rev. G, 13-Jun-11.

154. Datasheet for OPT101, “Monolithic Photodiode And Single-Supply Transimpedance Amplifier”, manufactured by Burr-Brown Products from Texas Instruments, SBBS002A – January 1994 – Revised October 2003.

155. Specification sheet of I.C TL072CP.” TL07xx Low-Noise JFET-Input Operational Amplifiers”. Manufactured by Texas Instruments”. SLOS080M – SEPTEMBER 1978–REVISED JUNE 2015.

156. Specification sheet of Gelatin filter.” Gamcolor, deep dyed polyester color”. Manufactured by Gamcolor.

157. Specification sheet of band pass filter.” 334-492nm Bandpass interference filters”. Manufactured by Edmund Optics.

158. Specification sheet of band pass filter.” 500-694nm Bandpass interference filters”. Manufactured by Edmund Optics.

159. Rishabh Sharma. July 02, 2014. what is Arduino? Retrieved from: http://myelectronicshub.blogspot.com/2014/07/what-is-arduino.html

160. Martyn Currey. 19.09.2015. HC-05 FC-114 and HC-06 FC-114. Part 2 – Basic AT commands. Retrieved from: http://www.martyncurrey.com/hc-05-fc-114-and-hc-06-fc-114-part-2-basic-at-commands/

161. Mechatrofice. LCD matrix interface with arduino. Retrieved from: http://mechatrofice.blogspot.com/2015/06/lcd-matrix-display-shield-interface-with-arduino-library.html

162. Crouch, Stanley; Skoog, Douglas A. (2007). Principles of instrumental analysis. Australia: Thomson Brooks/Cole. ISBN 0-495-01201-7.

163. Herrmann, R.; C. Onkelinx (1986). "Quantities and units in clinical chemistry: Nebulizer and flame properties in flame emission and absorption spectrometry (Recommendations 1986)". Pure and Applied Chemistry 58 (12): 1737–1742.

164. T. Vo-Dinh, Biomedical photonics handbook. Boca Raton, Fla: CRC Press, 2003.

165. Datasheet for 945-1122-ND, “Constant current LED driver”, manufactured by Recom, REV: 1/2016